A gene signature for Alzheimer's disease using RNAi in *C. elegans*

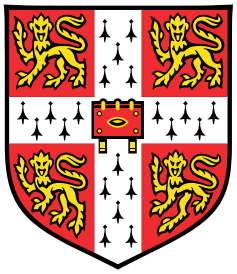

Prashanth Surya Ciryam

Supervisor: Prof Michele Vendruscolo

Department of Chemistry
University of Cambridge

This dissertation is submitted for the degree of
Doctor of Philosophy

St John's College

December 2020

Declaration

I hereby declare that except where specific reference is made to the work of others, the contents of this dissertation are original and have not been submitted in whole or in part for consideration for any other degree or qualification in this, or any other university. This dissertation is my own work and contains nothing which is the outcome of work done in collaboration with others, except as specified in the text and Acknowledgements. This dissertation contains fewer than 65,000 words including appendices, bibliography, footnotes, tables and equations and has fewer than 150 figures.

Prashanth Surya Ciryam
December 2020

A gene signature for Alzheimer's disease using RNAi in *C. elegans*

Prashanth Surya Ciryam

Alzheimer's disease (AD) is a complex multifactorial disorder that is responsible for the large majority of the 50 million cases of dementia worldwide. This disease is still incurable, a situation caused at least in part by the fact that its genetics are incompletely known. In our laboratory, we have developed a novel computational approach—Network-based Transcriptome-Wide Association Studies (nTWAS)—that seeks to identify the genes associated with AD by comparing gene expression patterns across tissues in the brain. nTWAS acts as an *in silico* pre-screen by providing a list of gene candidates, thus enabling us to pursue investigations into each gene candidate with significantly more depth. To that end, we use RNA interference in an AD model in the nematode worm *Caenorhabditis elegans* to validate the results of this pre-screen. *C. elegans* is a well-established research tool in biological and biochemical research for its ease of culture, small size, short generation time, and relative simplicity. Furthermore, the worm's facility for genetic manipulation and remarkably similar cellular characteristics to those of humans have allowed for numerous advances in the study of cancer, neurodegeneration, and ageing. Our approach takes advantage of an automated worm tracking platform, developed in our laboratory, that can simultaneously track hundreds of worms and make precise measurements of their motility, defects of which has been shown to correlate with neurological and muscular toxicity. While standard approaches typically only take data on dozens of worms, the vastly increased population size of our approach greatly improves the statistical power of our screen. We have leveraged these improvements in screening methods to associate the differences in distributions of these parameters with phenotypic changes across various siRNA conditions. Through both motility screening and validation by imaging, we identified *ckr-2*, *skr-21*, and *Y92H12A.2* as modulators of amyloid beta aggregation. While *skr-21* and *Y92H12A.2* are both components of the ubiquitin-proteasome system, *ckr-2* is an ortholog of a neuronal cholecystokinin receptor which has been suggested to be a biomarker of AD but for which no mechanism is known. The results of this work thus contribute to extending our understanding of the gene signature of AD.

Acknowledgements

No endeavour of any merit is undertaken alone. My postgraduate studies in Cambridge are no exception. In my time here, I have been truly blessed by the company of remarkable people. Where I have succeeded, it has been because of their guidance and generosity. And where I have faltered, it has been in spite of their best efforts. Without my colleagues, friends, and family, my adventures over the last five years would not have been nearly as exciting, intellectually rewarding, scientifically productive, or just plain fun. If in the coming pages I have forgotten anyone, this is undoubtedly due to the failure of my own memory, and not for lack of appreciation of their contributions.

I am extremely grateful to my supervisors Prof Michele Vendruscolo and the late Prof Sir Christopher Martin Dobson, without whom I would never have become a scientist. When I left Duke University, I departed with a vast, disconnected assortment of facts about biology but knew very little about the process of science. Under the tutelage of Prof Vendruscolo and Prof Dobson, I learned how to develop rigorous lines of scientific inquiry and to assemble arrays of facts and figures into coherent narratives. My conversations with Prof Dobson showed me the immeasurable worth of persistence in science. And my many discussions with Prof Vendruscolo shaped my understanding of economy in experimentation and, perhaps most valuable of all, how to decide when a question has been answered. I will be forever thankful for their investment in my development as a scientist.

I have also been very lucky to have enjoyed the guidance of other senior scientists. Prof. Ellen Nollen graciously gave me the opportunity to stay with her research group for a month at the University of Groningen, where I learned RNA interference methods in *C. elegans* with great help from Dr Mandy Koopman and Renee Seinstra. And Prof. Mario de Bono both opened his facilities at the Laboratory for Molecular Biology to me and personally taught me how to perform DNA microinjections and aerotaxis assays on the worms. The work presented in this thesis would not have been possible without their assistance.

I am immensely fortunate to have had the chance to work alongside some truly exceptional people in the Centre for Misfolding Diseases at the Yusuf Hamied Department of Chemistry. Although their benefactions may be too many to count, I will in my hubris attempt to count them anyway. I thank Dr Janet Kumita for so often shepherding me through difficult situations and for teaching me to navigate complex working relationships in a large research institute. My frequent debates with Dr Florian Buhr have made me a more thoughtful man, and his constant encouragement and endless patience are what I credit to my betterment as an experimentalist. I will always remember our arguments over beer and board games fondly, and I hope our collaborations—scientific and otherwise—will last far into the future. I am grateful for wonderful colleagues in my cohort like Dr Michele Sanguanini, who from my first day in Cambridge was a friend and confidant. And for Dr Sam Ness, who was my very first friend in Cambridge from my days as an undergraduate intern. Dr Ana Bernardo-Gancedo frequently reminded me that science is not the only thing in life, as much as I sometimes wanted it to be. I am thankful for the diligent work of Sam "Cass" Casford and Nancy Hanna, two fantastic research technicians whose dedication, hard work, and great company made life in the lab more vibrant. Over the years, many lab mates have become old friends, like Roxine Staats, Katarina Pisani, Dr Phil Lindstedt, Dr Marta Castellana-Cruz, Dr Maarten Hardenberg, Oded Rimon, Thomas Löhr, Prof Ryan Limbocker, Ryan Geiser, Mathias Schneider, Rosie Bell, Akhila Jyothy, Raphaël Jacquat, Dr Quentin Peter, Klara Kulenkampff, and Marc Oeller. And I am equally thankful for new friends, like Alyssa Miller, Alicia Gonzalez, Michael Metrick, Ross Taylor, Dillon Rinauro, Samuel Dada, Mady Hazemi, and Jiacheng Lin. I wish we had more time to spend together. Among this group is the CMDxWord gang, without whom I would not have left lockdown with any sanity. In fact, without any of these people, no low would have been as tolerable and no high as sweet. I will dearly miss working with them all.

I will always be indebted to Karen Valleli, my surrogate mother in Cambridge as she was for many others, for her patience and kindness. On so many occasions I found myself taking refuge in her office when I felt overwhelmed, and she always managed to help me disentangle myself from whatever bureaucratic nightmare I managed to get stuck in (less her 10%, naturally). And, on especially hard days, I could always count on her to be there to raise my spirits and spread some "hot goss".

St John's College has supported my education in Cambridge both in and out of the laboratory. My Tutor, Sylvana Tomaselli, made sure I wanted of nothing while I was under her care, even if I was occasionally rebellious. Danny Bennett is a constant

reminder of the joy of science, and our late-night riverside walks will be missed. Adam Lerner and Sipke Ó Seachnasaigh opened my mind to new worlds. I hope we speak more often.

I must also give thanks to Dr Divya Venkatesh, Prof Callie Vandewiele, and Dr Nelis Drost, who so readily welcomed me into their lives. Although we have now spread far across the globe, I hope we can reunite for board games soon.

Alejandro Enrique Figueroa Medina is my oldest friend, and none of my achievements would have been possible without his companionship. Our friendship is my most prized possession. John Byrum, Arpan Bhandari, James Fenwick, and Zach Carpenter have always challenged and humbled me, and I so look forward to spending more time with them all in person after many years away. Vanessa Osman's sage advice has been a necessary component of any undertaking almost from the moment we met. Jared Schwartz has accompanied me on countless adventures, and our conversations are a reminder that there are people who will always be on your wavelength. John Barker will never cease to amaze me, and I am infinitely better for our friendship. I have kept Hann Henson on the phone for far longer than is kind, and he has always been there to hear me out. Meredith Eaton King always screws my head on straight, no matter how askew I manage to leave it. And Ilya Strunilin is my long-lost brother, our bond forged through hardships of all kinds. These are lifelong friends, and I do not know what I would do without them.

My love of learning and passion for educating is the product of many great teachers in my formative years. Therefore, I must thank Mrs Amanda Turner, who taught me to keep practicing; Mrs Sue Sams, who helped me find the beauty of mathematics and physics in the mundane; and Mr Justin Holt, who taught me the true meaning of luck: where preparation meets opportunity. And I must give special thanks to Ms Jennifer Gallagher, whose support for me over the years has been a source of strength. It was in after-school sessions in Ms Gallagher's classroom that I first took serious interest in science, an interest she fostered despite my repeated (unintentional) destruction of her lab equipment. Ms Gallagher encouraged me to take her advanced chemistry course, where I was first introduced to the elegance of reactions and molecular phenomena that set me on the path toward research. I strive to have the kind of impact on the scientific careers of my students that she had on mine.

And, finally, there is no greater gratitude than that which I hold for my loving family. My father and mother have always pushed me to dream bigger and work harder, and any work ethic I possess is due to them. I will always cherish the

biomarker of AD but for which no mechanism is known. The results of this work thus contribute to extending our understanding of the gene signature of AD.

Table of contents

List of figures

List of tables

Expansion means complexity, and complexity decay.
Cyril Northcote Parkinson, *In Laws and Outlaws* (1962)

It's not easy with this complexity.
Eagles of Death Metal, *Complexity* (2015)

1 Introduction

1.1 Précis

Alzheimer's disease (AD) is the most common form of dementia, affecting roughly 850,000 people in the United Kingdom alone and 54 million people worldwide [1]. By 2050, the global figure is expected to rise to 140 million people [2]. Not only does AD represent a economic significant burden and logistical challenge to healthcare systems, the insidious nature of the disease robs people of their memories, their identities, and, eventually, their lives. Despite decades of fastidious research and copious amounts of funding, there is still no cure for the disease, although some medications may slow down the progression of the disease. Although the fact that aggregates of amyloid-β and tau are involved in the aetiology of AD has been known since the mid-1980s [3], there is still much to be learned about the precise molecular mechanisms by which these aggregates modulate the disease. Even less is known about what gives rise to sporadic AD—the most common form of the disease, representing roughly 98% of total cases [4].

In the following chapter, we will lay out the basic facts of AD, beginning with a generic review of protein misfolding and aggregation—the processes that underlie this disease and several others. From there, we will discuss AD specifically and

a selection of hypotheses regarding its pathogenesis, including the amyloid cascade hypothesis. Finally, we will present an approach to AD research focused on generating a gene signature for the disease.

1.2 Protein misfolding and aggregation

Many of the basic operations of a cell—from metabolism and ion transport to gene expression itself—are mediated by proteins. An essential condition for most proteins to carry out their intended functions is their folding into their native states. That is to say, they must fold correctly. Other proteins are intrinsically disordered, and therefore may occupy any number of conformational states, including functional, non-functional, and dysfunctional forms. AD is a protein misfolding disorder, a class of disorders that includes, among others, Parkinson's disease, Huntington's disease, and Type II Diabetes [5–8]. Because the original work presented in the coming chapters primarily focuses on the development of improved animal models for AD, it is important that we understand the fundamental cellular dysfunctions that underlie AD and other protein misfolding pathologies. In this section, we will address three important questions regarding the molecular underpinnings of amyloidogenic protein misfolding disorders:

1. What causes proteins to misfold and occupy the amyloid state?
2. Why do misfolded proteins persist in and around the cell?
3. By what mechanism do amyloid aggregates cause disease and cytotoxicity?

1.2.1 What causes proteins to misfold and occupy the amyloid state?

The native structure of a protein is influenced by its primary structure, which greatly limits the conformations that a protein may fold into and occupy [9]. While a stochastic search for the correct conformation may appear to be the driver of protein folding, the primary structure of a protein constrains the energy landscape to such an extent that only a few viable conformations remain [10–12]. Significant evidence for this lies in the fact that many proteins first fold around a characteristic folding nucleus, which then dictates how the remainder of the protein will fold and, ultimately, condense into its native state [13]. The spontaneity of folding is partially driven by the interaction of hydrophobic residues [14].

The folding process often begins on the ribosome during translation, although some proteins may not complete folding until after synthesis is complete [15–17]. While primary structure is a major determinant of the final conformation of the protein, folding also depends on the nature of the solvent [18, 19]. Namely, solvent salt concentration, temperature, and pH all exert influence on protein folding. These solvent characteristics vary across subcellular compartments, and indeed many proteins complete their folding after trafficking to non-cytosolic cellular compartments or in the extracellular space.

With all its many dependencies, it is not surprising that protein folding is not infallible. During translation, the nascent chain of the protein is exposed to the cellular environment. The very hydrophobic residues that assist in normal protein folding are, at this point, susceptible to inappropriate interactions with other components of the cell [18]. Although there are systems in place, such as molecular chaperones, to assure correct folding both during and after translation, proteins may still misfold [19].

Although amyloid aggregates are frequently formed from polymers of misfolded proteins, not all misfolded proteins readily form amyloids *in vivo*. The amyloid state is defined by cross-beta linkages and beta-sheet secondary structure formation that permit peptides to form long, unbranched fibrils [20]. The name amyloid derives from Rudolf Virchow's early erroneous identification of these structures as deposits of starch, rather than the proteinaceous material from which they are actually composed [21]. Sequence-specific characteristics, such as alternating hydrophobic and hydrophilic amino acid residues, may increase the likelihood of a protein to form cross-beta linkages and beta-sheets [22]. Amyloid structures found in many diseases are often composed of polymers of a single protein or peptide, but other proteins, sugars, and cellular components may be sequestered within inclusions and plaques [23–25].

The route a protein takes from translation on the ribosome to its functional native state offers numerous opportunities for conversion to the amyloid state (**Fig 1.1**). Unfolded proteins may proceed along various paths that interconvert with one another. They may be tagged for degradation directly by the unfolded protein response (UPR), form functional protein through intermediates, oligomerise through off-pathway mechanisms, or even be directly recruited to amyloid fibrils [26, 6]. The size of the population of these various conformational states and the rates of interconversion between them are governed by their thermodynamic stabilities, rates of synthesis and degradation, propensity to interact with molecular chaperones

and UPR components, free energy barriers, and proclivity for post-translational modification [6].

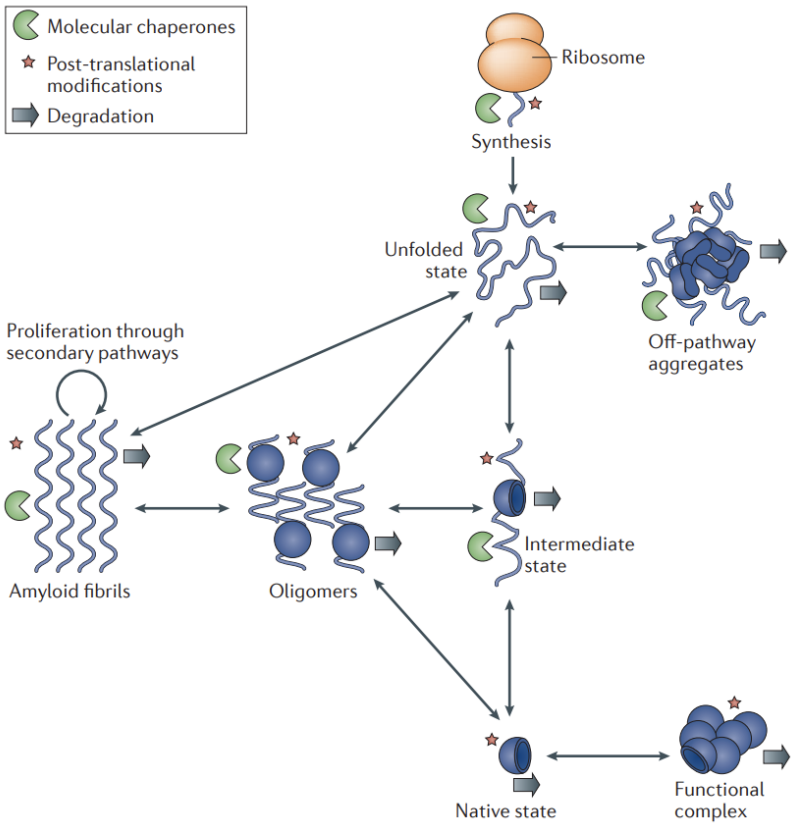

Fig. 1.1 **Proteins may occupy various conformations that may interconvert to both functional and aggregated states.** Proteins that do not co-translationally fold may occupy various non-native states. While these are typically transitional conformations that lead to the native state of the protein, several other pathways are possible. Proteins may form aggregation-prone species that oligomerise and, eventually, form amyloid fibrils, or may form unstructured, off-pathway aggregates. The interconversion among these states depends on a number features of a given protein, including their thermondynamic stabilities, free energy barriers between these states, rates of synthesis and degradation, and propensity to undergo post-translational modification. *Figure reproduced with permission from [6]*

Kinetic analysis of amyloid formation reveals a generic sigmoidal fibril growth curve in the presence of small quantities of soluble monomer (**Fig 1.2**) [6, 27]. The aggregation reaction begins with a slow lag phase, during which protein monomers polymerise to form oligomers, or soluble protein polymers formed from relatively few subunits [6, 27]. These oligomers may then associate to form protofibrils and, with time, mature amyloid fibrils. As the reaction proceeds, it enters a rapid growth

phase driven by the elongation of fibrils by addition of monomers at either of its ends. The swiftness of this phase of the reaction is sustained by fibril fragmentation, which exposes more sites to which monomeric species may attach, and secondary nucleation, which catalyses the production of oligomers from monomers [6, 27]. When the quantity of monomer in the environment is fixed, the growth phase is followed by a slowing of the reaction rate until a plateau is reached, caused by a drop in the concentration of available monomer as they continue to be recruited to fibrils [6]. The lag phase may be significantly shortened by the addition of preformed aggregates to the reaction, which suggests that nucleation processes have a consequential effect on amyloid aggregation kinetics [6].

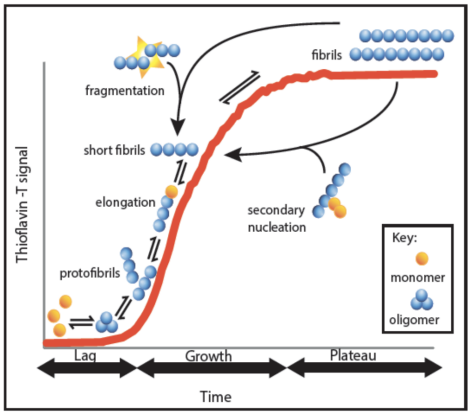

Fig. 1.2 **The kinetics of amyloid fibril formation and the mechanisms relevant to each phase.** The rate of the amyloid formation reaction is typically measured using a Thioflavin-T fluorescent signal. Thioflavin-T fluoresces upon interaction with cross-beta linkages that are characteristic of amyloid fibrils. This reaction proceeds through a lag phase during which monomers aggregate into oligomers, which in turn aggregate to form protofibrils and mature fibrils; a growth phase during which fibrils elongate and fragmentation, seeding rapid fibril growth; and a plateau phase during which the reaction rate slows due to monomer depletion. *Figure reproduced with permission from [27]*

1.2.2 Why do misfolded proteins persist in and around the cell?

Understanding how misfolded proteins are able to persist in the cell is central to our comprehension of the aetiology protein misfolding disorders. After all, if misfolded proteins were reliably and effectively degraded by the cell, these diseases may not even take hold in the first place. Even aggregated proteins in the extracellular space—such as amyloid-β—should be able to be endocytosed and degraded by canonical

pathways. With highly-conserved systems in place to prevent amyloid formation and hasten their degradation—systems such as molecular chaperones and the UPR [28–30]—and natural selection against common amyloidogenic motifs [22, 31, 32], how is it possible that misfolded proteins can convert to the amyloid state and remain in intracellular and extracellular spaces?

Protein homeostasis is maintained by a network of cellular mechanisms that contend with the diverse range of issues that may affect the regulation of proteins. Reaching far beyond simple protein quality control mechanisms, protein homeostasis machinery must contend with stressors that can potentially dysregulate transcription, translation, trafficking, processing, subcellular localization, processing, folding, and degradation of proteins [33]. It is precisely due to the variegated nature of the protein homeostasis network that some issues may slip through the cracks; communication between different homeostatic components may break down and insults to one part of the network may precipitate the breakdown of the network as a whole [28, 33]. Furthermore, protein misfolding diseases tend to be ageing-associated, and the effectiveness of protein homeostasis components declines with age [33].

Furthermore, even in the best of times cells only have a limited set of resources to deploy against perturbations in protein homeostasis. As a result, evolutionary pressures have pushed cells toward triage [34–38], although the actual decision-tree for homeostatic triage remains unclear [39]. Protein misfolding disorders may exploit these triage mechanisms to propagate unabated in their early stages before overwhelming protein homeostasis machinery [30]. This contention is supported by genetic evidence in AD, where certain mutations in Apolipoprotein E (ApoE) may reduce the cell's ability to degrade the amyloid-β peptide. These mutations are sufficiently linked with AD pathogenesis that they act as genetic markers for the disease [40, 41].

1.2.3 By what mechanism do amyloid aggregates cause disease and cytotoxicity?

Having now explained how amyloid aggregates form and evade the mechanisms in place to rid them from the cell, we must now answer the question of how these aggregates cause dysfunction. The answer to this question is less clear and the subject of much debate. One theory is that as these aggregates grow in size, they physically interfere with normal cellular functions [42]. Large aggregates may, for example, prevent other proteins from being trafficked to their target subcellular

compartments and organelles, thus producing aberrant cellular behaviours [42]. This explanation, however, is insufficient. Not only is it the case that several of the toxic species in the most common protein misfolding disorders (AD and PD) misfold and persist extracellularly, it has been demonstrated experimentally that treatment of cells with mature amyloid fibrils does not result in cytotoxicity [18]. Treatment of cells with oligomeric species, however, does produce cytotoxicity and disease phenotype [40, 43–47]. These findings suggest that it is the pre-fibrillar form of amyloidogenic peptides that results in the disease state [48].

Not all oligomers are created equal, and distinctions can be made among them in terms of their level of toxicity. Toxic oligomeric species are more likely to be small—and therefore ease diffusibility, owing to greater surface-to-volume ratios—and to have exposed hydrophobic residues [46]. They are also more likely to exhibit relative disorganisation in their core structures [43].

It is now commonly-held that disease-associated oligomeric species derive at least some of their character from toxic gain-of-function [49, 50]. Toxic oligomer assemblies have been shown to effect changes in vesicular trafficking [51] and form novel complexes [52], including calcium channels [53, 54], that disrupt neurotransmission and standard cellular function. While mature amyloid fibrils and plaques are, as stated previously, largely inert [55, 56], the oligomers from which they are composed and which they shed can cause severe disease phenotypes during fibrillar assembly [40, 43–47, 49, 50]. As a result, one proposed therapeutic strategy suggests accelerating fibril assembly to sequester toxic oligomers into these chemically-inactive plaques [57–60, 59, 61].

1.3 Alzheimer's disease

AD is an ageing-related neurodegenerative disorder of the central nervous system and is by far the most common cause of dementia, representing between 60 and 70% of all cases [62]. As a result, both the general public and clinicians often fail to make a distinction between diagnoses of AD and other dementias, even in the face of negative diagnostic results. Thus, it is important that we precisely define the disease. In the following section, we will discuss the pathogenesis of the disease, as well as the molecular mechanisms of the toxicity exhibited AD. The discussion of these mechanisms will begin with a critical appraisal of the amyloid cascade hypothesis, followed by an examination of more peripheral toxic mechanisms.

1.3.1 Current Hypotheses of AD Pathogenesis

Clinically, patients suffering from AD may first present with mild cognitive impairment many years before formal diagnosis can be made [63]. This cognitive decline, usually first manifesting as short-term memory loss, eventually results in severe impairment of learning and memory [62] (sometimes including long-term memory [64]), loss of language fluency [65], apraxia [66], agnosia [67], and—often as a result of these deficits—an inability to live independently [68]. This, however, is insufficient to distinguish AD from other dementia syndromes.

On the molecular level, AD is characterised by the appearance of extracellular amyloid plaques—composed primarily of the peptide fragment amyloid-β—and intracellular neurofibrillary tangles (NFTs), comprised of tau proteins, the intrinsically disordered splice variants of the gene *MAPT* (Microtubule-Associated Protein Tau) [69, 70]. It is the appearance of these two structures—plaques and NFTs—that distinguishes AD from other dementias. This has been the dominant mode of diagnosis since Alois Alzheimer first described these as the hallmarks of the disease in 1906 [71].

While tau proteins are themselves functional—both in their stabilisation of axonal microtubules and negative regulation translation through their ribosome-binding activity—amyloid-β is a cleavage product of amyloid precursor protein (APP), an integral membrane protein whose function is not completely understood [6]. There are three main categories of APP processing and cleavage: amyloidogenic (generated through successive cleavages by β- and γ-secretases), non-amyloidogenic (generated through successive cleavages by α- and γ-secretases), and alternative pathways (generated by a number of processes, including cleavage by caspases or σ- and η-secretases) (**Fig 1.3**) [72]. The various cleavage pathways for APP result in the production of at least 14 distinct families of peptides, whose effects range from neurotoxicity to neuroprotection [72].

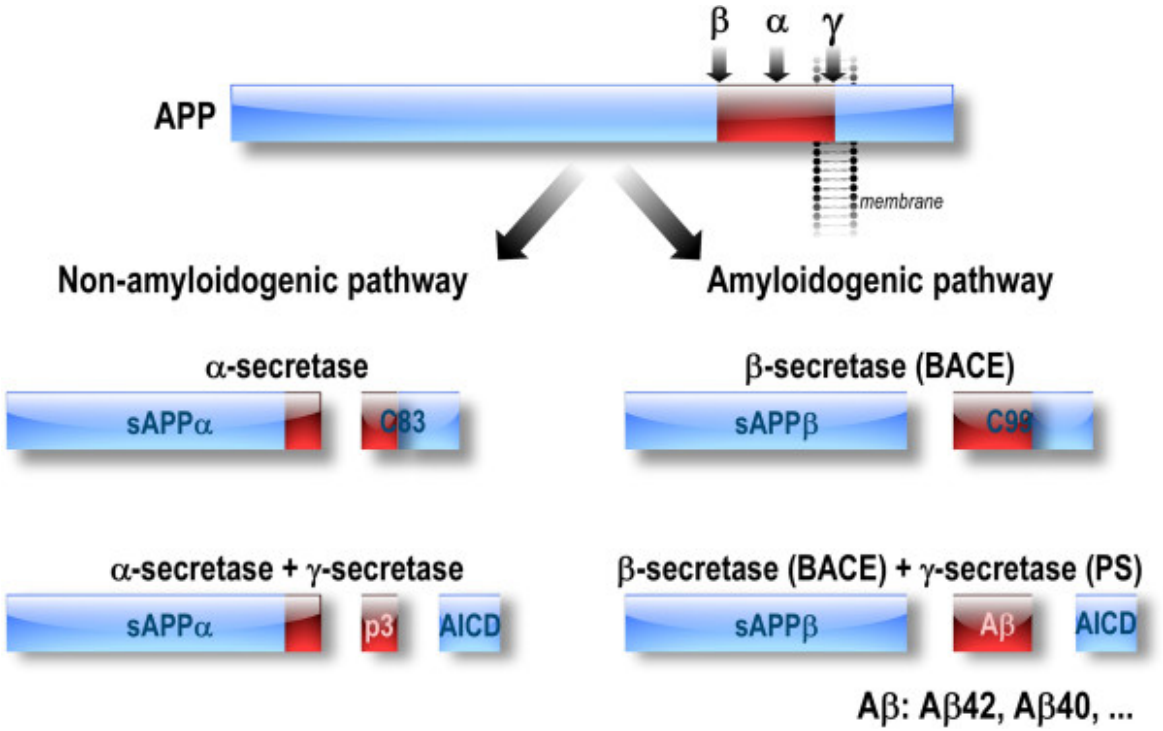

Fig. 1.3 **Amyloidogenic and non-amyloidogenic pathways of APP cleavage.** APP may be cleaved either successively by α-secretase and γ-secretase in the non-amyloidogenic pathway to yield sAPPα, p3, and AICD, or successively by β-secretase and γ-secretase in the amyloidogenic pathway to yield sAPPβ, Aβ, and AICD. The AICD formed by the amyloidogenic pathway is transcriptionally active, unlike the same peptide formed by the non-amyloidogenic pathway. *Reproduced under Creative Commons Attribution License from [72]*

The amyloidogenic pathway produces amyloid-β species of various lengths, and the specific species is typically denoted by which of the amyloid-β-generating APP residues are included in the final peptide fragment (e.g. $A\beta_{1\text{-}42}$ or $A\beta_{3\text{-}40}$). In this pathway, APP is first cleaved by β-secretase within its ectodomain, liberating the sAPPβ fragment [72]. The remaining membrane-bound portion of APP is then cleaved by γ-secretase, generating amyloid-β and the APP intracellular domain (AICD). Interstingly, even though both the amyloidogenic and and non-amyloidogenic pathways ultimately both produce AICD, they seem to serve different roles [72, 73]. While AICD generated from the amyloidogenic pathway localises to the nucleus and acts as a transcription factor for neprilysin, an amyloid-β-degrading enzyme, AICD produced from the non-amyloidogenic pathway is quickly degraded [74, 75]. This is in spite of the fact that there seem to be no differences in the sequences of AICD produced from these two pathways.

Although the majority of this work focuses on peptides generated through the amyloidogenic cleavage pathway, it is important to note that highly toxic oligomers can form from a mixture of amyloid-β species generated from the amyloidogenic and non-amyloidogenic pathways [76]. Some of these heterogeneous oligomeric species are less likely to accumulate in fibrils, possibly leading to increased toxicity and hastened disease onset due to failure to sequester toxic oligomers [76, 77]. While toxic species formed from non-amyloidogenic pathways are relatively low in abundance, they could play a part in the initial stages of the disease. Their role in AD pathogenesis is certainly meritorious of further study and consideration.

AD can be broadly categorised into two variants: familial (fAD) and sporadic (sAD). fAD is less common, representing roughly 2% of cases, and seems to be dominantly inherited [4, 69]. This variant of the disease seems to be caused by mutations in presenilin 1 (*PSEN1*), presenilin 2 (textitPSEN2), and/or APP, albeit other genes may also be involved [69]. PSEN1 is a core protein of the γ-secretase complex, while PSEN2 either regulates this complex or is itself a protease [69]. Disease-associated mutations in these genes increase production of amyloid-β, leading to development of AD. fAD is distinct from sAD in its early onset, with presentation of clinical phenotype occurring prior to the age of 65 [78]. Meanwhile, sAD, as the name suggests, arises without significant inheritance, although certain risk factors—such as the ApoE4 allele of Apolipoprotein E—can be inherited [79]. Besides the changes in the age of onset, fAD and sAD have roughly the same clinical presentation. As a result, and because of the relative ease with which one can reproduce the genetic causes underlying fAD in the laboratory, most animal models for AD attempt to recapitulate fAD.

The progression of AD through the brain follows a predictable path. Braak staging, a widely-accepted and formally defined staging system for AD, is defined by the progression of NFTs through the brain (**Fig 1.3, lower**) [80]. Braak stages I and II refer to periods when NFTs are confined to the transentorhinal brain region [80, 70, 81]. In stages III and IV, there is also involvement of the limbic regions including the hippocampus. And in stages V and VI, NFTs form in neocortical regions. The deposition of amyloid-β plaques is highly spatially correlated with the formation of NFTs, and therefore follows a similar—although not identical—path through the brain (**Fig 1.3, upper**). Braak staging shows us that AD has a long fuse, with the earliest events in the disease occurring decades prior to presentation of a clinical phenotype. It can take 30 years to progress from stage I to stage III, and 48 years to progress from stage I to stage V [81].

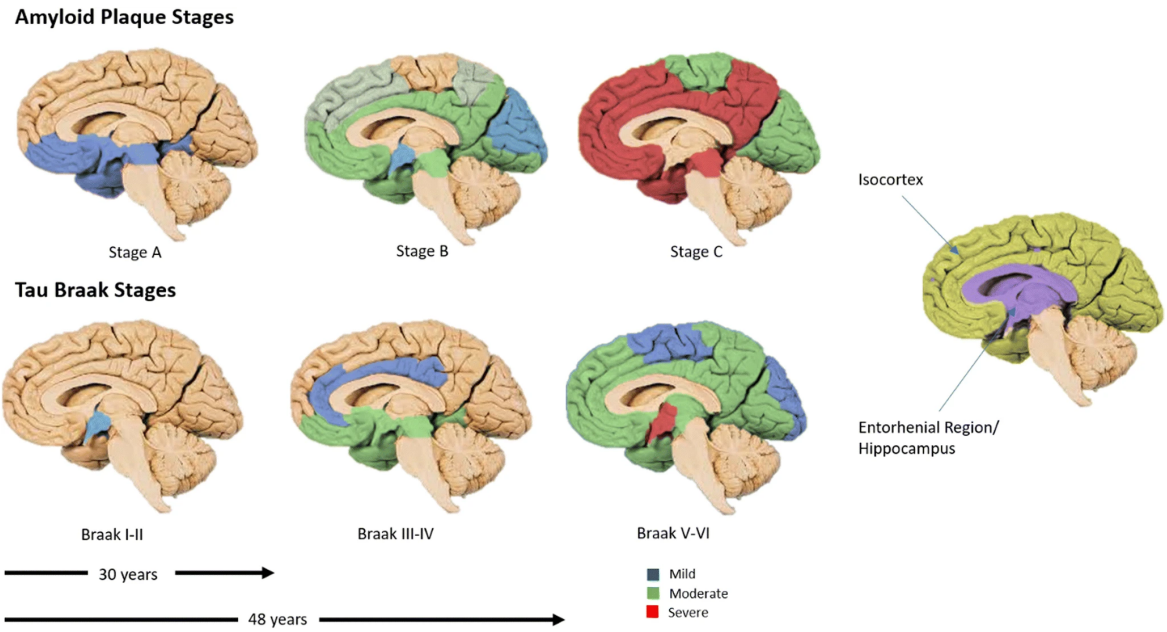

Fig. 1.4 **Braak staging of AD.** Visual schematic of the Braak stages of AD, both in terms of tau NFT formation and amyloid-β plaque deposition. *Reproduced with permission from [81]*

The mechanisms by which amyloid-β and tau are related to disease pathogenesis have been the subject of much debate. While the majority of researchers believe that the aggregation of amyloid-β and tau represent some of the earliest events in the development of AD, there are schools of thought that eliminate the involvement of these peptides as causative agents altogether, suggesting instead that aggregation of these proteins is downstream of another root cause. Here we will review and critically appraise some of the most popular hypotheses surrounding the pathological processes of AD.

The Amyloid Cascade Hypothesis

The Amyloid Cascade Hypothesis (ACH) has been proposed as a way of connecting the most salient features of the disease with a molecular mechanism of toxicity, and has become the ascendant paradigm for AD pathogenesis. The original formulation—first proposed by Hardy and Allsop in 1991, and expounded upon by Hardy and Higgins in 1992—is as follows: "Our hypothesis is that deposition of amyloid-β protein, the main component of the plaques, is the causative agent of Alzheimer's pathology and that the neurofibrillary tangles, cell loss, vascular damage, and dementia follow as a direct result of this deposition" [82, 83]. de Strooper and Karran

(2016) suggest three basic tenets must hold in order for the hypothesis to be true [84]:

1. The parenchymal deposition of the amyloid-β peptide is important pathophysiologically.
2. Amyloid-β peptide deposition occurs prior to the frank neuronal and synaptic loss that is the hallmark of AD.
3. The evidence from mutations that cause familial AD is informative and relevant to sporadic AD.

The phrasing of this formulation of the ACH is important, as it stresses that it is the *deposition* of amyloid-β that results in disease pathology. The ACH, as originally conceived, proposes that the causative agent of AD are those aggregates of amyloid-β that have grown to sufficient size to have crashed out of solution: fibrils and plaques. However, as we reviewed in the last section, modern evidence suggests that it is the lower molecular weight, soluble, oligomeric species—and *not* fibrils—that engender cytotoxicity.

Furthermore, Braak and colleagues found in a large-scale study of human brains that pretangles and NFTs actually appeared prior to amyloid-β plaques [70]. However, it should be noted that there is a good deal of evidence suggesting that amyloid-β expression can modulate tau accumulation and deposition, while tau expression does not seem to have the same effect on amyloid-β [85]. There are also numerous studies finding amyloid-β deposition prior to NFT accumulation [85], though the controversy on this point may be due to differences in visualisation and quantification methods.

In order to bring this nearly three-decade-old hypothesis in line with modern evidence, Selkoe and Hardy have put forward revisions to the sequence of pathogenic events that elicit AD (Fig 1.5) [85]. This revised version of the ACH highlights the importance of amyloid-β oligomers in neurotoxicity, while maintaining that the deposition of amyloid plaques is central to the disease process. Specifically, amyloid plaques may shed oligomers and, more importantly, amyloid plaque formation may recruit a number of inflammatory responses that disrupt cellular homeostasis and lead to the alterations in kinase and phosphatase activities that ultimately spur on the formation of NFTs. This would resolve at least some of the issues with establishing causation between amyloid-β deposition and the disease process.

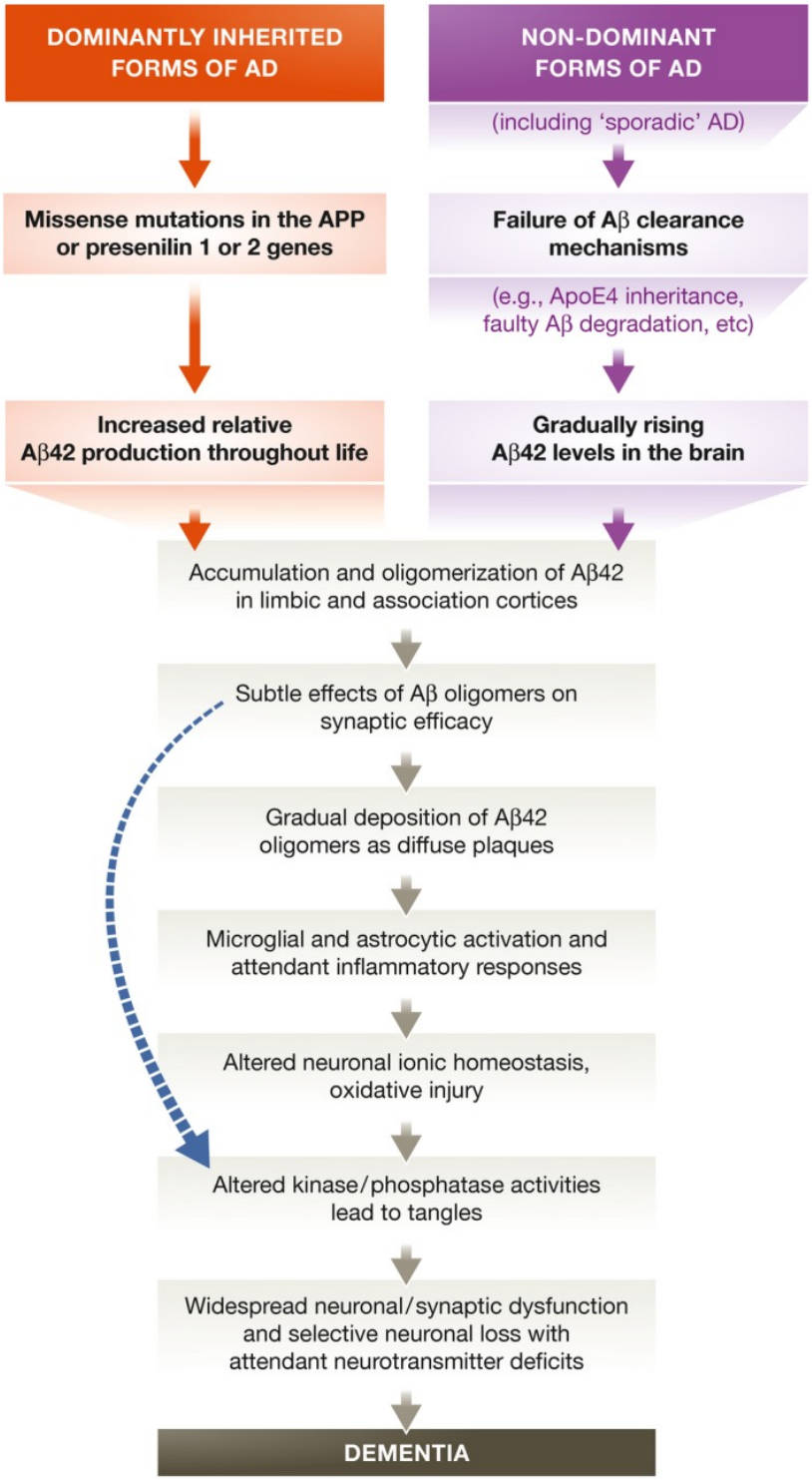

Fig. 1.5 **Schematic of revised ACH.** The modernised revision of the ACH takes into account oligomerisation as a driving force of toxicity in AD. It also articulates the downstream effects in greater detail, including neuroinflammation brought on by amyloid deposition leading to the production of tau NFTs. *Reproduced with permission from [85]*

While it may be the case that amyloid-β deposition is indeed important to the disease process, the contentiousness of this point may also be a matter of definitions. Amyloid-β plaques help define the disorder, but this is primarily because these are features of the disease that (1) distinguish it from other dementias and (2) are relatively easy to visualise, giving them diagnostic utility. Given that amyloid-β oligomers are now believed to be the toxic species, it is unfortunate that neither oligomer concentration in the blood nor in the cerebrospinal fluid correlates well with disease progression [86]. Our reliance on amyloid-β plaques and tau NFTs for diagnostics may merely be products of our time, and new technologies and insights into the earliest disease processes—those that probably have no visible physical features—may improve such that we define AD in terms of features other than plaques and NFTs.

Despite the advances in our knowledge of the genetics and molecular mechanisms of AD over the last 30 years, we are no closer to a successful treatment, let alone a cure. Some have blamed this lack of therapeutic progress on a dogmatic adherence to the ACH, while others merely suggest peripheral mechanisms of toxicity that may act in parallel to the cascade. As a result, many scientists have begun pursuing lines of research that do not fit neatly into the model the ACH puts forth. The following sections are a brief review of a selection of these hypotheses.

The Presenilin Hypothesis

As discussed previously, mutations in *PSEN1* and *PSEN2* are associated with amyloid-β accumulation and onset of AD through their relationships with the γ-secretase complex [69]. However, it should be noted that the γ-secretase complex has fairly promiscuous proteolytic activity, cleaving substrates with fairly different sequences, and is involved in the Notch signalling pathway [73, 87]. Therefore, it has been theorised that at least some, if not all, of the cytotoxicity associated with the *PSEN1* and *PSEN2* mutations in fAD are associated with changes in the proteolytic activity of γ-secretase that are unrelated to amyloid-β [73]. Defects in presenilin activity could interfere with Notch signalling and directly induce apoptosis. This seems unlikely, however, as sAD is not associated with defects in presenilin yet produces nearly the same phenotype, suggesting that both diseases are likely linked to the accumulation of amyloid-β. As a result, this line of reasoning ought to be dismissed as it is not sufficiently conservative. Kelleher and colleagues attempted to resolve these problems with the Presenilin Hypothesis by suggesting that amyloid-β could act as a competitive inhibitor for γ-secretase [88], but there is no direct evidence that

this is the case. While non-amyloidogenic defects in presenilins may play a role in the pathogenesis of fAD and sAD, these roles must be minor, if they exist at all.

The Neuroinflammation Hypothesis

Another line of AD research suggests that the worst of the effects are associated with neuroinflammation [73, 89]. The *ApoE4* allele of ApoE—which we alluded to earlier as a significant risk factor for sAD—is linked to the ACH through its involvement in amyloid-β clearance [6]. The theory is that when ApoE is defective, amyloid-β can aggregate and accumulate [6, 85]. However, ApoE has a number of other roles, including a connection to innate immunity. For example, ApoE suppresses the secretion of TNF-α, a pro-inflammatory cytokine, from macrophages [73]. Loss of ApoE, then, results in an increase in the inflammatory response. Under the Neuroinflammation Hypothesis, it is the loss of ApoE—among other inflammation-related factors—that results in the disease state. Proponents of this theory point to studies in which treatment of various models of neurodegenerative disease with a mimetic of the receptor-binding domain of ApoE (the portion thought to mediate the immune response) has alleviated symptoms of these diseases [90, 91]. AD models treated with this mimetic have also shown reduced amyloid-β and tau deposition [92].

There are number of issues with this hypothesis. First and most obviously, if the Neuroinflammation Hypothesis were true, any event that causes neuroinflammation, such as a stroke, should produce AD-like symptoms. Since this is not the case, there must be other factors at play. Given the pronounced deposition of amyloid-β and tau, Occam's razor tells us that they must be involved at least to some extent. Neuroinflammation clearly plays a role in AD, and those who subscribe to the ACH believe that it partially drives the changes to the cellular environment that result in tau phosphorylation and NFT formation [85]. If neuroinflammation is responsible for some of the toxicity associated with the disease, it makes sense that a reduction of that toxicity would alleviate symptoms. But this effect is not dependent on whether neuroinflammation plays a causative or downstream role.

The Calcium Hypothesis

The Calcium Hypothesis of AD is in many ways a fork of the ACH. The idea, in broad strokes, is that amyloid-β oligomerisation causes changes in cellular calcium homeostasis that directly lead to widespread synaptic loss (**Fig 1.6**) [93]. The key

difference between this and the traditional view of the ACH is that the ACH has a number of mechanistic steps—some of them including tau—that lie between amyloid-β accumulation and pervasive neuronal and synaptic loss.

There is good evidence for this hypothesis. For example, amyloid-β oligomers may act as calcium channels, increasing the amount of Ca^{2+} that accumulates in the cell [93, 85, 54, 53]. Amyloid-β oligomers may also act as substrates for NMDA receptors, enhancing Ca^{2+} entry via receptor-operated ion channels. Moreover, release of AICD may further remodel the calcium signalling system by upregulating the ryanodine receptor and downregulating calbindin through AICD's role as a transcription factor [72]. There is also evidence that interference in the activity of the presenilins results in profound changes in stores of intracellular Ca^{2+} [94, 95].

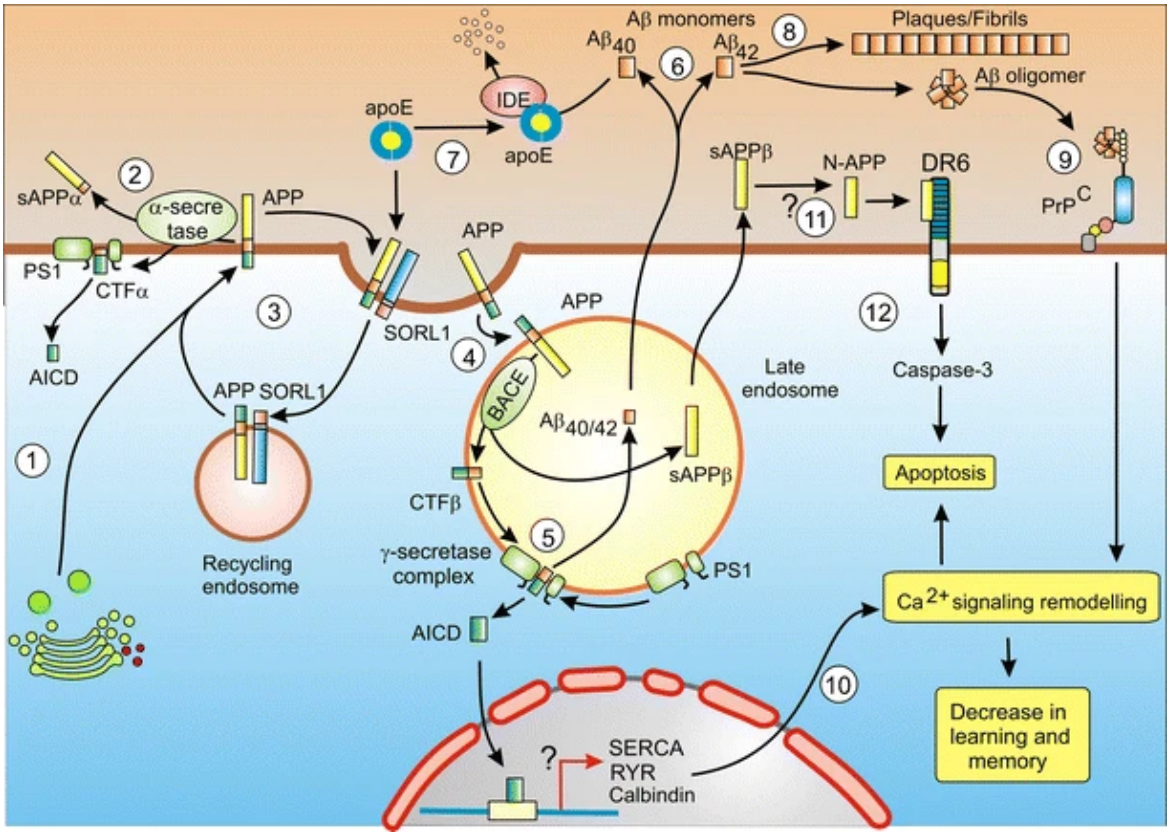

Fig. 1.6 **Calcium Hypothesis of AD.** Under the Calcium Hypothesis of AD, amyloid-β oligomerisation results in remodeling of calcium homeostasis in the cells of the central nervous system, leading directly to cellular dysfunction and apoptosis. *Reproduced with permission from [93]*

There is significant evidence that this kind of gross remodeling of calcium signalling and homeostasis can result in loss of synaptic plasticity and, ultimately, cell

death [93, 95]. Mechanistically, this matches well with disease phenotype: changes in synaptic physiology leads to memory loss in the early stages of the disease, and cell death becomes widespread in the later stages.

However, these mechanisms of toxicity can be true without necessarily rejecting the ACH. They just add to the long list of possible gains-of-function of amyloid-β oligomers. So while it is possible that the toxicity of amyloid-β is mediated exclusively though disruption of calcium homeostasis, it is at least equally likely (if not more so) that these mechanisms represent a part of the cascade.

1.3.2 Network-Wide Perturbations: An Integrative Solution

Up to this point, we have reviewed and assessed the validity of the ACH and several other alternative or peripheral hypotheses of AD pathogenesis. While it may seem that we have dismissed these alternative hypotheses in favour of the ACH, this is not quite true. The ACH clearly serves as a useful framework for studying AD, but the criticisms these hypotheses raise are largely valid. And it remains an inconvenient truth for proponents of the ACH that the numerous clinical trials of drugs designed exclusively on the basis of this hypothesis have failed.

The defining feature of the ACH is the contention that amyloid-β is the causative agent of the disease. Under the ACH, it is amyloid-β that sets off the cascade and is therefore considered the cause of the disease. Consequently, many of the clinical trials we have undertaken so far have focused on reducing the amount of APP that is cleaved into toxic forms of amyloid-β. But perhaps it would be more useful to reframe our understanding AD around the insults that set the stage for improper APP cleavage and amyloid-β accumulation. In the case of fAD, the causes are fairly clear: mutations in *PSEN1*, *PSEN2*, and *APP* lead to amyloid-β production and accumulation that directly result in a cascade that ends with widespread dysfunction. But without a clear genetic basis, this case is harder to make for sAD. While the aggregation of amyloid-β may be the proximate cause of the cascade in sAD, it is not clear why it accumulates and causes synaptic dysfunction and neuronal loss in some people and not others. If amyloid-β is the bullet, tearing its way through the central nervous system and leaving a trail of cytotoxicity in its wake, the question is: what loads the gun?

In the study of cancer, finding gene signatures has been a successful method of developing novel therapeutic strategies [96–98]. Mutations in different genes can cause failure to exit the cell cycle in the same groups of cells, meaning that different insults can bring about the same type of cancer. With the many peripheral

processes that are related to disease pathogenesis, it seems likely that AD may be caused by disruptions in the protein homeostasis network that regulates any number of processes—for example, calcium signalling, mTOR signalling, synaptic vesicle cycling, or protein degradation pathways—that then lead to either increased production of amyloid-β or an inability for cells to deal with the amyloid-β that has begun to accumulate within them. Neurons in the central nervous system are post-mitotic [99], meaning they must maintain integrity of DNA over a lifetime. Over the decades of a natural life, at least some mutations will occur. Most of these are innocuous, but, together, these seemingly small insults could give rise to network-wide perturbations in protein homeostasis. Though different people will accrue different collections of these mutations over a lifetime, the end result is still amyloid-β aggregation that initiates a cascade resulting in the phenotype we recognise as AD.

Using this framework, we may refine our approach to the study of AD. The gene signature of AD, then, is the collection of genes whose dysregulation results in sufficient imbalance of protein homeostasis that toxic amyloid-β oligomers may accumulate. As our understanding of this gene signature improves, we may be able to successfully recapitulate sAD in animal models. Once our models improve, drugs tested in these models will more reliably serve as interventions for the real disease. The development of novel therapies may also be hastened by a new collection of druggable targets. Furthermore, establishing a gene signature may help us find reliable biomarkers for sAD prior to the onset of symptoms, ensuring interventions are delivered before the worst of the cognitive decline sets in.

The focus of the work presented in this dissertation is chiefly on the improvement of animal models for sAD. I believe that our work in *Caenorhabditis elegans* detailed in Chapters 4 and 5 represents a small but meaningful contribution to that goal. I am hopeful that by placing network-wide perturbations in protein homeostasis at the start of AD pathogenesis, better models, better diagnostics, and better drugs may follow.

Progress depends on the interplay of techniques, discoveries, and new ideas, probably in that order of decreasing importance.

Sydney Brenner, *Biology in the 1980s* (1980)

I've got science for every occasion. Postulating theorems, formulating equations.

Beastie Boys, *The Sounds of Science* (1989)

2

Network-based Transcriptome-wide Association Studies

The work presented in this chapter is based on the unpublished findings of Dr Andrea Possenti.

2.1 Précis

An important step toward greater understanding of AD is the establishment of a gene signature. As we noted in Chapter 1, gene signatures can aid our search for druggable targets and novel diagnostic methods. Necessary to both of these goals is the production of reliable animal models, which are currently poorly suited to the study of sAD. However, given the human-centric nature of the disease, any pursuit of a gene signature must be grounded in patient-derived data. To this end, Dr Andrea Possenti—then a doctoral candidate in our group—devised a computational method to accomplish this task. The method, Network-based Transcriptome-wide Association Studies (nTWAS), leverages information we already have about the progression of the disease to extract a list of genes associated with the progression of AD. Using Braak staging as a guide, nTWAS examines those genes that are associated

with those that have either a positive or negative expression gradient over successive stages of the disease. In this chapter, we will review the nTWAS method and the gene list it provides. This gene list serves as the starting point for the research presented in Chapter 4 of this work.

2.2 The nTWAS Method

Among the most common methods of investigating the genetic aetiologies of human disease is the Genome-Wide Association Study (GWAS). The underlying principle behind GWAS is simple: assuming a disease has a genetic basis, patients suffering from that disease are likely to share single-nucleotide polymorphisms (SNPs) that healthy individuals do not. First used to determine a genetic basis for susceptibility to myocardial infarction [100], GWAS has since been adapted for the study of a wide range of diseases, including major depressive disorder [101], schizophrenia [102], anorexia nervosa [103], and AD [104]. Although GWAS has conferred us with new insights into the genetic origins of disease, it is not without significant limitations [105]. The search space of a GWAS is massive: typically, the entire human genome. Correction for multiple hypothesis testing therefore vastly reduces the statistical power of the study. As a result, GWAS is not able to identify all genes related to the disease being studied. Furthermore, SNPs identified in GWAS often appear in non-coding DNA [106], a result that can be difficult to interpret. Even those SNPs that appear in coding sequences pose potential problems for further investigation, as GWAS is frequently unable to uncover the gene-gene interactions that account for much of the heritability of complex traits [107].

To avoid some of these problems, nTWAS takes a different tack. nTWAS was developed to identify a gene signature for AD, and it intentionally leverages what we already know about the disease to improve its performance. Braak staging of AD gives us critical spatiotemporal information on the progression of the disease [80], and nTWAS operates by identifying hub genes whose expression level either trends up or down across successive Braak stages. It then identifies those genes whose expression varies with these hub genes. The advantages of such an approach exceed simply considering extant knowledge of AD. By analysing gene expression rather than whole-genome sequences, the search space is reduced from 3 billion base pairs to something on the order of 25,000 genes——dramatically increasing the statistical power of the study. And because nTWAS specifically analyses co-expression with hub genes, it may capture some crucial information on gene-gene interactions. A

complete list of the human genes produced by nTWAS arranged by KEGG pathway can be found in Table 2.1.

The fundamental assumptions of nTWAS are that (1) Braak regions (that is, regions of the brain that are involved in any of the 6 Braak stages) are more vulnerable to AD than non-Braak regions and (2) brain regions involved in earlier Braak stages are more vulnerable to AD than those involved in later ones. On this premise and using microarray data from the Allen Brain Atlas, nTWAS seeks to uncover a more complete gene signature than traditional methods.

The first step of nTWAS is to establish a Guide Gene Set (GGS), a set of genes associated with AD progression. The GGS was obtained through an analysis of microarray data from healthy (non-AD) brains. Specifically, a Vulnerability Score (V_g) was calculated for all genes. V_g is itself an amalgam of two metrics: the δ-score and the gradient of δ-scores across Braak regions. The δ score of a gene is calculated by taking the difference between the average expression of that gene in Braak regions and non-Braak regions. The second metric, the gradient, is given by determining the trend of δ-scores across the 6 Braak regions. Because the number of tissues from the Allen Brain Atlas that map to each Braak stage varies greatly, there is a problem of heteroskedasticity. To solve this, the average value associated with each stage was weighted by its standard error. V_g is then given by the product of δ-scores in Braak I regions and the additive inverse of the gradient. As a result, high V_g indicates that a gene is either highly expressed in Braak I and has successively lower expression over Braak stages or poorly expressed and has successively higher expression over Braak stages (Fig). The GGS was then defined as those genes whose V_g was in the top 5% of all genes. This gene list was then validated by mapping them onto pathways from the Kyoto Encyclopedia of Genes and Genomes (KEGG pathways) using NCBI's DAVID [108, 109]. The results demonstrate that these genes are over-represented in the biochemical pathways that are commonly associated with neurodegenerative diseases [110, 111]. This suggests that V_g is able to capture the relationship between the histopathology of AD and its molecular underpinnings.

Next, the GGS was used to find more genes that might be associated with AD. Accordingly, the GGS was used in a differential co-expression analysis comparing healthy and diseased tissues, which is the heart of the nTWAS method. The principle of nTWAS is to find network motifs: closed structures of genes co-expressed with members of the GGS. Although motifs are usually defined as directed and recurrent functional relationships among a group of genes [112, 113], relationships in co-expression networks are undirected by definition. Consequently, any fully-

connected group of 3 genes in the co-expression matrix was considered a motif. This strategy is well-evidenced, given local structures and co-expression networks have previously been found to reveal cellular functions and molecular mechanisms of disease in a host of animal models [114–116]. A denoising step was then applied to the correlation matrix [117], both to increase the signal-to-noise ratio and prune weak connections among genes in the network.

With these motifs defined, a method was needed to study the extent of perturbations among the motifs in AD. To this end, two co-expression networks were built: one for non-pathological ageing and another for AD, each consisting of 14,306 gene nodes. The link between each of these genes was quantified as a Pearson's correlation coefficient of the expression levels of each pair of genes. To measure the perturbations occurring in the diseased state, a metric was devised as a function of the clustering coefficient of each gene within the motif and the weight associated with each edge connecting the genes within the motif. By analysing the differences in this metric between the two networks (non-pathological ageing and AD), the perturbations occurring upon disease could be quantified. After analysing the connectivity of the perturbation network, 878 hub genes were identified as being co-expressed with the GGS and significantly perturbed. This list was then filtered by mapping these genes to KEGG pathways using DAVID and extracting only those genes that were associated with pathways that are over-represented in the set. The genes on this list were considered candidate members of the AD gene signature (**Table 2.1**).

2.3 The AD Gene List

The AD Gene List generated by nTWAS (Table 2.1) is divided into the 9 KEGG pathways that were over-represented in the dataset. Namely, these pathways are: synaptic vesicle cycle (hsa04721), long-term potentiation (hsa04720), dopaminergic synapse (hsa04728), mTOR signalling (hsa04150), ubiquitin-mediated proteolysis (hsa04120), glutamatergic synapse(hsa04724), cholinergic synapse (hsa04725), insulin signalling (hsa04910), and neuroactive ligand-receptor interaction (hsa04080).

The fact that the above selection of KEGG pathways were found to be enriched amongs our AD-associated genes is unsurprising. Some, like ubiquitin-mediated proteolysis, have fairly obvious connections to AD pathogenesis. If clearance of misfolded or aggregated proteins is impaired, the disease can be allowed to progress

KEGG Pathway	Gene names
Synaptic vesicle cycle	VAMP2, ATP6V0D1, UNC13C, STX1A, RAB3A, CPLX1, SYT1, RIMS1, STX1B, DNM1, CLTC, NSF, ATP6V0A1, ATP6V1C1, ATP6V0C, ATP6V1A
Long-term potentiation	PPP1R1A, **PPP3R1**, ARAF, **CAMK2A**, **CAMK2B**, **ITPR1**, **RPS6KA3**, GRIA1, ATF4, RAP1A, **MAPK1**, **MAPK3**, **ADCY1**, **BRAF**, PRKACA, **PRKCB**, GRIN2A, CALM1, CREBBP, RAF1, **CAMK4**
Dopaminergic synapse	KCNJ9, **KCNJ3**, **CAMK2A**, **CAMK2B**, **CAMK2G**, **ITPR1**, SCN1A, **PRKACB**, GSK3A, **MAPK9**, **GSK3B**, **MAPK8**, **MAPK10**, MAPK13, **GNG3**, **CALM3**, KIF5A, KIF5C, **DRD1**, **AKT3**, **GRIA3**, **GNB5**, **GRIN2B**, **PRKCB**
mTOR signalling pathways	AKT1, EIF4B, RPS6KB1, RPS6KB2, RRAGA, **RPS6KA3**, PIK3CA, MLST8, **PIK3CB**, PTEN, **MAPK1**, **MAPK3**, TSC1, **PIK3R1**, RRAGD, **AKT3**, **BRAF**, ULK3, PIK3R2, RPTOR, IKBKB, EIF4E2, AKT2, RIC- TOR, **PRKCB**, EIF4E1B
Ubiquitin-mediated proteolysis	TRIM32, SKP1, SKP2, ANAPC4, ANAPC10, ANAPC11, MDM2, UBE2K, WWP2, TRIM37, UBE3A, UBE2I, CUL3, CUL1, UBE2QL1, CDC16, CDC27, BIRC2, MGRN1, FBXW11, UBA1, UBE2D1, UBE2D3, UBE2D2, UBE2E1, UBE2Z, UBE4B, TRAF6, STUB1, HERC4, ANAPC7, ANAPC5
Glutamatergic synapse	**GRM5**, **GRM7**, GLS, GLS2, **KCNJ3**, **ITPR1**, DLGAP1, SLC1A1, **PPP3R1**, **ADCY1**, **GRIA3**, **PRKACB**, DLG4, PPP3CB, **GNB5**, HOMER1, GRK3, **GRIN1**, **PLCB1**, **GNG3**, **GRIN2B**, **PRKCB**
Cholinergic synapse	KCNQ5, **CAMK2B**, **CHRM3**, **KCNJ3**, **ITPR1**, **CAMK2G**, **PIK3CB**, **KRAS**, **AKT3**, **PIK3R1**, **ADCY1**, **PRKACB**, **GNB5**, **PLCB1**, **GNG3**, **CHRNB2**, **CAMK4**, **CAMK2A**, KCNQ3, **PRKCB**
Insulin signalling pathway	PRKCZ, SHC3, **MAPK8**, **PIK3CB**, **KRAS**, PRKAB2, AKT3M, PIK3R1M, **PRKACB**, PRKAR1B, **MAPK9**, **GSK3B**, **MAPK10**, PDPK1, **CALM3**, PRKAR2B
Neuroactive ligand-receptor interaction	NPY1R, **GRM5**, **GRM7**, **CHRM3**, CCKBR, MTNR1A, HTR5A, GLRA3, RXFP1, **DRD1**, OPRM1, **GRIA3**, NPY5R, HTR1F, GABRA3, HTR1E, GABRA4, THRB, GABRB3, FSHR, GABRB2, **GRIN1**, GABRA1, GABRD, PTH2R, MCHR2, **CHRNB2**, **GRIN2B**, GABBR2, HRH2

Table 2.1 **AD Gene List.** List of the genes in the AD gene list produced by the nTWAS method arranged by KEGG pathway. Genes in bold appear in multiple KEGG pathways.

unhindered. Long-term potentiation, too, has a clear connection to disease phenotype. Among the defining features of dementia is an impairment of learning and memory. The sustained synaptic transmission associated with long-term potentiation is considered to be the molecular basis of both learning and memory. The specific pathways of the dopaminergic synapse, glutamatergic synapse, and cholinergic synapses also recapitulate some of the nuances of the disease that have been revealed in recent years. Impairment in the function of dopaminergic neurons has been repeatedly been shown to be associated with Parkinson's disease [118–124], a related neurodegenerative protein misfolding disorder, and impediments to synaptic plasticity and dendritic loss of glutamatergic neurons are amongst the earliest events in the pathogenesis of AD [125]. Cholinergic neurons are involved in cognition [126, 127], and their association with AD has been formalised in the Cholinergic Hypothesis of AD [128–131]. Acetylcholinesterase inhibitors have been proposed as potential treatments for AD [132–135]. Although treatment with these drugs has not slowed down disease progression, cognition and memory have been improved among dementia patients by treatment with these drugs [136]. Other pathways have less obvious connections. Insulin-signalling may on the surface appear to be unrelated to AD, but insulin dysregulation has long been implicated in the disease [137–140]. The characteristic insulin resistance in the central nervous system amongst sufferers of AD has even lead some researchers, perhaps somewhat irreverently, to refer to AD as "Type III Diabetes" [137].

Although the nTWAS method is robust, it still requires experimental validation. The first iteration of this process, an RNA interference screen in *C. elegans* is presented in Chapter 5.

All models are approximations. Essentially, all models are wrong, but some are useful.

George E.P. Box,
Empirical Model-Building and Response Surfaces (1987)

Wiggle, wiggle, wiggle.

Snoop Dogg, *Wiggle* (2014)

3

Caenorhabditis elegans as a model organism

3.1 Précis

The nematode worm *Caenorhabditis elegans* has been a mainstay of biological and biochemical research for the last fifty years. Although its use as a model system was popularized by Sydney Brenner and colleagues in the 1960s, *C. elegans* and other nematodes have been critical to the advancement of scientific knowledge since the late 19th century. In the last few decades, *C. elegans* has been used to advance molecular and neurobiology. And in the course of conducting these experiments, we have come to understand the worm in incredible detail.

C. elegans was the first multiceullular organism to have its whole genome sequenced and remains, to date, the only animal for which a complete neural connectome has been made. The annotation of the *C. elegans* genome is of unparalleled detail, lowering the difficulty of genetic studies. And the relative ease and low expense of culture, small size, short generation time, and relative simplicity among multicellular organisms have made it a strong model for many biological and biochemical studies.

3.2 A brief history of *C. elegans* research

The earliest experiments done on nematodes were conducted with parasitic nematodes isolate from livestock or humans [141, 142]. In fact, in the period spanning 1880-1910, one such nematode, *Ascaris*, was used as perhaps the first model organism [142]. Edouard van Beneden, for example, used *Ascaris* in his discovery of the basic facts of meiosis. Somewhat presciently, in 1883, van Beneden remarked that in *Ascaris* he found "a wonderful material. I am convinced that the egg of this nematode will soon become a classical object of study to investigate and illustrate the phenomena connected with fecundation" [142, 143]. Parasitic nematodes continued to be used in research of development for many years, in no small part due to the fact that individual stages of the life cycle of these worms localised to particular regions of the host, allowing for study of relatively large populations of worms at particular developmental stages [142, 144].

This advantage, however, proved to be problematic in the long-term. As obligate parasites, culture of these worms required extraction from a host, reducing the number of environmental controls one could reasonably employ [142]. As a result, a small number of scientists began working with the free-living nematodes, which largely inhabit soil. The first to isolate and characterise *C. elegans* was a librarian and biology hobbyist named Émile Maupas, who did so with the explicit intent of using it as a model for reproduction and development [145]. In his publications in 1899 and 1900, Maupas was the first to describe the molts of *C. elegans*—including the dauer larval stage—and its modes of reproduction [145, 146]. In the next two decades, several more researchers, including Paula Hertwig, Karl Bělař, Hikokura Honda, and Eva Kruger, would build on the knowledge base laid by Maupas to give us greater understanding of the life cycle of rhabditid worms [142, 147–151].

The next great innovations in *C. elegans* research came with the standardisation of culturing conditions. Although Haven Metcalf was the first to use solid agar (rather than liquid) as the culturing medium for *C. elegans* [152], the culturing conditions were not yet strictly controlled. This changed when Victor Nigon, then a student at the Faculté des Sciences in Toulouse, was sent home during the second World War [153]. His supervisor, Albert Vandel, being somewhat familiar with the work of Maupas and others—and sharing some of the same proclivities as many senior scientists—suggested that Nigon search for free-living nematodes in his garden and conduct experiments at home. From the soil samples in his garden, Nigon was able to isolate *C. elegans* and, using only a rudimentary microscope and a scalpel, set up

cultures and crosses from single worms [153]. After the war, Nigon teamed up with the American physician scientist Ellsworth Dougherty, who until that point had only worked with parasitic nematode species, to develop culturing protocols to make *C. elegans* experiments sufficiently reproducible for their work on metabolism and nutrition [154–156]. Many of these same protocols have survived largely untouched into the modern day, including methods for both solid and liquid culture, although current methods have converged on a standardised medium: Nematode Growth Medium (NGM) [142].

In the 1960s, Sydney Brenner began a search for new scientific frontiers. Having just elucidated much of the central dogma of molecular biology, Brenner felt that "most of molecular biology had become inevitable" [157]. Instead, he turned his eyes toward development and neurobiology, which he referred to s the "future of molecular biology" [158]. His first quest was to find an appropriate model organism for his goals. It had to be easily grown, have a short life cycle, have relatively few neurons (such that knowledge of its neurological system could be come complete), and fit in the viewing window of an electron microscope [159]. After literally going through a zoology textbook organism by organism, Brenner came across the free-living nematodes [159]. In 1963, he received worm samples and protocols from Dougherty and drafted his one-page proposal to the Medical Research Council [142]. The famously ambitious goals laid out within that proposal would be considered arrogant from anyone other than Brenner: "To start with we propose to identify every cell in the worm and trace lineages. We shall also investigate the constancy of development and study its control by looking for mutants" [157]. By 1986, Brenner and his team had completed the first connectome of the worm [160], and by 1997 the entire genome of *C. elegans* was sequenced [161]. The rest, as they say, is history.

3.3 Life Cycle

This section as well as those covering anatomy and genetics have been adapted from WormBook except where indicated otherwise [162, 163]

As is the case with many other nematodes, the life cycle of *C. elegans* is comprised of an embryonic stage, four larval stages, and adulthood. Larval stages are separated by moults, characterised by the shedding of the outer cuticle and a temporary ceasing of pharyngeal pumping—the mechanism by which *C. elegans* consumes food.

Worms tend to live between 2 and 3 weeks, although that can be extended or shortened based on genetics or culturing conditions. Worms begin laying eggs on the first day of adulthood. The larval stages are named in the order in which they occur: L1, L2, L3, and L4. The length of each of these stages is dependent on the temperature at which the worm is raised, with higher temperatures resulting in faster development. Each stage typically lasts between 8 and 14 hours within the normal range of experimental culturing temperatures (16-25°C). In cases of starvation, overcrowding, or extreme temperatures, *C. elegans* L1 and L2 larvae can enter an alternative developmental mode called the dauer stage (borrowed from the German "dauer," meaning "duration"). The dauer stage is characterise by a thickened cuticle and is generally much hardier, allowing the worm to survive in a kind of stasis for up to 4 months. Entry into the dauer stage is regulated by the daf-2/insulin-like pathway and the daf-7/TGF-β pathway. A summary of the life cycle of the worm at 22°C can be found in **Fig 3.1**.

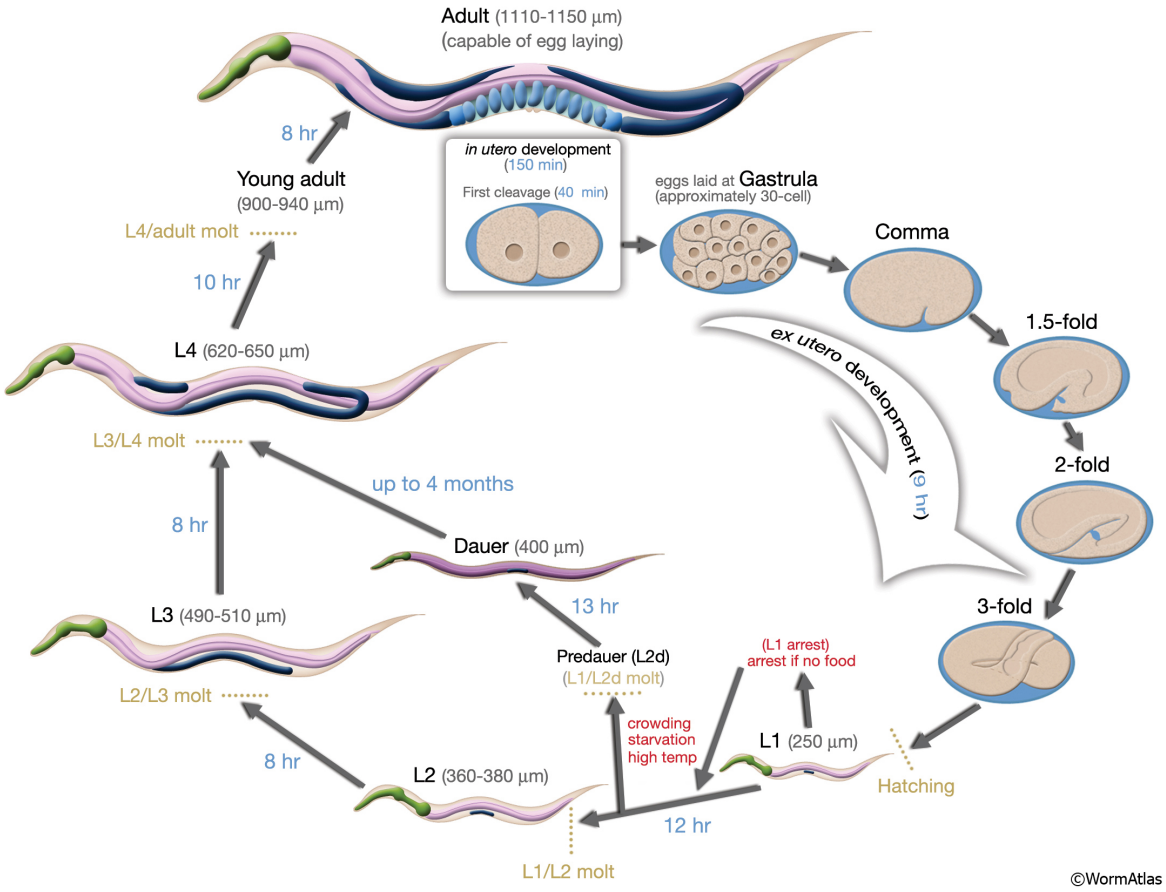

Fig. 3.1 **Developmental stages of *C. elegans* at 22°C.** *C. elegans* hatch from eggs and proceed through four larval stages (L1, L2, L3, and L4) before reaching adulthood. Starvation or environmental stressors may induce entry into the dauer larval stage, characterised by fat accumulation and long life. Although the worm may exit the dauer stage and enter adulthood when environmental stressors are removed, transcriptional changes may persist throughout life. *Figure reproduced with permission from WormAtlas* [164]

3.4 Anatomy

3.4.1 Anatomy of the adult hermaphrodite

The *C. elegans* hermaphrodite is the most common of the two sexes and is capable of self-fertilization. The body itself is cylindrical with tapered ends at the head and tail and is unsegmented and bilaterally symmetrical. The body is roughly 1 mm in length and 80 µm in diameter at its widest point. it has a total of 959 somatic cells, of which 302 are neuronal and 95 are body wall muscles.

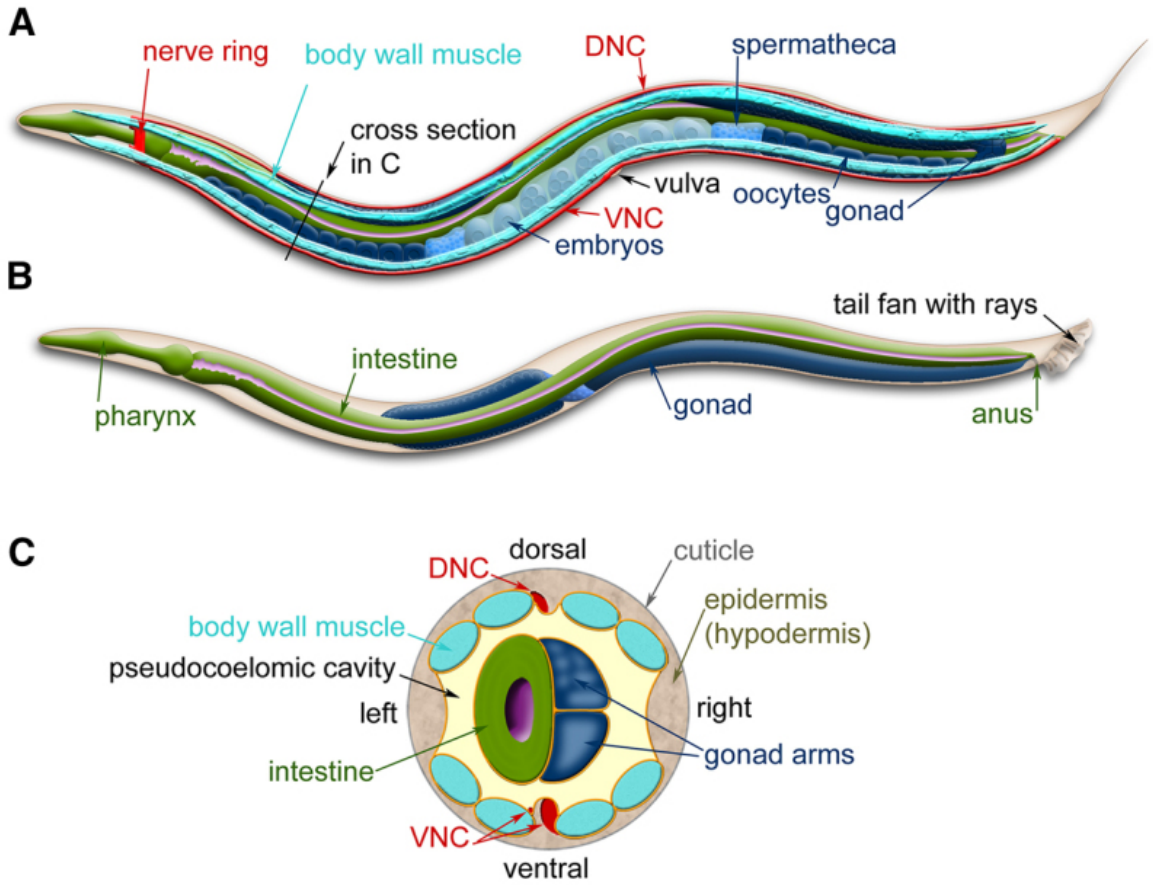

Fig. 3.2 **Anatomy of the *C. elegans* adult hermaphrodite.** (A) The most prominent features of the *C. elegans* anatomy. The major constituents of the nervous system include the nerve ring, dorsal nerve cord (DNC), and ventral nerve cord (VNC). The latter two structures run the length of the worm. (B) Anatomy of the worm highlighting the pharynx and intestine. The intestinal-pharyngeal valve lies just caudal to the pharynx. (C) Cross-section of the worm, detailing the arrangement of the body wall muscles, DNC, VNC, gonad arms, and intestine, among other structures. *Figure reproduced with permission from WormBook [165]*

The head of the worm houses the mouth, pharynx, and nerve ring (**Fig 3.2A**). The nerve ring is the primary neuropil of the worm, and as a result the majority of neurons extend their processes through either the dorsal or ventral nerve cord to the nerve ring. The pharynx is bilobed, and operates largely autonomously, having its own musculature, nervous system, and epithelium. The pharynx pulls nutrition from the environment through the mouth, grinds it, and passes it to the intestinal system via the intestinal-pharyngeal valve (**Fig 3.2B**). The intestine is composed of 20 cells arranged in a tube shape wit ha central lumen. Microvilli protrude from the apical surface of these cells into the lumen to absorb nutrients. Waste products are

passed from the intestine through the intestinal-rectal valve and excreted via the anus/cloaca. Of note is the autofluorescence of the intestine, which fluoresces in the GFP range and may correlate with the health of the worm [166–168].

Abutting the intestine are the two arms (proximal and distal) of the syncytial gonad. These arms are each connected to the uterus through the spermatheca. As germ cells draw closer to the uterus, they enlarge and eventually pinch off from the syncytium to form oocytes. These oocytes, in turn, are fertilized either by sperm in the spermatheca or (less frequently) sperm supplied by a male. The resultant zygotes are then stored in the uterus and laid through the vulva. Blockage or malformation of the vulva results in the "bag of worms" phenotype, wherein fertilized eggs hatch within the mother without being excreted.

The intestines and gonad are surrounded by the pseudocoelomic cavity, immediately outside of which are the body wall muscles (**Fig 3.2C**). the body wall muscles are separated into four quadrants each containing a pair of muscle cells. These muscles are controlled through the neurons that occupy the nerve cords or nerve ring, and each muscle projects arms to motor neurons contained therein.

Surrounding these structures is the hypodermis, formed from concentric rings of syncytial cells. On the lateral sides of the worm, the hypodermis is interrupted by the seam cell syncytium, which shares many features with the hypodermis but also produces the alae, ridge-like structurs of unknown function protruding longitudinally from the worm. The seam cell syncytium is connected to the hypodermis along its apical borders by adherens junctions and along its lateral borders by gap junctions. The hypodermis and seam cells together secrete the cuticle, a thick, collagenous membrane surrounding the entirety of the worm except for openings at the orifices.

3.4.2 Anatomy of the adult male

Adult males are relatively rare, appearing at a rate of only one per thousand worms under normal conditions. While self-fertilized hermaphrodites typically lay 300 eggs over their lifetime, hermaphrodites fertilized by males can lay up to 1400 eggs in the same period. Adult males have a total of 1031 somatic cells, with the extra cells being predominantly neurons involved in male mating behaviours. Despite having more cells than the hermaphrodite, males are typically slightly shorter at just 0.8 mm and are quite slender. To the untrained eye, males can easily be mistaken for L3 or L4 larvae. A comparison of the *C. elegans* female hermaphrodite and male can be found in **Fig 3.3**.

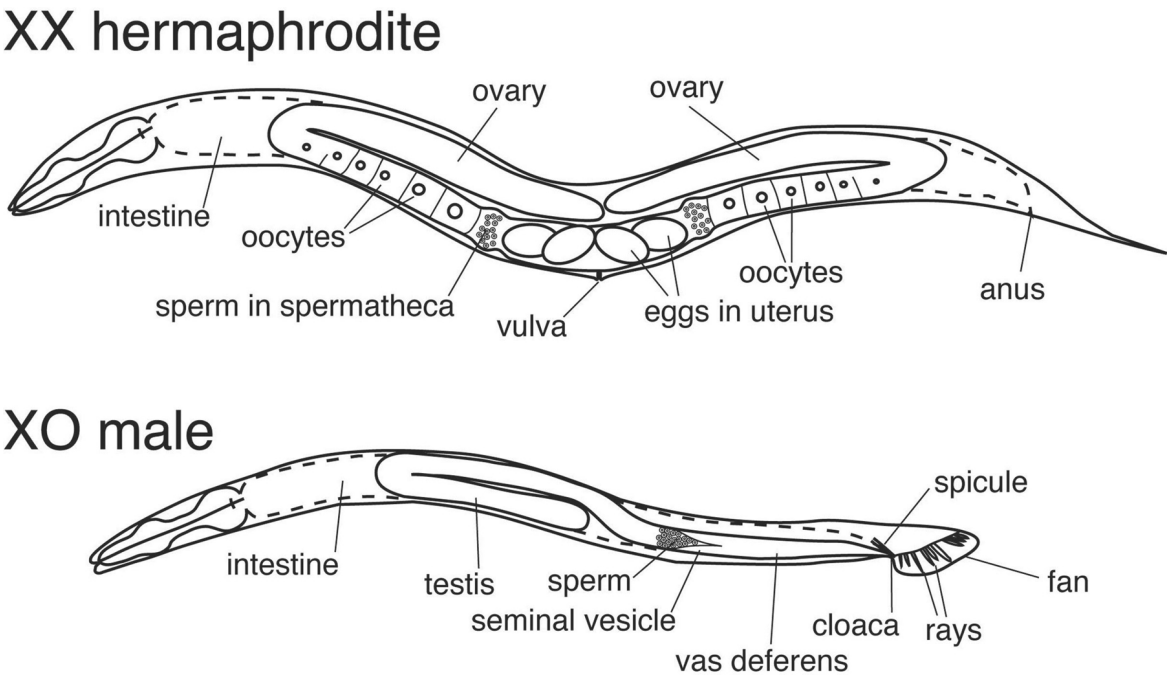

Fig. 3.3 **A comparison of the major anatomical features of the female hermaphrodite and male worm.** As one would expect, the major differences between the two sexes of the worm are in the reproductive system. The tail of the male worm includes the spicule, fan, and rays. The vas deferens connects the seminal vesicle (where sperm are generated) to the cloaca, from whence they are excreted. *Figure reproduced with permission from WormBook [165].*

The major defining feature of the male anatomy is, as one might suspect, the reproductive system. The two major structures of the male reproductive system are the gonad and the copulatory apparatus. The gonad, which produces sperm, runs one-half to two-thirds of the way down the length of the worm and terminates in the tail. The tail houses the copulatory apparatus, including the anus/cloaca, spicules, and sensilla. The tail of male worms is sufficiently distinctive as to distinguish it from larval hermaphrodites, and features a fan containing sensory rays.

3.5 Genetics

The *C. elegans* genome is 100 Mb, spread across five autosomes and one allosome. Hermaphrodites have two X chromosomes while males have only one. The genome of *C. elegans* is unusually information-rich. Protein-coding regions alone make up 25.5% of the *C. elegans* genome, and genes (including introns and other regulatory regions) make up a full 40%. There are an estimated 20,470 *C. elegans* genes, 35%

of which of human orthologs. The completeness of the sequencing of the *C. elegans* genome has made its annotation extremely detailed as well, which, along with the ease of genetic manipulation of the worm, have made it an excellent model for molecular biology and genetics. The most common techniques for genetics research in *C. elegans* can be broadly categorized into forward and reverse genetics.

3.5.1 Forward genetics

Forward genetics research begins with the observation of a phenotype and seeks to find the underlying genetic basis for that phenotype. Typically this is done through mutagenic screens, followed by gene mapping and sequencing.

Much of the early genetics work carried out by Brenner and colleagues consisted of mutagenic screens, and mutagenesis remains a standard part of the *C. elegans* toolkit today. Chemical mutagenesis using ethyl methanesulfonate (EMS) followed by scoring of F2 progeny is the most common and reliable method, but other chemical mutagens (e.g. TMP or ENU) are also used.

When large deletions or complex rearrangements are required at a high frequency, radiation mutagenesis can be employed, although at the cost of an increased mortality rate.

Non-directed insertional mutagenesis with transposons——both endogenous (Tc1) or exogenous (Mos1)——can be used to make mapping and sequencing easier once a phenotype has been identified. Although this method reduces the mortality rate and eases downstream analysis, this method is ten times less mutagenic than EMS and, as a result, requires ten times the worm population to employ.

As is the case with several other model organisms, many *C. elegans* genes are named for the physical features (e.g. *dpy* for dumpy, or *sma* for small) or behavioural phenotypes (e.g. *egl* for egg-laying defect) that arise from mutation of the gene. Many of the most essential *C. elegans* genes are named in this fashion, and gene mutants with strong phenotypes are often used as markers for transgene expression. Quantification of behavioural measures such as body bends per minute, rate of omega turns, and touch sensitivity have, as a result, become mainstays of *C. elegans* genetic research.

3.5.2 Reverse genetics

Reverse genetics, aptly, is conducted in the opposite direction to forward genetics. That is to say, expression of specific genes is abated (usually through knockdowns

or knockouts) and the resultant phenotype is then assessed. The easiest and most common method of accomplishing this is through RNA interference (RNAi).

Although RNAi was first identified in plants in the early 1990s, the mechanism was not elucidated until Craig C. Mello and Andrew Fire published the findings of their experiments on *C. elegans* in 1998 [169]. Together, they described the potent knockdown effects they observed after injecting worms with double-stranded RNAs (dsRNA). Endogenous RNAi pathways exist and are thought to be key epigenetic regulators in *C. elegans* and many other organisms. Notably, the insulin-regulating pathway in *C. elegans* is under epigenetic control by endogenous RNAi mechanisms.

The mechanism of RNAi is fairly straightforward. First, dsRNA encoding a portion of the target gene enters the cell from an exogenous source. This dsRNA is then cleaved by Dicer, a conserved RNase III enzyme [170]. The result of this cleavage are short sequences roughly 21 nucleotides in length called short interfering RNAs (siRNAs) [170]. These siRNAs are then recruited to the RNA-induced silencing complex (RISC). RISC is composed of proteins in the Argonaute family, which bind various classes of non-coding RNAs [170]. Once bound to RISC, the siRNAs are separated into individual strands: the guide strand and the passenger strand. The guide strand, which is antisense to the target mRNA, remains bound to RISC, while the passenger strand is (usually) degraded. RISC, now bound to the guide strand, attaches itself to the target mRNA. Once bound, the target mRNA sequence is degraded on RISC [170, 171]. Depending on the conditions of the knockdown, RNAi can also be heritable by progeny.

One aspect of RNAi that is very helpful to experimentalists is its ability to amplify within target cells [171]. Not only do siRNAs bind RISC and their target, but they can also be recruited by RNA-dependent RNA polymerases (RdRPs). RdRPs use bound siRNAs as guides for synthesis of further double-stranded siRNAs, which can then be bound by RISC and strengthen the knockdown effect.

Practically, RNAi is very easy to administer to *C. elegans*. The process can be done three ways, each with trade-offs. RNAi may be administered by directly injecting dsRNA into the gonad as one would do for transgene expression, and some of the progeny of injected worms will exhibit the knockdown. This method results in the strongest phenotypes, although it is quite time-consuming. Furthermore, inducing a knockdown after larval development is not possible in RNAi by injection, which is sometimes necessary when knockdowns result in embryonic-lethal phenotypes.

RNAi may also be administered by soaking. *C. elegans* worms can be left to soak in a high-concentration dsRNA solution, and they or their progeny can then be

scored for phenotypes. This method is suitable for worm populations in the tens to hundreds, and is less labour intensive than RNAi by injection. RNAi by soaking requires significantly more dsRNA than does RNAi by injection, but can be done on worms of any age.

The least labour-intensive and most cost-effective method of inducing RNAi in *C. elegans* is RNAi by feeding. In this method, bacteria expressing dsRNAs are fed to worms in place of their normal food source. This method produces results that are more variable than either RNAi by soaking or RNAi by injection, but can be rapidly scaled with limited increases in labour.

3.6 Scale and scalability

When Sydney Brenner first began his search for a model organism for neurobiology research, he was well aware that the scale of experiments would be critical to his success [142]. Mutagenic screens require many animals to produce usable results; in a typical EMS screen in *C. elegans* containing 12,000 haploid genomes, one can expect to recover 6 mutations in any particular gene——not dissimilar from mutation rates in other species [172]. In light of this necessity for large populations,*C. elegans*was in part chosen because of its short life cycle and limited need for incubator space [142].

The ability to rapidly scale experiments has continued to be at the heart of *C. elegans* research and is typical of both forward and reverse genetics. Whole genome RNAi screens, for example, are done with relative frequency, and are often run in the 96-well format, saving both time and space. These studies have helped make the *C. elegans* genome among the best annotated, and screens conducted on transgenic backgrounds have even helped to characterize human proteins.

The usual trade-off in large-scale screening is a loss of data resolution. Screens run in the 96-well format in particular suffer from this limitation as each condition only represents a population of a few worms. These issues are compounded by human error when phenotypic scoring is conducted manually.

3.7 The Wide-Field Nematode Tracking Platform

In recent years, several groups have begun attempting more automated versions of these protocols, including automated scoring. Our own Wide-Field Nematode Tracking Platform (WF-NTP)——originally developed for drug screening in *C. elegans*——is capable of scoring hundreds of worms simultaneously, and its adaptation

to RNAi screening is described in greater detail in the Materials and Methods section of Chapter 4 of this work.

The WF-NTP requires a relatively simple set-up. Worms are washed onto thin, agar assay plates in a small amount of buffer. A high-resolution video is taken of the worms thrashing for 60-120 seconds, and the video is then fed into a software package that can extract various health-correlated measurements of worm thrashing behaviour, including body bends per minute and the bend distance (distance bent from the medial axis of the worm). These measures are recorded for each worm in the video.

There are great advantages to using the WF-NTP over traditional methods. Scoring is done automatically, thus eliminating human error. Further, the maximum population of worms that can be simultaneously scored by the computer is quite high—in the hundreds—and is in practice only limited by the number of worms that can be placed in a plate without colliding with one another. Finally, since the analysis is carried out after the videos have been taken, old data may be re-analysed if significant updates have been made to the tracking software.

The subtle are the causes, the gross the effects.

Swami Vivekananda, *Raja Yoga* (1896)

I burned too many brain cells now, to be worried about my brain cells now.

Chance the Rapper, *Brain Cells* (2012)

4

Expression of amyloid-β in a single pair of *C. elegans* neurons

The work presented in this chapter was done in collaboration with Dr Tessa Sinnige, Samuel Casford, and the group of Prof Mario de Bono at the Laboratory for Molecular Biology [173]. Specifically, Dr Sinnige designed the constructs and carried out staining experiments, Mr Casford conducted worm maintenance, and the group of Prof de Bono generously provided equipment and protocols for the CO_2 assays.

4.1 Précis

Although the aggregation of the amyloid-β peptide has been implicated in the aetiology of AD, the precise mechanism by which amyloid-β aggregates perturb neuronal function remains unclear. While *C. elegans* has been used as a model for amyloid-β aggregation *in vivo*, these models tend to overexpress the protein either in the entirety of the musculature or in all neurons. There are, however, two major limitations to these approaches: (1) overexpression of amyloid-β is not typical of the most common variants of AD and (2) tissue-wide expression of amyloid-β peptide

prevents direct interrogation of cellular and subcellular phenomena associated with amyloid-β aggregation.

In order to overcome these limitations and better investigate the early events affecting neuronal signalling, we developed a *C. elegans* strain that expresses a single copy of the 42-residue form of amyloid-β in a single pair of glutamatergic sensory neurons, the BAG neurons, which sense reduced oxygen in the environment. In behavioural assays, we found that our model displayed a subtle modulation of its response to increased CO_2 compared to wild-type controls. Interestingly, Ca^{2+} imaging showed that the BAG neurons in our model were more strongly activated than in controls, and this increased neuronal activation remained intact until old age. Taken together, these results suggest that the low expression level of amyloid-β in our model was sufficient to modulate the behavioural response but insufficient to cause neurotoxicity. It is possible that further perturbations of the cellular environment, in conjunction with low-level expression of amyloid-β, will prove to be valuable tools in elucidating the early events leading to neuronal dysfunction and neurotoxicity in AD.

4.2 Introduction

As previously discussed, protein misfolding and aggregation underlie a large number of neurodegenerative disorders [6, 61, 7, 8], including AD. Tau NFTs and amyloid-β plaques made up of these misfolded and aggregated peptides comprise the two most prominent features of the disease [6, 85]. These large extracellular deposits of protein, however, seem to form relatively late in the progression of AD. Smaller aggregates called oligomers do form in earlier stages of the disease, and there is a significant body of knowledge that indicates that these oligomeric species may be among the most neurotoxic [85]. Unfortunately, there remains much to be understood about the molecular mechanism by which these species disrupt cellular function. And even less is known about the role that amyloid-β aggregates may play in the earliest events of AD, where intervention may one day be possible.

In order to unravel these early molecular events, robust *in vivo* models of AD are necessary. The use of *C. elegans* as a model for neurodegenerative disorders is now commonplace, owing in large part to its ease of use and the completion of its connectome [160]. Amyloid-β models of AD in *C. elegans*, too, are common. Although *C. elegans* does have an APP ortholog in *apl-1*, this gene does not contain the human amyloid-β sequence [174]. Therefore, most *C. elegans* amyloid-β AD models

simply express the human peptide [175, 176]. Current *C. elegans* models of AD are usually lacking in at least one of two regards. The first shortcoming is the frequent overexpression of amyloid-β. Overexpression models are favoured because the high concentrations of amyloid-β they produce lends itself well to aggregation and cytotoxicity. But these extremely high concentrations of amyloid-β do not accurately simulate the sporadic——and the overwhelmingly most common——variant of the disease, where as-yet-unclear events result in the formation of amyloid aggregates from relatively low levels of amyloid-β.

The second limitation of these approaches is the widespread nature of tissue-wide expression. That is, expression of amyloid-β is often put under the control of promoters that are active in an entire tissue (e.g. the unc-54 promoter, which drives expression in the body wall muscles) [176]. This is done partly because tissue-wide promoters tend to be well-characterized and partly because the failure of an entire tissue (due to cytotoxicity and cell death) results in easily-quantifiable behavioural phenotypes. Some models overexpress amyloid-β in the body wall muscles, resulting in deposition of amyloid plaques and progressive paralysis within the first several days of adulthood [176]. Others have opted for pan-neuronal expression, resulting in defects in chemotaxis and learning, as well as shortened lifespan [177]. Unfortunately, not all neurons are created equal, and the death of one may have little impact on the behavioural phenotype while the death of another may have an immediately noticeable impact. Since the death of or aberrant signalling in one neuron may cause disease-relevant changes in others——and because behavioural phenotypes remain an important tool for probing cellular health and function in *C. elegans*–pan-neuronal models may not be able to elucidate the mechanisms of the earliest stages of the disease; namely, those that occur due to misfolding and aggregation of amyloid-β in single neurons in isolation.

In the experiments outlined in this chapter, we sought to create a model that was suited to answer questions about these early events in AD at the single-neuron level. In service of this goal, we expressed a single copy of the 42-residue form of amyloid-β in only two sensory neurons. We felt that it was essential that the neurons chosen were representative of those that are most vulnerable to AD and whose function was linked to some behavioural phenotype for easy assessment. The BAG neurons—a pair of neurons that sense low O_2 levels in the environment—seemed to fit this bill. The BAG neurons are glutamatergic and tonically activated [178], just as the neurons most vulnerable to AD are [179–182]. Further, health of these neurons can be assessed by counting Ω-turns in response to hypoxic conditions [178].

Ω-turns, as the name suggests, are locomotory movements in which the head and tail of the animal are brought close together in roughly the shape of the Greek letter omega. These turns represents one of two mechanisms for worms to change direction while moving on solid media—the other being reversals, during which the animal backs up and resumes movement in a new direction. In chemotaxis assays, the number of Ω-turns can be used to quantify the strength avoidance behaviours, as worms will change direction more often when attempting to avoid unpleasant stimuli [178]. If the BAG neurons cease to function, then one can expect avoidance of hypoxia to diminish and the number of Ω-turns to diminish along with it.

The ability of the BAG neurons to sense low oxygen is mediated by the soluble guanylate cyclases *gcy-31* and *gcy-33* [183, 184]. Both of these enzymes are activated by O_2 downshifts. Activation of these enzymes results in the synthesis of cGMP from GRP, in turn opening TAX-2/TAX-4 cGMP-gated ion channels and stimulating the neuron [185, 186].

4.3 Results and Discussion

4.3.1 A *C. elegans* model expressing amyloid-β in th pair of BAG neurons (BAG-Aβ worms)

In order to develop our model, we first designed a construct encoding the 42-residue human amyloid-β (codon-optimized for *C. elegans* and targeted it to the secretory pathway with a signal peptide, which results in the 42-residue amyloid-β peptide after the signal has been cleaved. One common issue with the expression of amyloid-β in *C. elegans* is the accidental expression of amyloid-$\beta_{3\text{-}42}$ due to miscleavage——highly problematic because amyloid-$\beta_{3\text{-}42}$ has been shown to have different biophysical properties than amyloid-$\beta_{1\text{-}42}$ *in vitro*. To avoid this issue, two additional amino acids were inserted between the signal peptide sequence and the amyloid-β sequence, a strategy that has been successfully employed in other laboratories to develop overexpression lines [175]. Expression of amyloid-β was driven by the flp-17 promoter, and induced robust expression exclusively in the BAG neurons. Due to its small size at just 42 residues, the amyloid-β peptide could not be linked with a fluorescent tag as an expression marker without compromising its biophysical properties. Instead, we included mCherry after an SL2 trans-splice site, resulting in an operon that co-expressed cytoplasmic mCherry. To ensure that the line reproducibly expressed low

levels of amyloid-β, Mos1 single-copy insertion was used to integrate our construct into the genome (**Fig 4.1A**) [187].

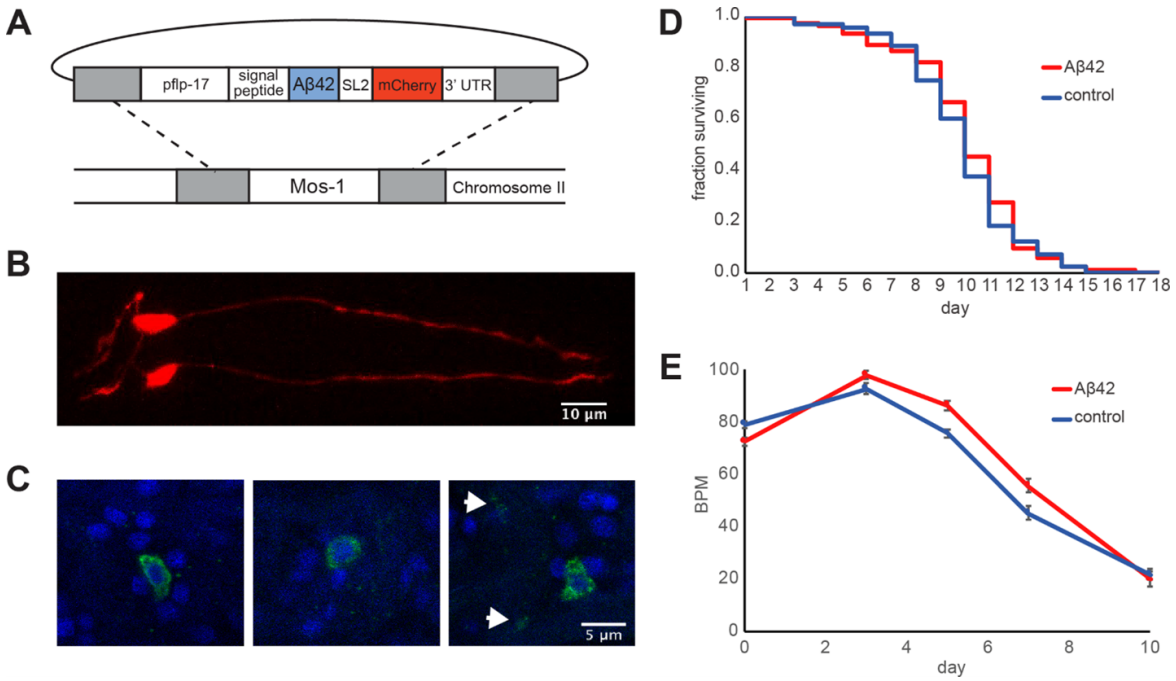

Fig. 4.1 **Construction of a *C. elegans* model that expresses Aβ42 in the two BAG neurons.** (A) Design of the construct for Mos1 insertion. (B) Confocal image of the Aβ42 strain showing mCherry expression in the BAG neurons. (C) Staining with the 4G8 anti-Aβ (17–24) antibody (green), which shows that Aβ is localized primarily around the nuclei (visualized by DAPI staining, blue). In some cases, weak staining was observed in a region that may correspond to the BAG axons (white arrows). (D) Lifespan assay. The worms were scored daily in response to gentle prodding with a platinum wire, and the number of animals that remained alive was plotted as a fraction of the number of L4 worms at the start of the experiment. The assay was performed in a blinded fashion and two independent experiments showed no difference in lifespan between Aβ42 and control strains. (E) Motility assay. Body bends per minute are plotted for BAG-Aβ and control strains, averaged over two independent experiments. Error bars indicate standard error of the mean.

Expression was verified through fluorescence imaging and antibody staining (Fig 4.1B,C). We observed mCherry expression throughout the entirety of the BAG neurons (Fig 4.1B), but antibody staining revealed that amyloid-β localized to the area immediately outside the nucleus, stained with the DNA-binding dye DAPI (Fig 4.1C). This intracellular localization of amyloid-β is unsurprising despite the secretory signal peptide we included; prior studies have shown that cleaved amyloid-β accumulates intracellularly despite extracellular localization signals, bringing our

findings in line with the suggestion that amyloid-β is unable to be excreted in these models. The cleavage of the signal peptide from amyloid-β ensures, however, that the biophysical characteristics of amyloid-β should remain unchanged, save for the possibility of post-translational modifications. That being said, the cleavage of the signal peptide was not directly observed or tested for.

As a control, we also generated a line expressing only mCherry in the BAG neurons. In order to characterize our line, we then performed lifespan assays at 25C–—the temperature that has been previously shown to maximize aggregation and toxicity in a strain expressing amyloid-β in the body wall muscles [48, 188]——and found virtually no difference in lifespan between the two strains: a median of 10.9 days for the amyloid-β strain and a median of 10.8 days for the mCherry control (Fig 4.1D). Motility assays using the worm tracking platform were conducted on these strains over the first 10 days of adulthood and showed no difference in motility between the two strains. These results are in contrast to the reduced lifespan reported in a model overexpressing amyloid-β pan-neuronally and the strong, progressive paralysis reported in body wall muscle models [48, 188], indicating that our model does not cause widespread cytotoxicity or dysfunction.

4.3.2 Modulation of Ω-turn behavioural response in BAG-Aβ worms

We next endeavoured to characterize the BAG-Aβ worm model using behavioural assays. As previously explained, the BAG neurons are activated through a signalling cascade triggered by low levels of O_2 and mediated by two guanylate cyclases [183, 184]. The BAG neurons are responsible for an avoidance response to hypoxic conditions, the strength of which can be quantified by counting the number of Ω-turns performed by the animals.

In this behavioural assay, animals were allowed to crawl on NGM plates that were seeded with E. coli 24-48 hours prior, and covered by a microfluidic chamber that was pumped with the desired mixture of O_2, CO_2, and air. Hypoxic conditions were induced by increasing the amount of CO_2 in the mixture. Measurements of speed and fraction of worms making Ω-turns were determined programmatically using custom-written software produced within the de Bono Group [178]. We observed a reduction in the fraction of animals making Ω-turns as compared to controls, while the speed of the animals remained comparable (Fig 4.2A). In order to confirm that the observed effect was due to expression of amyloid-β and not due to off-target mutations caused by Mos1-insertion, we independently verified our results using an overexpression model. This transgenic model overexpresses amyloid-β exclusively

in the BAG neurons, and was created in an *npr-1* mutant background which requires that the behavioural assay be performed at 7% O_2. The neuropeptide npr-1 mediates both feeding and O_2 behaviours, and its expression and activity vary naturally in *C. elegans*. The mutant *npr-1* strain expresses the low activity isoform of the gene, allowing for consistent observation of aerotaxis response. Under these conditions, amyloid-β overexpression was associated with a reduction in the fraction of Ω-turns compared to controls (Fig 4.3). In contrast, a strikingly different phenotype was observed when subjecting pan-neuronal amyloid-β expression models to this assay. In this case, animals were incubated at 25°C overnight prior to the assay, a requirement to induce phenotype in this model, and we observed a prolonged period of Ω-turns and a strong reduction in overall speed compared to wild-type N2 worms (Fig 4.2B). This phenotype is likely caused by amyloid-β-induced aberrant signalling occurring simultaneously in several types of neurons, including interneurons and motor neurons. This difficulty in linking neuronal dysfunction in the pan-neuronal model to specific, quantifiable behavioural outputs highlights the importance of creating and characterizing models with neuron type-specific amyloid-β expression.

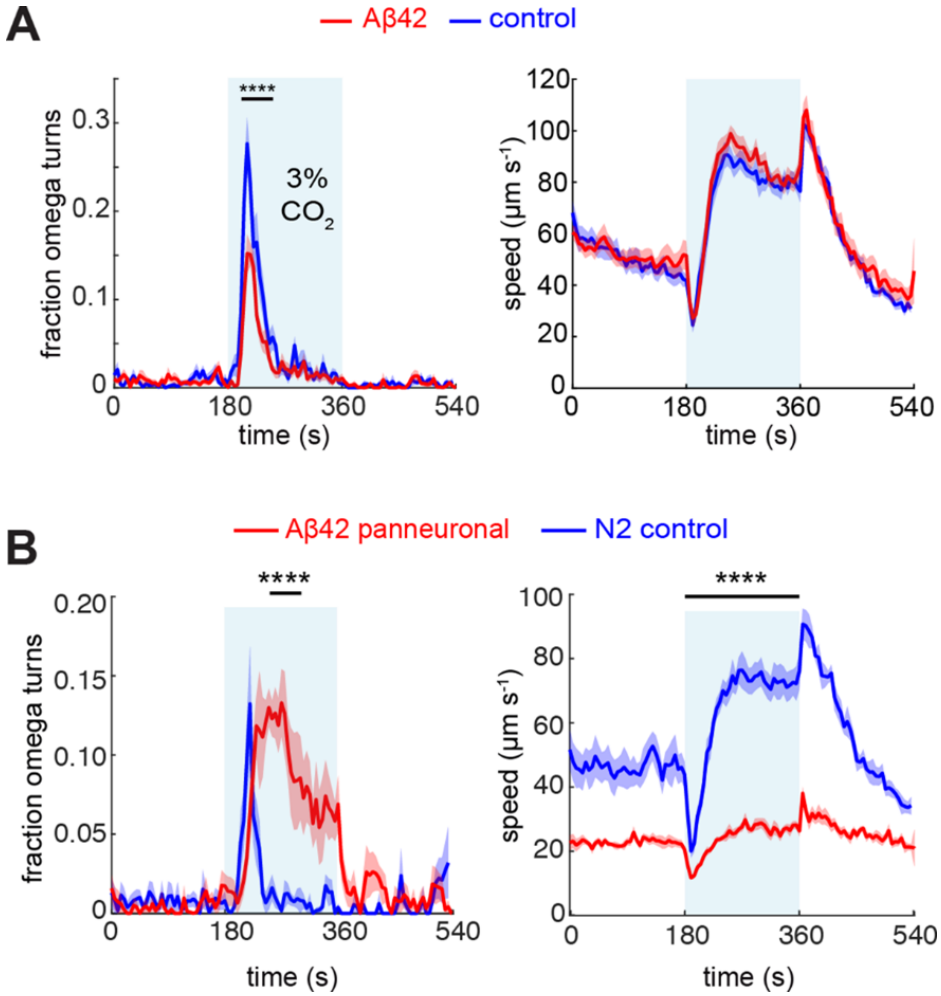

Fig. 4.2 **CO_2 assay of Aβ-expressing strains.** (A) Fraction of Ω-turns (top) and speed (bottom) of BAG-Aβ worms (red, n = 221) and mCherry controls (blue, n = 228) in response to 3% CO_2. (B) CO_2 assay of strain CL2355 with panneuronal Aβ-overexpression (red, n = 172) and N2 controls (blue, n = 170). Statistical tests were performed with a Mann-Whitney U-test, **** $p < 0.0001$.

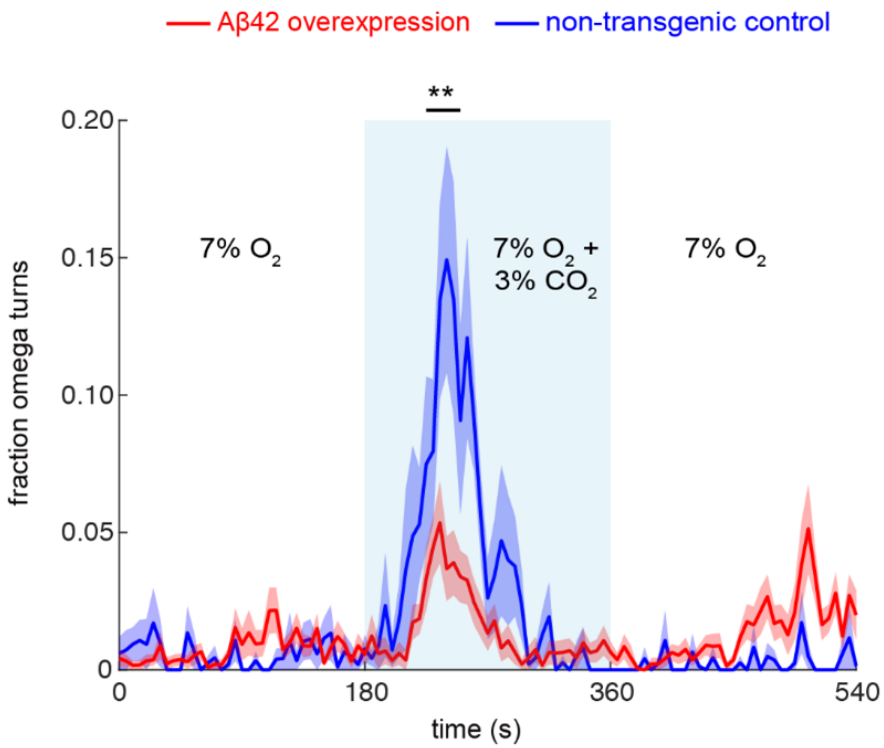

Fig. 4.3 **Behavioural response of animals overexpressing Aβ42 in BAG in *npr-1* background.** CO_2 response of *npr-1* animals overexpressing Aβ42 in BAG (red, n = 280) and non-transgenic siblings (blue, n = 89) in 7% O_2 background.

When starved animals are subjected to hypoxic conditions, a reduction in speed is usually observed in addition to an increase in the fraction of worms making Ω-turns [184]. Like the Ω-turn response, this speed reduction is mediated by the BAG neurons. Both of these responses have been shown to be abolished in BAG-ablated animals in prior studies [184]. In order to fully characterize the BAG-Aβ model, we performed a hypoxia assay using starved animals and quantified their speed and number of reversals (Fig. 4). We found that both BAG-Aβ and control animals slowed down (Fig 4.4A) and increased their reversals (Fig 4.4B) at a similar rate upon a downshift of 21% to 7% O_2. This suggests that although amyloid-β causes some degree of neuronal dysfunction, the deficits are not sufficiently severe such that the neuron ceases to function entirely. Incidentally, we also found that maximum Ω-turn response in BAG-Aβ worms remained below that of the controls, but this effect was not statistically significant (Fig 4.4C).

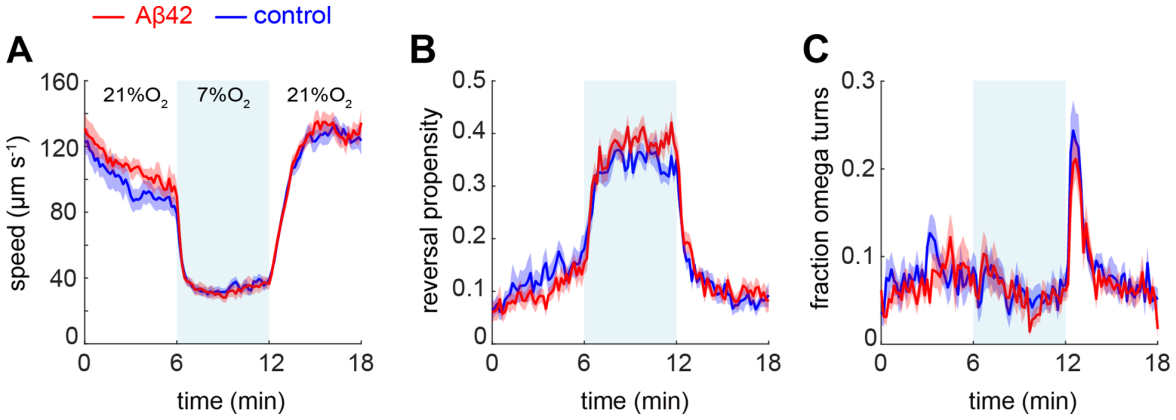

Fig. 4.4 **Hypoxia assay of starved BAG-Aβ and mCherry control animals.** (A) Speed response, (B) reversal propensity, and (C) fraction of Ω-turns of BAG-Aβ (red, n = 201) and control (blue, n = 209) animals in response to a downshift from 21% to 7% O_2 and upshift back to 21% O_2.

In light of these results, we became interested in the effects of amyloid-β expression on BAG-dependent learning and memory. Learning and memory, we reasoned, could potentially be more susceptible to amyloid-β-induced toxicity, and it has been recently shown that the BAG neurons mediate experience-dependent changes to chemotaxis behaviour along a CO_2 gradient [189]. To test this, we raised nematodes at an elevated CO_2 concentration of 3% prior to performing the hypoxia assay. We found that control worms raised at this increased CO_2 concentration had a steeper decrease in speed than did their counterparts raised in ambient air (Fig 4.4A, right), but both had the same propensity for Ω-turns (Fig 4.5A, left). In contrast, BAG-Aβ

worms raised with 3% CO_2 saw an increase in Ω-turn propensity than did BAG-Aβ worms raised in ambient air in addition to the more rapid decline in speed (Fig 4.5B). The speed decline in both the BAG-Aβ and control worms was similar (compare right panels of Fig 4.5A and B), indicating the amyloid-β did not abolish experience-dependent modulation of the behavioural response. While the increase in Ω-turn propensity after conditioning for BAG-Aβ worms is of interest, it should be noted that maximum fraction of Ω-turns for BAG-Aβ worms was lower than that of control worms either with or without conditioning. One interpretation of this finding is that BAG-Aβ worms require conditioning in order to have a strong avoidance response to hypoxia.

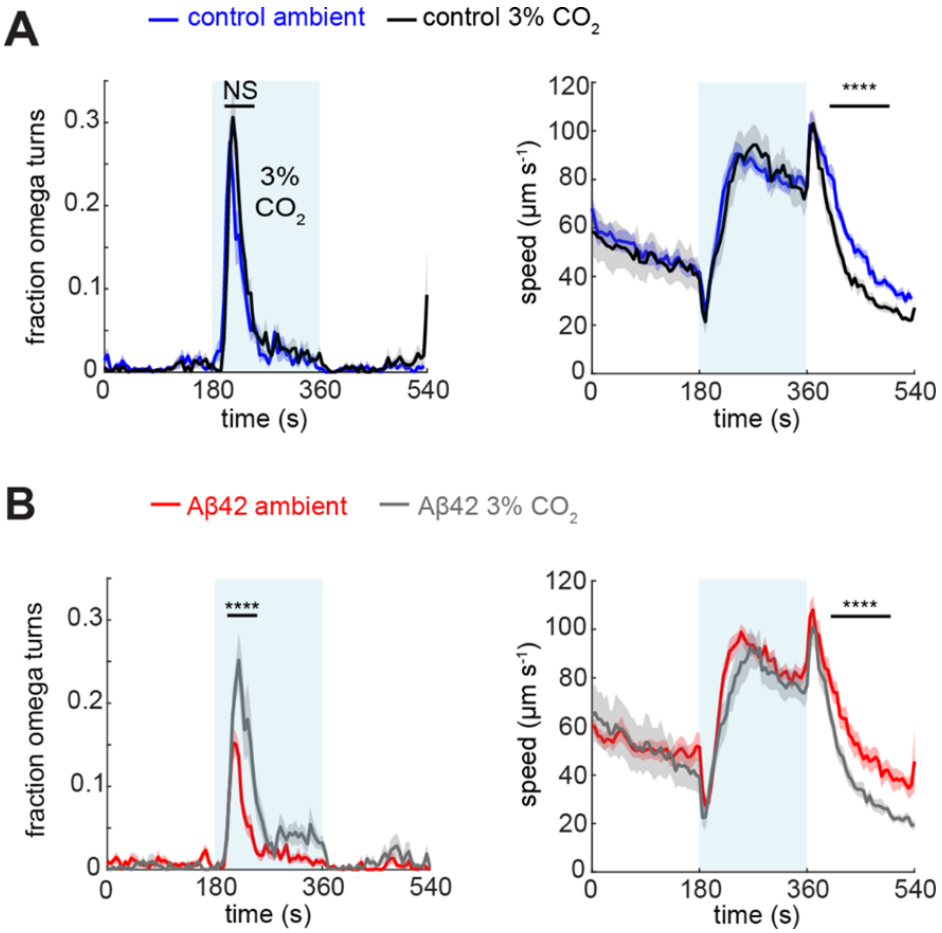

Fig. 4.5 **Experience-dependent modulation of the CO_2 response.** Behavioural response of (A) control animals raised at ambient atmosphere (blue, n = 228) or at 3% CO_2 (black, n = 216), (B) BAG-Aβ animals raised at ambient atmosphere (red, n = 221) or or at 3% CO_2 (grey, n = 215). Ω-turns were assessed using a Mann-Whitney U-test and speed with a t-test over the indicated intervals. **** $p < 0.0001$.

4.3.3 The Ω-turn response—but not neuronal activation—diminishes with age

Following our initial characterization of the BAG-Aβ model, we sought to determine the effects of ageing on the BAG-Aβ phenotype. To this end, we performed the hypoxia assay on adult BAG-Aβ worms at days 1, 2, and 3 of adulthood when raised at 25°C (Fig 4.6). We found that the difference in Ω-turn propensity between BAG-Aβ and control worms in response to hypoxic conditions did not increase with age, although fraction of Ω-turns declined strongly with age in both strains (Fig 4.6). This trend was also observed when animals were raised at 20C as well as in the N2 wild-type strain, indicating that this effect is unlikely to have been caused by mCherry expression of elevated culturing temperature (Fig 4.7). Conversely, the BAG-mediated "off-response"—a brief spike in speed immediately following cessation of the CO_2 stimulus—remained intact across all three days examined (Figs 6 and 7, lower panels). However, no consistent difference in speed between the BAG-Aβ and control worms could be observed, and a pronounced decrease in speed over ageing was observed in both strains—probably a result of decline in health of the musculature rather than due to neuronal dysfunction.

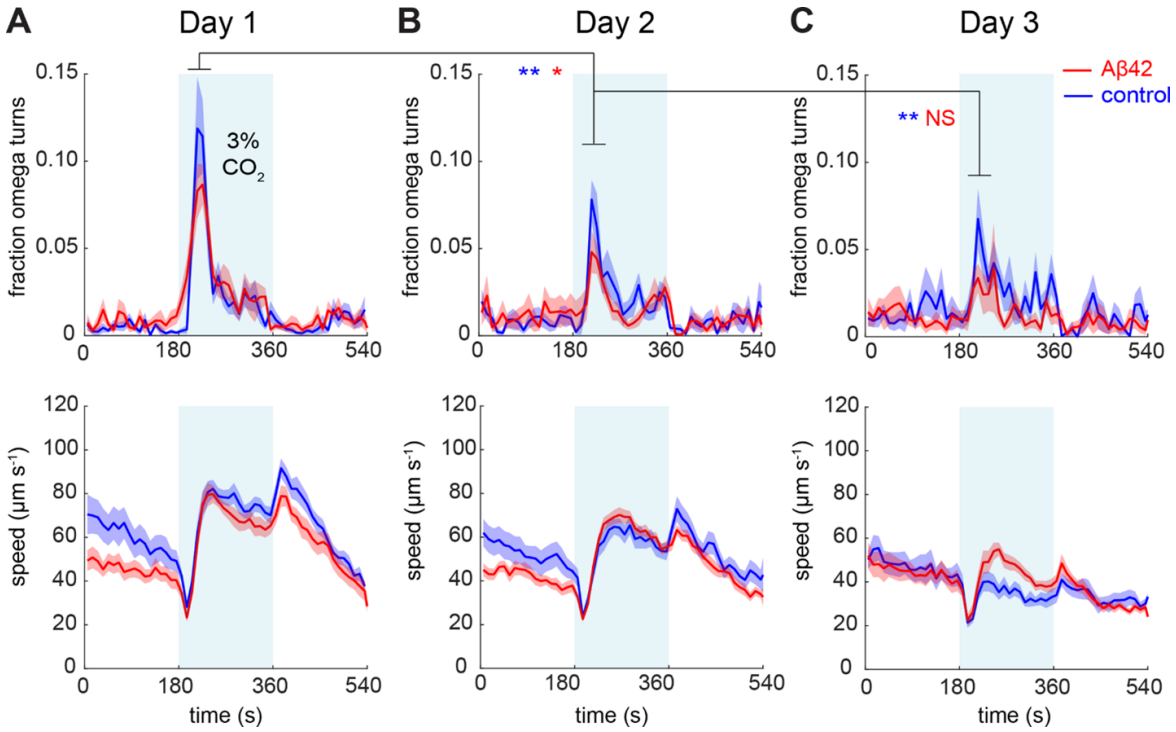

Fig. 4.6 **Locomotory responses to 3% CO_2 as a function of ageing.** Shown are the fraction of animals making Ω-turns (upper panels) and the modulation of speed (lower panels) in response to a 3% CO_2 stimulus (shaded in blue) at day 1 (A), day 2 (B) and day 3 (C) of adulthood. For each time point, naïve animals not previously assayed were taken from the same batch of animals. The data shown here were averaged over multiple independent experiments, Aβ n = 220–280, control n = 160–241. Statistics on the fraction of Ω-turns were performed with a Mann-Whitney U-test over the indicated time intervals. * $p < 0.05$, ** $p < 0.01$, NS not significant.

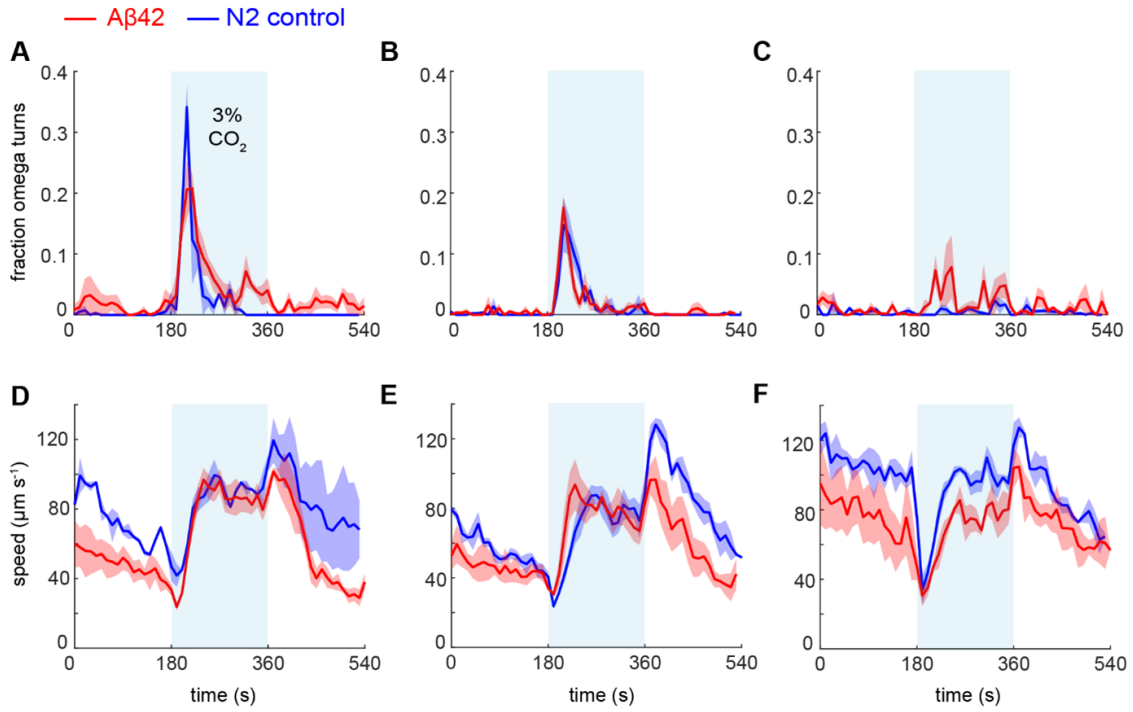

Fig. 4.7 **Behavioural response of the BAG-Aβ worms and N2 wild-type worms raised at 20°C.** A-C) The fractions of worms making Ω-turns in response to 3% CO_2 (shaded in blue) at day 1 (A), day 2 (B) and day 4 (C) of adulthood. D-E) Speed response at day 1 (D), day 2 (E) and day 4 (F). The data represent 2–3 assays for each time point and strain from one biological replicate, Aβ n = 66 (day 1), n = 71 (day 2), n = 47 (day 4); N2 n = 46 (day 1), n = 66 (day 2), n = 65 (day 4).

To directly probe the response of the BAG neurons to hypoxic stimuli, we employed Ca^{2+} imaging. To do this, we expressed the fluorescence resonance energy transfer (FRET) sensor YC3.60 [190] in the BAG neurons, and we used this to monitor the increase in intracellular Ca^{2+} concentration upon activation with 3% CO_2. We found that BAG-Aβ worms showed a significantly elevated Ca^{2+} response as compared to controls (day 1, p = 0.04; day 3, p = 0.03) (Fig 4.8A and B), although this difference was abolished as the animals aged (Fig 4.8C-E). This increase in Ca^{2+} influx is especially interesting in light of the fact that neuronal hyperactivation is thought to be an early event of the earliest stages of human AD, prior to the appearance of any clinical symptoms [191]. Moreover, the Ca^{2+} influx due to activation of the BAG neurons by the CO_2 stimulus persisted across all ages tested, showing no clear signs of impairment as a result of amyloid-β expression or natural ageing, including on the 12th day of adulthood——that is, beyond the median lifespan of 11 days. Insofar as Ca^{2+} influx can be used as a measure of neuronal function, the BAG neurons seem to remain functional throughout the lifespan of *C. elegans*

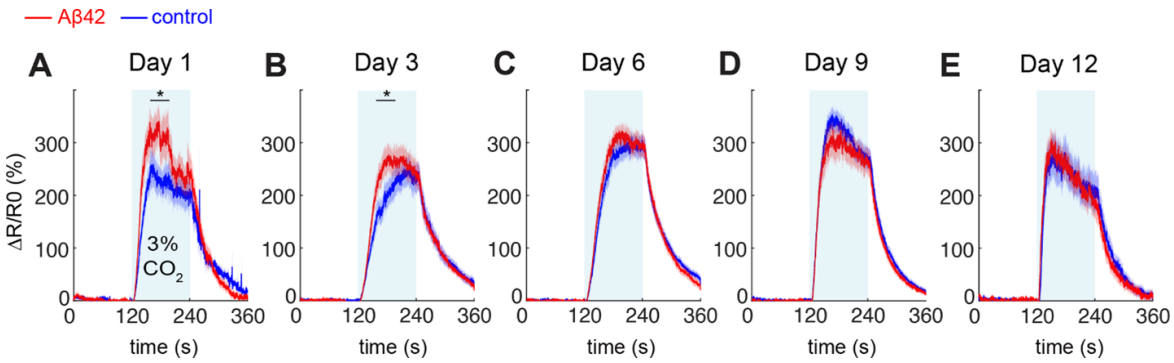

Fig. 4.8 **Ca^{2+} response in the Aβ-BAG worms and corresponding controls.** (A) Day 1 of adulthood, (B) day 3, (C) day 6, (D) day 9, (E) day 12. For each measurement, naïve animals not previously exposed to elevated CO_2 levels were taken from the same batch of age-synchronised animals. Data were averaged over 2–4 biological replicates for each time point, n = 23–28 per strain for day 1, 3, 6, 9 and n = 11–13 for day 12. ΔR/R0 represents the percent increase in YFP/CFP ratio, normalized to the baseline value. Statistics were performed using a t-test between 160 s and 200 s, * p < 0.05.

Finally, we attempted to measure amyloid deposition——if any——in the BAG-Aβ worms using the amyloid-binding dye X-34 (Fig 4.9) [192]. Using this technique, no amyloid deposits could be found, a finding consistent with the modest phenotype of the BAG-Aβ worms. This does not, however, rule out the possibility that soluble

oligomeric amyloid-β species may be present and responsible for the behavioural phenotype and increased Ca^{2+} influx observed in the BAG-Aβ model.

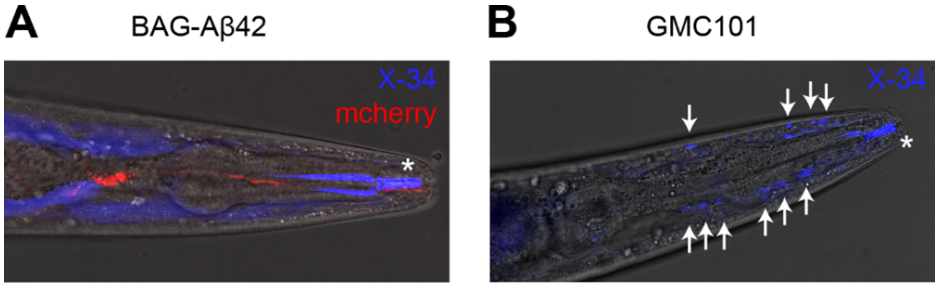

Fig. 4.9 **Staining with X-34 does not reveal amyloid deposits in BAG-Aβ worms.** (A) BAG- Aβ42 animal grown until day 7 at 25°C followed by live staining with X-34. X-34 staining (blue) is observed diffusely throughout the body and at the mouth cavity (asterisk), but not observed to co-localise with the BAG neurons (red). (B) GMC101 animal overexpressing Aβ42 in the body wall muscle cells grown until day 7 at 25°C, showing deposits positive for X-34 (blue, deposits marked with arrows).

4.4 Conclusions

Here, we have reported the creation and characterization of a model of AD in *C. elegans* that expresses a single copy of amyloid-β in a pair of sensory neurons. While more traditional *C. elegans* AD models which overexpress amyloid-β throughout entire tissues can illustrate amyloid-β toxicity in a dramatic fashion (e.g. paralysis, shortened lifespan, and locomotory defects) our model appears generally healthy apart from several specific alterations to the behavioural responses to hypoxia mediated by the BAG neurons. We hypothesize that these changes reflect perturbations in neuronal signalling and function caused by soluble amyloid-β species, which we believe may be relevant to the human disease. An alternative explanation is amyloid-β modulates synaptic transmission and plasticity in young *C. elegans* animals as part of its physiological role.

Altogether, these results lend credence to the strategy of modelling AD by creating perturbations of sufficient severity that they modulate specific, quantifiable physiological processes, but adequately weak and localized that they do not cause more widespread toxicity. Subjecting these models to additional perturbations could result in a reasonable facsimile of the early molecular events in AD, giving us greater insight into the aetiology of the disease. Indeed, the strategy of subjecting subtle *in vivo* models of AD to minor insults in order to create a stronger phenotype is a

general theme of this work, and the next chapter represents our attempt to follow through on this line of reasoning.

4.5 Materials and Methods

4.5.1 *C. elegans* strains

Nematodes were maintained on nematode growth media (NGM) plates seeded with Escherichia coli OP50 at 20°C, unless stated otherwise. Strain EG6699 was maintained on NGM plates seeded with *E. coli* HB101 at 15°C. For age-dependent studies, a synchronized worm population was generated by a 4 h synchronized egg-lay at 20°C, after which incubation was continued at 25°C throughout the experiment unless stated otherwise.

The strains of *C. elegans* used in this study include:

N2 (Bristol)

EG6699 ttTi5605 II; unc-119(ed3) III; oxEx1578([eft-3p::GFP + Cbr-unc-119]

AX204 npr-1(ad609) X

AX6171 npr-1(ad609) dbEx[pflp-17::Aβ1–42::unc54 3′ UTR + ccRFP]

CMD01 ttTi5605 camIs[pflp-17::Aβ1–42::SL2mCherry::let-858 3′ UTR + Cbr-unc-119] II; unc-119(ed3) III

CMD06 ttTi5605 camIs[pflp-17::mCherry::let-858 3′UTR + Cbr-unc-119] II; unc-119(ed3) III

AX2073 dbEx[pflp-17::YC3.60]

CMD12 ttTi5605 camIs[pflp-17::Aβ1–42::SL2mCherry::let-858 3′UTR + Cbr-unc-119] II; unc-119(ed3) III; dbEx[pflp-17::YC3.60]

CMD13 ttTi5605 camIs[pflp-17::mCherry::let-858 3′UTR + Cbr-unc-119] II; unc-119(ed3) III; dbEx[pflp-17::YC3.60]

CL2355 smg-1(cc546) dvIs50 [pCL45 (snb-1::Aβ 1–42::3′ UTR(long) + mtl-2::GFP]

GMC101 dvIs100 [unc-54p::Aβ 1–42::unc-54 3′-UTR + mtl-2p::GFP]

4.5.2 DNA cloning

DNA constructs were created using MultiSite Gateway Cloning (Thermo Fisher Scientific). As a promoter sequence, we used 2 kb upstream of flp-17 in position 1. The sequence for human Aβ42 preceded by a signal peptide, as used previously [175], was codon-optimized for *C. elegans* using Jcat [193], and synthesized by GeneArt

(Thermo Fischer Scientific). This construct was cloned into position 2, and the SL2::mCherry sequence in position 3. The 3′ UTR region of let-858 was inserted into the backbone of pCFJ150 [187] in which the full construct was assembled. For the control line, mCherry was inserted in Gateway position 2 and the let-858 3′ UTR in position 3, followed by assembly into pCFJ150. For overexpression of Aβ42, the 3′ UTR of unc-54 was inserted into gateway position 3, and the construct with pflp-17 in position 1 and Aβ42 with signal peptide in position 2 was assembled into pDEST. The constructs were verified by Sanger sequencing.

4.5.3 Creation of transgenic lines

Strains were generated by Mos-1 single copy insertion following published protocols [187], by micro-injection of plasmid DNA into the gonads of young adults of strain EG6699. Mos-1 insertions were verified by PCR with LongAmp Taq polymerase (New England Biolabs) followed by Sanger sequencing. The Aβ42 plasmid for overexpression was micro-injected into the gonads of young adults of strain AX204 together with a plasmid encoding cc::RFP, and transgenic offspring was selected based on RFP expression in the coelomocytes.

4.5.4 Antibody staining and imaging

Animals were fixed at day 3 of adulthood in 4% formaldehyde in PBS for 24 hours at 4°C, followed by β-mercaptoethanol and collagenase treatment to digest the cuticle, as described previously [194, 195]. Fixed and permeabilised animals were probed with anti-amyloid-β antibody 4G8 (epitope residues 17–24), followed by Alexa-488 conjugated anti-mouse secondary antibody (both obtained from Biolegend UK Ltd). Stained animals were mounted in ProLong Gold antifade reagent with DAPI (Life Technologies) and imaged on a Leica SP8 confocal microscope using a 63x water immersion objective. To visualize the BAG neurons in living animals, the nematodes were anaesthetized with sodium azide and mounted on an agarose pad. Imaging was performed on an Andor Revolution spinning disk microscope with a 20x objective and a Leica SP8 confocal microscope using a 40x oil or a 63x oil objective.

4.5.5 Lifespan assay

For lifespan assays, 150 nematodes per strain derived from a 4 h synchronized egg-lay were placed on 3 cm NGM plates containing 75 µM 5-fluoro-2′-deoxyuridine (FUDR, Sigma) at the L4 stage, and incubated at 25°C. In an independent experiment, FUDR was omitted and the nematodes were transferred daily to fresh plates during their reproductive phase. The worms were counted daily and scored as dead when they did not respond to gentle prodding with a platinum wire. Worms that crawled up against the side of the plate were excluded from the analysis. The lifespan assays were scored blindly.

4.5.6 Motility assay

The motility assay was performed as described previously [188]. In brief, an age-synchronised population of animals was generated by bleaching, and worms were transferred to NGM plates containing 75 µM FUDR (Sigma) at L4 stage and incubated at 25°C. The motility assay was performed on ca. 500 animals for each strain and timepoint, and body bends per minute were determined using custom-written software.

4.5.7 Behavioural assays

For behavioural assays, worms were grown on NGM plates either at room temperature (20–22°C) or at 25°C. CO2 conditioning was performed by raising the animals in a chamber filled with 21% O2 + 3% CO2 starting after a synchronised egg-lay. Assays on aged nematodes were performed by daily transfer to fresh NGM plates to separate the adults from their offspring. Naïve animals from the same batch that were not previously assayed were used for each time point, and at least three independent experiments were performed for each of the assays. For the CO2 assay, NGM plates were seeded with 20 µL of an overnight culture of E. coli OP50 approximately 20 hours before the assay. For each assay, 20 nematodes were placed onto the resulting food lawn and a 1 cm × 1cm × 200 µm polydimethylsiloxane (PDMS) chamber was placed on the plate, with gas inlets connected to a PHD 2000 Infusion syringe pump (Harvard Apparatus) as described previously [178]. The animals were allowed to adjust for several minutes before the start of the assay, followed by exposure to a 1.5 mL/min gas flow consisting of 21% O2 for 3 min, 21% O2 + 3% CO2 for 3 min, and finally 21% O2 for 3 min. For the assays of npr-1 animals, the gases used

were 7% O2 for 3 min, 7% O2 + 3% CO2 for 3 min, and 7% O2 for 3 min. Videos were recorded using FlyCapture on a Leica M165FC microscope with a Point Gray Grasshopper camera at 2 frames per second. The hypoxia assay was performed on animals starved for 4–6 h, and transferred to unseeded 3 cm NGM plates sealed with a copper ring to contain the worms within the field of view of the camera. The gas flow was applied using a custom-made setup at approximately 1–1.5 mL/min with 21% O2 for 6 min, 7% O2 for 6 min, and 21% O2 for 6 min. Videos were recorded using Dino-Lite Digital Microscope cameras at either 6 or 10 frames per second. Custom-written Matlab software was used to track the nematodes and to determine the fraction making Ω-turns, reversals and speed [178].

4.5.8 Ca^{2+} imaging

Aβ42 and mCherry control lines were crossed with strain AX2073 expressing Ca2+ sensor YC3.60 [190] under the flp-17 promoter, driving expression in BAG. The assay was performed on freely moving animals using the set-up described previously [43]. Individual animals were placed on 5 cm agarose plates (17 g/L agarose, 3 g/L NaCl, 5 mg/L cholesterol, 1 mM MgSO4, 1 mM CaCl2) seeded with a 3 µL concentrated drop of E. coli OP50. A PDMS chamber was placed on top and the gases were applied at 1.4 mL/min, with 21% O2 for 2 min, 21% O2 + 3% CO2 for 2 min, and finally 21% O2 for 2 min.

Videos were recorded at 10 frames per second using 100 ms exposure time on a Nikon AZ100 microscope with an AZ Plan Fluor 2x lens. A TwinCam adaptor (Cairn Research, UK) and two ORCA-Flash4.0 V2 digital cameras (Hamamatsu, Japan) were used to simultaneously record YFP and CFP fluorescence. The neurons were tracked and the YFP/CFP ratios (R) calculated using custom-written Matlab software. R0 was defined as the initial value averaged over the first 100 frames (10 s) and ΔR/R0 expressed as the percentage increase.

4.5.9 X-34 staining

Animals were grown at 25°C until day 7 of adulthood, washed in M9 buffer and incubated in 1 mM X-34 (Sigma) in 10 mM Tris-HCl pH 8.0 at room temperature for 3 h. They were then transferred to seeded NGM plates and allowed to destain for ca. 16 h. Imaging of anaesthetised animals was performed as described above on a Leica SP8 with 63x oil objective.

4.5.10 Statistical methods

A Mann-Whitney U-test was applied for statistical analysis of the Ω-turn response over the time intervals as indicated in the figures. A Student's t-test was used to examine speed, unless the data were not normally distributed in which case the Mann-Whitney U-test was applied. Ca2+ levels were assessed with a t-test over the interval of interest. The data were considered statistically significant at $p < 0.05$.

Most people stop looking when they find the proverbial needle in the haystack. I would continue looking to see if there were other needles.

Albert Einstein

We'll put you on the hit list.

Run-D.M.C., *Can I Get a Witness* (1993)

5

A Gene Signature for AD using RNA interference in C. elegans

In this chapter, I present the results of a high-resolution RNAi screen in *C. elegans* to validate the gene signature of AD described in Chapter 2, using the nTWAS approach. The 142 genes screened in the experiments reported here are the *C. elegans* orthologs of those in the gene signature. I will explain how a list of *C. elegans* orthologs of these genes was extracted from the human gene list provided by nTWAS. RNAi knockdowns of each of the 142 genes were conducted and then assayed for motility phenotype using the Wide-Field Nematode Tracking Platform (WF-NTP), a tool that allows hundreds of worms to be simultaneously scored along a number of motility-related parameters. Hits from these experiments were then validated by using the amyloid-specific dye NIAD-4 to stain the worms to quantify amyloid formation. The results of the motility assays and NIAD-4 staining, as well as a description of the setup and workflow of the screen itself, will also be presented.

5.1 Compilation of the initial gene list

Protein sequences of genes on the human gene list were obtained from the NCBI protein database and run through NCBI BLASTp in order to identify potential candidate *C. elegans* genes [196]. To ensure that the genes included in the screen had both sequence and functional homology with their human counterparts, a custom BLAST database consisting of those genes that occupied similar KEGG pathways in *C. elegans* was created. This database was BLASTed against the human gene list, and those genes with high sequence homology were selected. It should be noted that several of the KEGG pathways from the original gene list had no equivalent in *C. elegans* while others required stand-ins. Calcium signalling was used in place of Long-term Potentiation due to the number of orthologs shared between them, and Longevity-regulating Pathway was used in place of Insulin Signalling for the same reasons. A further filter on the list was the availability of RNAi stocks. Only those genes that are represented in the Ahringer RNAi library [197, 198] were considered for this screen. A complete list of these genes arranged by KEGG pathway can be found in **Table 5.1**. A large percentage of the genes on the list (59/142, or nearly 42%) are involved in ubiquitin-mediated proteolysis. This is probably due in equal measure to the fact that ubiquitin-mediated proteolysis is a highly-conserved pathway and this pathway has a great deal of redundancy in *C. elegans* [199, 200], thereby increasing the number of *C. elegans* genes that map to each human one.

5.2 Results and Discussion

5.2.1 Phase I of the Motility Screen

In order to screen the list of 142 *C. elegans* genes for modulators of Aβ aggregation and toxicity, we conducted an RNAi screen using a liquid thrashing assay scored by the WF-NTP as a measure of worm health. To this end, a suitable worm strain had to be selected. When selecting the strain, the primary constraint was that the strain had to express Aβ in the neurons of the worm, as many of the genes on our list are neuronal. As a result, the commonly-used GMC101 [176] strain—which over-expresses Aβ in the body wall muscles was not ideal for our purpose. Instead, we selected the CL2355 worm strain, which exhibits pan-neuronal expression of Aβ

KEGG Pathway	**Gene names**
Synaptic vesicle cycle	*dyn-1*, ***nmr-1***, *rab-3*, *snb-1*, *snt-1*, *unc-10*, *unc-31*, *unc-64*, *unc-13*
Calcium signalling	*K03A1.4*, *Y50D7A.3*, ***acy-1***, *cal-1*, *cal-2*, *cal-4*, *cmd-1*, *cnb-1*, ***gar-3***, *itr-1*, *let-23*, *plc-3*, *plc-4*, ***ser-1***, ***ser-7***, *unc-43*, *unc-68*, ***mgl-2***
mTOR signalling pathways	*C44H4.6*, *R03D7.5*, ***aak-2***, ***age-1***, ***akt-1***, ***akt-2***, ***daf-15***, *daf-18*, ***daf-2***, *gsk-3*, *ife-1*, *ife-2*, *ife-3*, *ife-4*, ***let-363***, *mpk-1*, *par-4*, *raga-1*, *rho-1*, *rict-1*, *rskn-1*, ***rsks-1***, *sem-5*, ***skpt-1***, *strd-1*, *unc-51*, ***aak-1***
Ubiquitin-mediated proteolysis	*Y48G1C.12*, *Y92H12A.2*, *apc-10*, *cul-1*, *cul-2*, *cul-3*, *cul-4*, *cul-5*, *cul-6*, *emb-27*, *fzr-1*, *let-70*, *lin-23*, *mat-3*, *oxi-1*, *prp-19*, *rbx-1*, *rbx-2*, *rfl-1*, *sel-10*, *sel-11*, ***skpt-1***, *skr-1*, *skr-12*, *skr-13*, *skr-15*, *skr-16*, *skr-17*, *skr-19*, *skr-2*, *skr-20*, *skr-21*, *skr-3*, *skr-5*, *skr-6*, *skr-8*, *skr-9*, *sli-1*, *such-1*, *uba-1*, *uba-2*, *ubc-1*, *ubc-12*, *ubc-16*, *ubc-17*, *ubc-18*, *ubc-20*, *ubc-21*, *ubc-22*, *ubc-24*, *ubc-25*, *ubc-6*, *ubc-7*, *ubc-8*, *ubc-9*, *ubr-5*, *uev-2*, *ufd-2*, *chn-1*
Longevity regulating pathway	***aak-2***, ***acy-1***, ***age-1***, ***akt-1***, ***akt-2***, ***daf-15***, ***daf-2***, *jkk-1*, *kgb-1*, *kgb-2*, ***let-363***, *pmk-1*, *pmk-2*, *pmk-3*, ***rsks-1***, *sek-1*, ***aak-1***
Neuroactive ligand-receptor interaction	*ckr-2*, *dop-1*, *dop-2*, *dop-3*, *gab-1*, *gar-1*, *gar-2*, ***gar-3***, *gbb-2*, *lgc-37*, *lgc-38*, *mgl-1*, ***nmr-1***, *nmr-2*, *npr-10*, *npr-11*, *npr-4*, *npr-6*, *npr-9*, *seb-3*, ***ser-1***, *ser-2*, ***ser-7***, *tkr-1*, *tkr-2*, *unc-49*, ***mgl-2***

Table 5.1 *C. elegans* orthologs of the AD Gene List. Genes in bold appear in more than one KEGG pathway.

[177](Fig. 5.1A) and was previously characterised using the WF-NTP [188]. Unlike Aβ expression in the body wall muscles—whose decay and death leads to a decrease in thrashing behaviour and, ultimately, paralysis—expression of Aβ in the neurons creates a considerably more subtle phenotype. When compared to the N2 Bristol worms of the same age, the motility of CL2355 worms is not substantially different from controls (Fig. 5.1B). We opted not to use the BAG-Aβ strain depicted in Chapter 4 of this work because the assays required to assess the health of the BAG neurons cannot be conducted in a high-throughput manner.

To determine whether our protocol for RNA interference by feeding would be successful, we tested knockdown of *uba-1*, the sole E3 ubiquitin ligase in *C. elegans*. When fed to L1 larvae, uba-1 reliably led to larval arrest at the L2 stage. When fed to L4 larvae, adults developed with significantly smaller body sizes. Loss of *uba-1* results in cell cycle arrest, and both the larval and adult phenotypes we observed were consistent with those of *uba-1* mutants. From this we concluded that our knockdown by feeding protocol was sound.

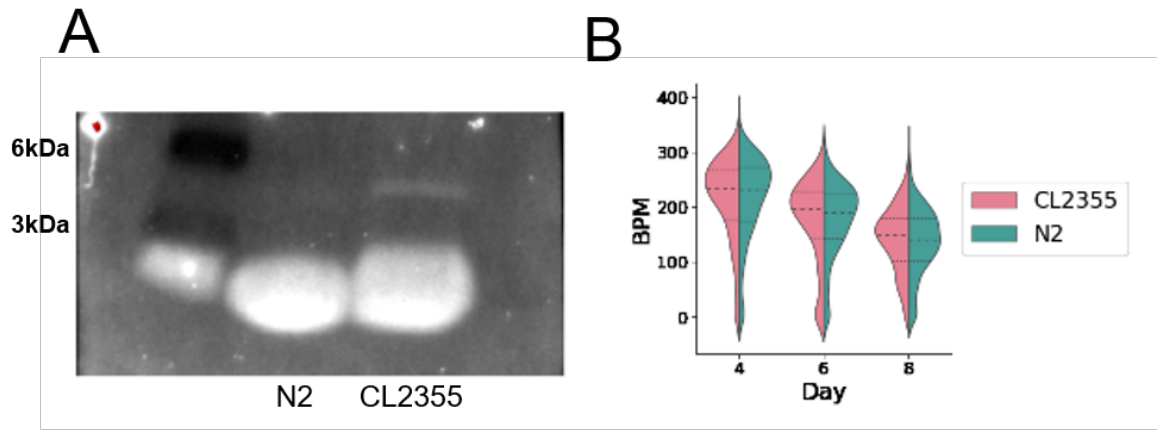

Fig. 5.1 **Comparison of N2 and CL2355 worms.** (A) Western blot of N2 and CL2355 worm lysates stained with the W0-2 anti-Aβ antibody. A band at 4 kDa representing Aβ can be observed in the CL2355 strain. (B) Comparison of the BPM distributions between the N2 (green) and CL2355 (pink) strains. All the corresponding distributions have similar median values and standard deviations.

With the aim of reducing the number of plates to be screened, we made the decision to conduct the motility screen in two phases. The first phase consisted of conducting knockdowns of each of the 142 genes only on the CL2355 strain. The rationale for this procedure was that only knockdowns resulting in modulation of the phenotype in CL2355 worms are expected to be relevant to disease. For this

portion of the screen, time points were taken on days 4, 6, 8, and 10 of adulthood. The count of body bends per minute (BPMs) was chosen as the primary motility readout due to its clear relationship with neuronal health: as motor neurons and related neuronal circuits experience decline, BPMs should also decline. The mean BPM value for each gene knockdown was normalised by taking the difference between the mean BPM of the knocked down population and the mean BPM of worms fed E. coli expressing the L4440 empty vector control. These normalised values were termed the dBPM. For each gene, the dBPM across all time-points was averaged. When plotted as a histogram, it became obvious that the knockdowns arranged neatly into three clusters: one centred at zero dBPM (no difference between the knockdown and control), one centred at a positive dBPM (increase in BPM in the knockdown compared to control), and one centred at a negative dBPM (decrease in BPM in the knockdown compared to control) (Fig. 5.2). These clusters were separated using the k-means++ algorithm [201], and the latter two clusters of genes were deemed preliminary hits and moved on to the second phase of the screen. A list of these genes arranged by KEGG pathway can be found in **Table 5.2**.

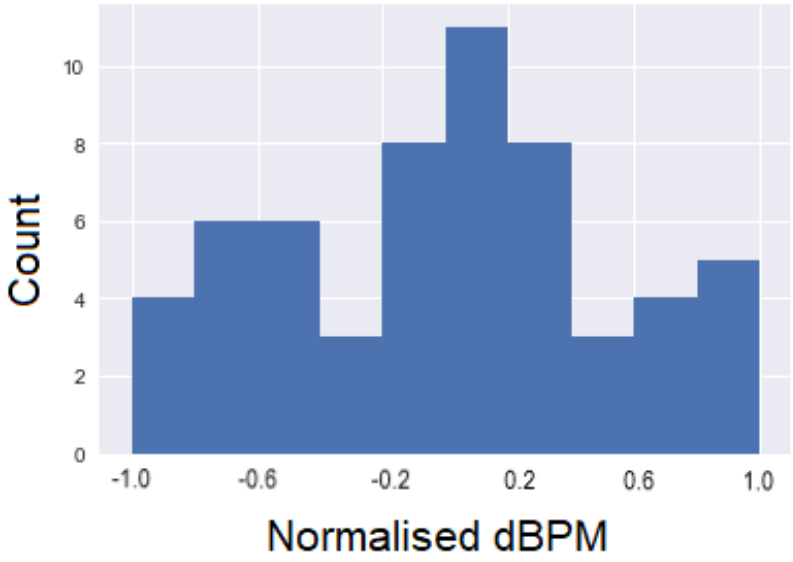

Fig. 5.2 **Histogram of Phase I dBPMs.** Histogram of dBPMs for all RNAi conditions administered to CL2355 worms in Phase I of the screen. Three clusters of genes can be clearly seen.

KEGG Pathway	Gene names
Synaptic vesicle cycle	*unc-13*
Calcium signalling	*K03A1.4*, *Y50D7A.3*, *cal-2*, *cmd-1*, *let-23*, ***ser-7***, *itr-1*
mTOR signalling pathways	*R03D7.5*, ***akt-1***, *daf-18*, *par-4*, *rict-1*, *rskn-1*, *skr-20*, *strd-1*, *unc-51*, *raga-1*
Ubiquitin-mediated proteolysis	*Y48GC1.12*, *Y92H12A.2*, *cul-2*, *cul-3*, *cul-4*, *cul-5*, *emb-27*, *fzr-1*, *let-70*, *mat-3*, *oxi-1*, *rfl-1*, *skr-16*, *skr-21*, *skr-5*, *uba-2*, *ubc-21*, *ubr-5*
Longevity regulating pathway	***akt-1***, *kgb-1*, *pmk-1*
Neuroactive ligand-receptor interaction	*dop-3*, *gab-1*, *gar-1*, *gbb-2*, *lgc-38*, *mgl-1*, *npr-6*, ***ser-7***, *tkr-1*, *ckr-2*

Table 5.2 Results of Phase I of the RNAi screen. Genes in bold appear in more than one KEGG pathway.

5.2.2 Phase II of the Motility Screen

In the second phase of the screen, these preliminary hits were re-screened following the same protocols and using both the CL2355 and N2 Bristol wild-type strain. We opted to use the N2 strain as a control for CL2355 (rather than the CL2122 strain that is typically used) because we found that the CL2122 strain was often sicklier and more difficult to culture than the CL2355 despite not expressing amyloid-β. As a means of determining whether the effect of the knockdown was due to an interaction with amyloid-β we sought to assess the differences between the dBPMs of each of the two strains. In this way, we wanted to determine whether the change in motility caused by the knockdown in the CL2355 strain exceeded the change in motility caused by the knockdown in the N2 strain. To do this, we computed the population mean BPM and standard deviation for each knockdown condition and the L4440 empty vector condition. The distribution of the dBPM was then computed as a simple combination of Gaussian variables (Eqs. 1 and 2),

1. $\mu_{total} = |\mu_{RNAi} - \mu_{control}|$
2. $\sigma_{total} = \sqrt{\sigma^2_{RNAi} + \sigma^2_{control}}$

and the resultant dBPM distributions from each strain were compared with a two-tailed Student's t-test. These comparisons were made across the two strains for each of the time-points, and conditions in which there was a significant difference in dBPM in the majority of time-points were considered hits.A prerequisite for this

type of analysis is that the BPMs in each condition are normally distributed. While this was usually the case, there were two scenarios we encountered that produced bimodal distributions. In the first scenario, developmentally delayed worms caused a second, lower mode to appear. In the second, the RNAi was not 100% effective. In these cases, one mode would appear at roughly the same mean as the control (no knockdown) and another either above or below it (successful knockdown). Both of these scenarios were dealt with in the same way: Gaussian mixture models were employed to deconvolute the distributions, and only the distribution representing successful knockdown of fully developed worms was considered. A visual summary of these methods can be found in Figure 5.3.

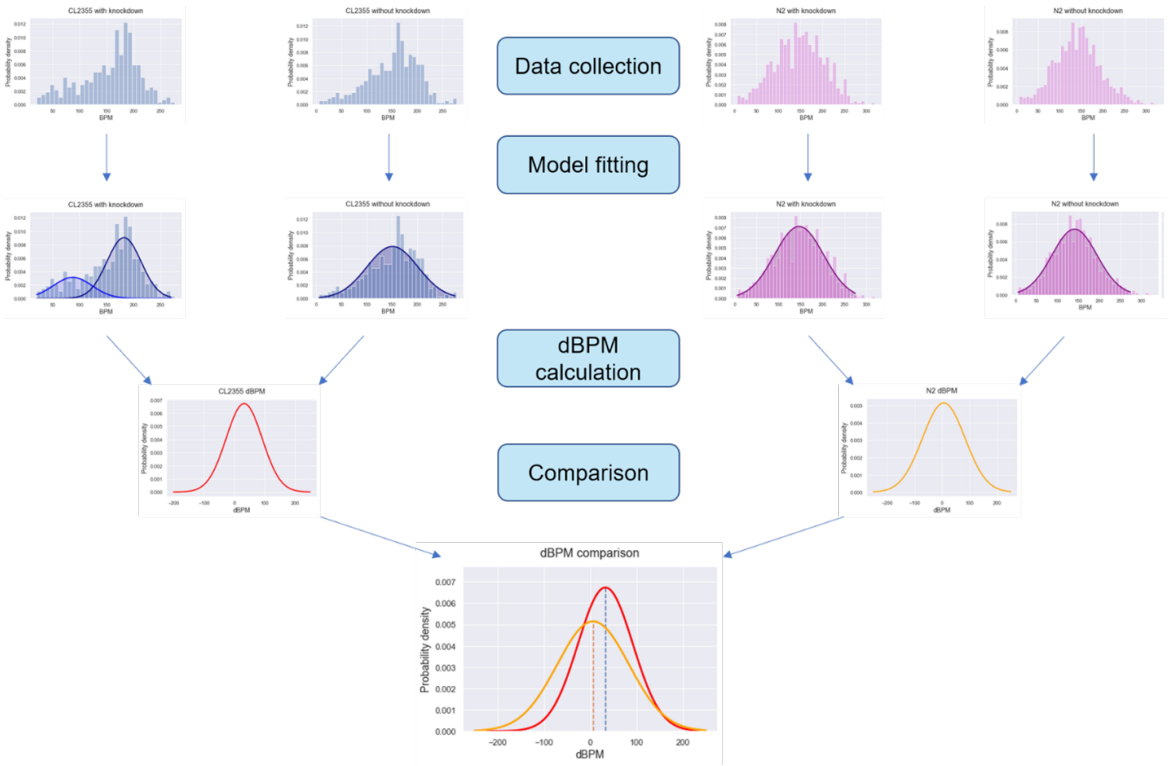

Fig. 5.3 **Schematic of Phase II data analysis.** Comparison of the differences in dBPM across strains. An example of deconvolution of a mixture of Gaussians is provided on the left.

Following this second screen, a total of 23 genes were determined to be true hits (**Table 5.3**). These hits were then carried forward to be evaluated by NIAD-4 staining and imaging, followed by aggregate quantification.

Nearly all the original KEGG pathways are represented among these hits, with the exception of the synaptic vesicle cycle, which is in many ways accordant with our understanding of the molecular biology of AD. The synaptic vesicle cycle is

KEGG Pathway	**Gene names**
Calcium signalling	*cmd-1*, *itr-1*, *ser-7*, *K03A1.4*
mTOR signalling pathways	*rict-1*, *R03D7.5*
Ubiquitin-mediated proteolysis	*cul-3*, *cul-5*, *fzr-1*, *oxi-1*, *rfl-1*, *skr-16*, *skr-21*, *skr-5*, *ubc-21*, *Y92H12A.2*
Longevity regulating pathway	*pmk-1*, *kgb-1*
Neuroactive ligand-receptor interaction	*gab-1*, *gbb-2*, *mgl-1*, *npr-6*, *ckr-2*

Table 5.3 Results of Phase II of the RNAi screen

a complex, multi-step process thought to be related to AD through the exocytosis and endocytosis of amyloid-β oligomers—a process that is very unlikely to be recapitulated in a worm model, even if that model is a neuronal one.

It is important to note that, unlike in muscular models of the disease, an increase in motility in neuronal models does not necessarily imply an increase in health. Neurodegeneration can result in an increase of certain movement behaviours; Huntington's patients notably exhibit chorea [202]. Therefore, the dBPM hit-selection method focuses on deviations from the normal BPM in either direction, rather than only increases or decreases in mean BPM.

5.2.3 NIAD-4 Staining and Image Analysis

While the putative hits from the motility assay give us an indication of the influence these genes have on worm health in disease models, they do not directly give us information on the modulation of Aβ aggregation. To this end, we stained treated and untreated worms for aggregates on three days of adulthood with NIAD-4 and took photos in both fluorescent (using a Cy5 filter) and transilluminated channels on an EVOS 5000 light microscope. NIAD-4 is an amyloid-binding dye that reduces its rotational mobility becoming planar after coming into contact with Aβ fibrils, thereby increasing its fluorescence intensity [203]. Although it was designed for high amyloid binding specificity and has a shape similar to thioflavin T (ThT), NIAD-4 can in theory planarize in other hydrophobic structures. In our hands, the greatest fluorescence intensity of NIAD-4 is indeed localized to dense collections of neuronal bodies in worms expressing Aβ, such as the head and tail ganglia (Fig. 5.4). That said, variations in fluorescence that are unlikely to be explained by amyloid binding

activity do occur and sometimes give rise to low-contrast images. As a result, image processing prior to aggregate quantification was deemed necessary.

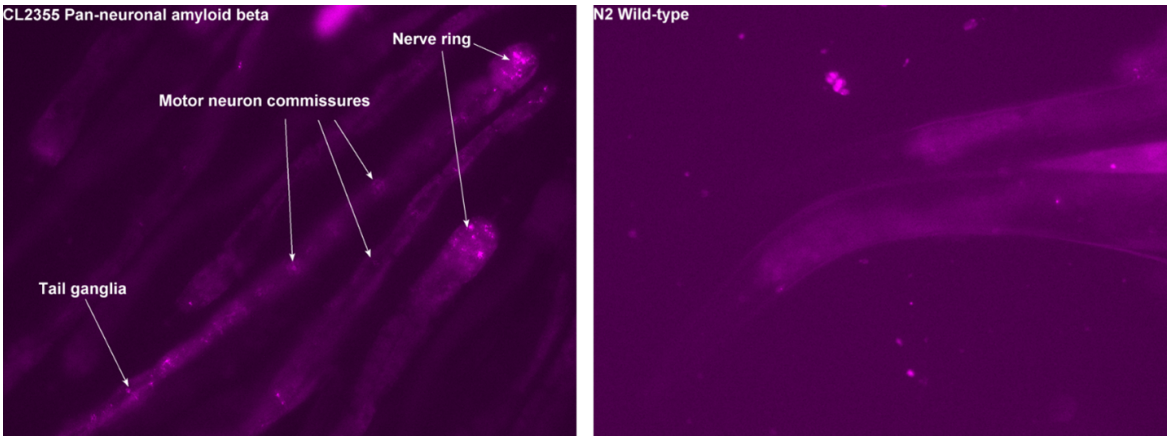

Fig. 5.4 **NIAD-4 staining of CL2355 and N2 worms.** The left panel shows clear visualization of aggregates in the densest collections of cell bodies.

To quantify aggregates in the worms, regions of interest were defined within the heads of the worms. We used this procedure because the head and tail ganglia often provided the highest contrast for imaging, and the head (unlike the tail) is a structure that is reasonably simple to demarcate. For the purposes of image analysis, the head was defined as the region between the mouth and a line just caudal to the pharynx, an easily-recognizable feature under a light microscope. The actual quantification of aggregates was performed by first thresholding the image using the Phansalkar local thresholding algorithm (with a radius of 20), followed by Fiji's built-in despeckling algorithm to reduce noise (Fig. 5.5). The Phansalkar algorithm [204] is a variation on Sauvola's thresholding method to deal with low-contrast images and in our experience typically outperformed the Sauvola algorithm. Following this step, data were collected on the particles that fell into the head region of the image. The percentage of the area of the head that the particles occupied was chosen as the most appropriate parameter for quantifying the extent of aggregation. This was done so as not to introduce bias due to natural variation in the size of worms. The percent area was then normalized using N2 controls as the baseline.

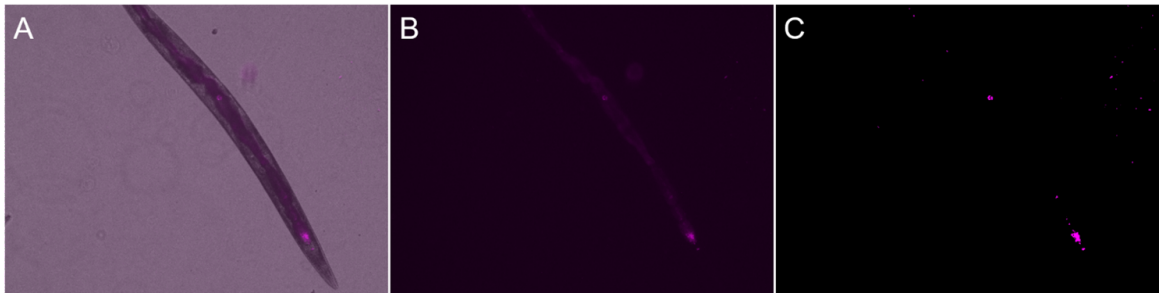

Fig. 5.5 **Montage of image processing steps.** (A) Composite image of a CL2355 worm after NIAD-4 staining under both a transilluminator and Cy5 filter. (B) Raw image of the same worm from only the Cy5 channel. (C) Image from the Cy5 channel after the application of the Phansalkar local thresholding algorithm and Fiji's despeckling algorithm for noise reduction.

Of the 23 genes identified as hits from the motility screen, we were able to test 6 by NIAD-4 staining (Fig. 5.6). We were unable to quantify changes in plaque deposition in the other 17 genes because plaques could not be visualised in untreated CL2355 controls from the same bleach. These 6 genes, with their human orthologs provided in parentheses, are: K03A1.4 (CALM1), ckr-2 (CCKBR), Y92H12A.2 (UBE3A), cmd-1 (CALM1, CALM3, PPP3R1), R03D7.5 (GSK3B), and skr-21 (SKP1). Apart K03A1.4, these genes showed a clear reduction in amyloid aggregates in CL2355 animals compared to controls.

The fact that plaque deposition could not be consistently visualised in untreated CL2355 worms was a serious concern and prompted further investigation. We initially believed that the CL2355 worms may have lost the transgene due to improper maintenance, which lead us to revive the line both from our own frozen stocks and from stocks obtained directly from the Caenorhabditis Genetics Center at the University of Minnesota. In both cases, we found that there was high variation in fluorescence from the GFP intestinal marker across animals. Furthermore, motility data obtained from testing these worms showed a high degree of variability, and did not match the results we obtained in previous phases of the screen. Indeed, the last point we can verify that CL2355 worms produced consistent motility phenotype across biological replicates (different bleaches) was in Phase I of this study. We concluded, that the CL2355 strain has significant variation in its phenotype, and that the extent of this variation may vary by batch. In light of this, interpretation of the results that follow is limited. An extended discussion of the limitations of this study can be found in Section 5.3.

When reviewing the motility data, these genes can be divided into two distinct groups: one where the direction of the motility effect was consistent (ckr-2, skr-21, Y92H12A.2), and another where the direction varied (R03D7.5, cmd-1). Although R03D7.5 and cmd-1 certainly merit further study, especially considering the imaging results, the inconsistency in motility data make the results here difficult to interpret. An increase or decrease in motility does not necessarily imply more or less fitness respectively. However, knockdowns resulting in a consistent effect—one that solely increased or decreased motility across several time points—suggest a clearer mechanism. An increase in dBPM suggests an increase in the activity of motor neurons and a decrease in dBPM suggests a decrease in activity of motor neurons, although the precise process by which this happens is more difficult to determine. Knockdowns where the direction varies may be exhibiting a type of chorea but may also be exhibiting erratic motility as a result of a complex combination of interactions of proteins downstream of the knockdown that varies over ageing. As a result, quantification of the magnitude of these dBPMs may not actually be meaningful, as the erratic motility itself may be the phenotype. The following sections will focus on results relating to ckr-2, skr-21, and Y92H12A.2, which are more straightforward to interpret.

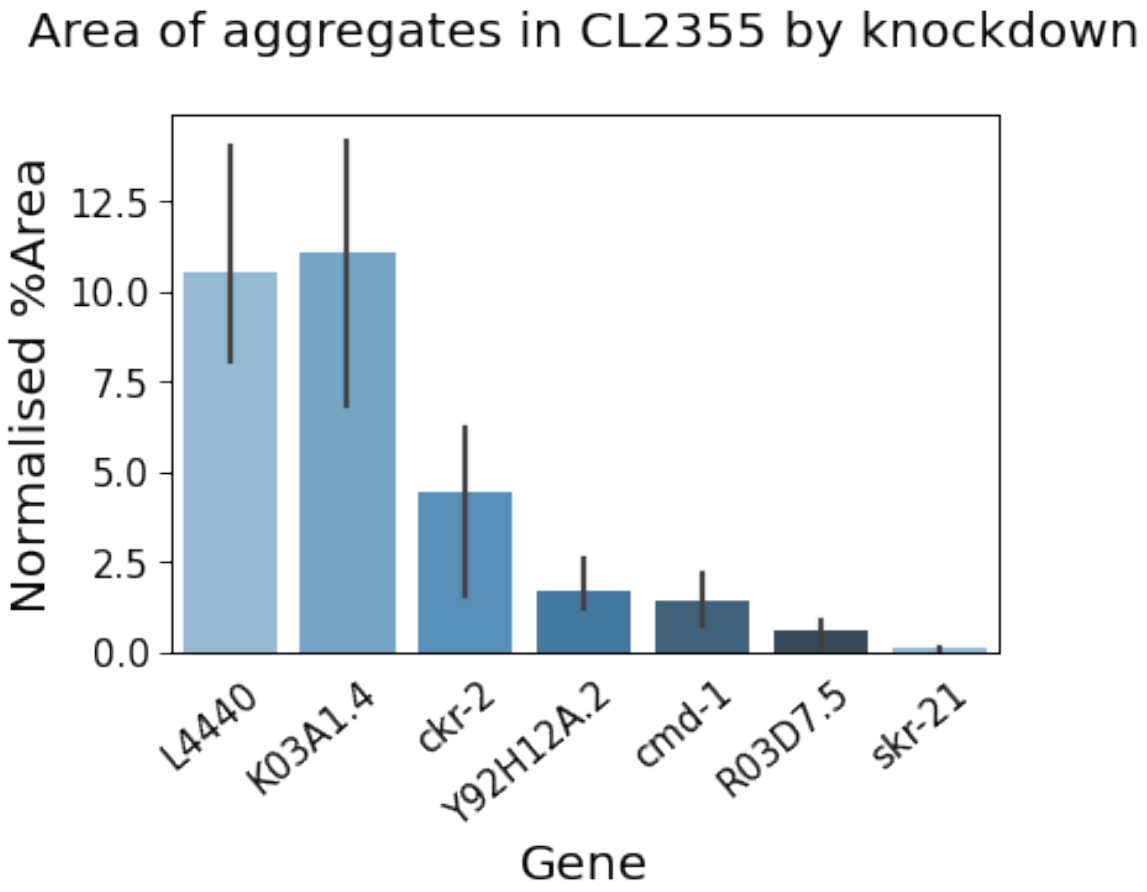

Fig. 5.6 **Normalised %Area of aggregates in CL2355.** All genes tested, with the exception of *K03A1.4*, showed a significant reduction in aggregates after knockdown. Error bars represent a 68% confidence interval.

5.2.4 Knockdowns of ckr-2 results in increased worm motility and a reduction of plaque formation

Cholecystokinin (CCK) is a peptide hormone that helps regulate satiety, and a neurotransmitter in the central and peripheral nervous systems [205, 206]. CCK-A receptors (CCKARs) are a class of G-protein coupled receptors (GPCRs) that are highly expressed in the gastrointestinal system and mediate pancreatic enzyme secretion as well as muscular contraction of the gallbladder and stomach. On the other hand, CCK-B receptors (CCKBRs) are highly expressed in the central nervous system [206], and their binding to CCK influences a variety of neurological phenomena as anxiety [207, 208], feeding behaviours [209, 210], and locomotion [211, 212]. Although the function of CCKBRs in the context of AD remains unknown,

a reduction in CCKBR expression has been found in the cerebral cortex of post-mortem AD brains [213], and may serve as a biomarker for the disease [206].

In *C. elegans* behavioural adaptation to changes in food availability are mediated by NLP-12, an ortholog of CCK [214]. NLP-12 is known to bind the CCKBR ortholog CKR-2, encoded by the ckr-2 gene. Although ckr-2 was once thought to be a requirement for NLP-12-mediated foraging behaviours, more recent evidence suggests that several other GPCRs that share homology with ckr-2 may provide redundancy for this role. Regardless, ckr-2 remains the only receptor for which there is robust evidence of NLP-12 binding [215]. Of note, ckr-2 was recently identified as a hub gene that responds to Aβ in a *C. elegans* model [216].

In N2 worms, knockdown of ckr-2 showed an increase in motility compared to controls only on day 4 of adulthood. In contrast, ckr-2 knockdown in CL2355 worms were comparable with controls on Day 4, but showed sustained high motility through the first 8 days of adulthood even as control worms experienced decline (Fig. 5.7).

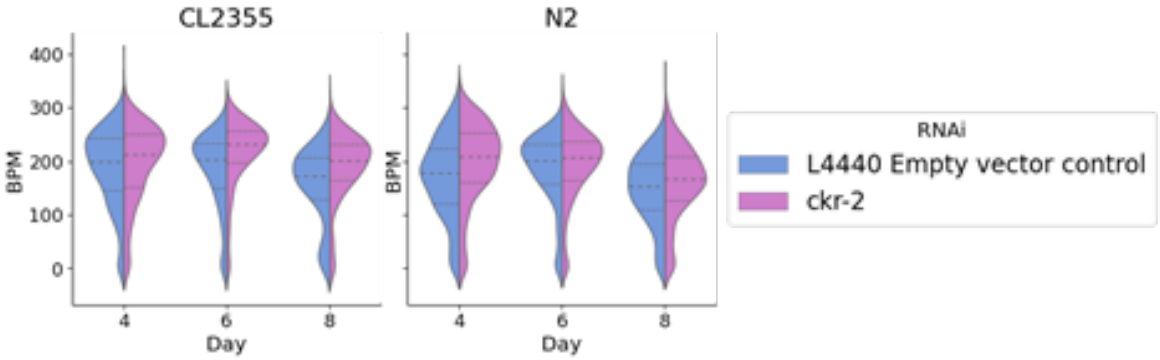

Fig. 5.7 **Results of thrashing motility assay upon *ckr-2* knockdown.** Results of thrashing motility assay on ckr-2 knockdowns and controls using the WF-NTP. A resistance to decline in motility over ageing in the CL2355 ckr-2 knockdown worms can be clearly observed.

Increases in plaque formation do not necessarily imply a decline in health. There is evidence that amyloid plaques may act to sequester monomers and prevent the formation of toxic amyloid oligomers [60, 59]. In light of this observation, there are two very different possibilities for the interpretation of these results. If we consider an increase in motility to indicate neuronal dysfunction, then the reduction in plaques in ckr-2 knockdown worms compared to controls may suggest a failure to sequester the toxic species. If we consider an increase in motility to demonstrate a protective effect, then the reduction in plaques may suggest enhanced disaggregation

and proteolytic activity. Both findings would be in line with previous observations in post-mortem AD brains [213]: the decrease in CCKBR expression in the cerebral cortex either indicates an enhancement of neurodegeneration by loss of CCKBR or an incomplete compensatory mechanism. Given that increased CCK correlates with decreased cognitive impairment, however, the first explanation seems more likely. In either case, these findings merit further study. Given the relationship between ckr-2 and changes in feeding behaviours, both feeding and tracking assays on solid media should be conducted. Furthermore, an assay quantifying oligomer concentration across ckr-2 knockdown and control conditions should also be performed.

5.2.5 Knockdown of skr-21 results in increased worm motility and a reduction of plaque formation

SKP1 is an essential component of the SCF complex, a type of E3 ubiquitin-protein ligase complex that regulates cell cycle control. This protein is widely expressed, with low tissue specificity. E3 ligases play important roles in ubiquitination, as they determine the substrate specificity of the reaction. While SKP1 is only represented once in the human genome, the skr (or SKP1-related) family in*C. elegans*is made up of at least 21 genes [217]. Previous RNAi studies of the skr family show no abnormal morphology or embryonic development when knocking down skr-21, unlike some other members of the family [217, 218]. Furthermore, skr genes have been found to be involved in hyperfunction-related ageing in *C. elegans* a process in which genes are overactive during adulthood lead to hypertrophy-associated pathology [219]. Skr-21, however, is mostly active during the later part of the life of the worm (after day 6 of adulthood) [219].

Given this information, it is possible that expression skr-21 mediates normal ageing of the worm. This explains why there is relatively little effect when knocking down skr-21 in N2 worms until day 8 of adulthood, wherein a significant increase in motility can be observed (Fig. 5.8). By contrast, knockdown of skr-21 shows a decrease in motility early in the life of CL2355 worms (day 4), but provides a substantial resistance to decline in motility over time. It is possible that expression of Aβ in CL2355 accelerates ageing, driving early expression of skr-21, and that knockdown of skr-21 suppresses some of this phenotype. However, transcriptomic or proteomic studies are necessary to further investigate this effect. The precise mechanism by which knockdown of skr-21 results in a decrease in amyloid plaque formation remains unknown.

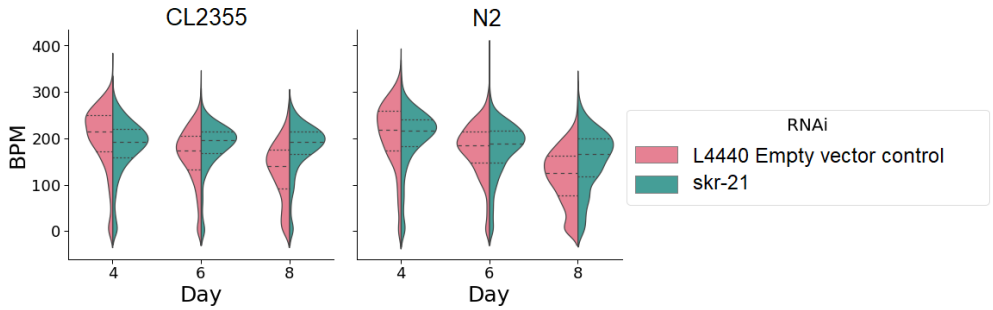

Fig. 5.8 **Results of thrashing motility assay upon *skr-21* knockdown.** Results of thrashing motility assay on skr-21 knockdowns and controls using the WF-NTP. *Skr-21* shows a decrease in motility early in life, but a resistance to motility decline over time.

5.2.6 Knockdown of Y92H12A.2 results in decreased motility and a reduction in amyloid plaque formation

The *C. elegans* gene Y92H12A.2 is an ortholog of the human ubiquitin ligase UBE3A. In addition to its role in misfolded protein clearance through the UPS, UBE3A is also involved in normal synaptic function and plasticity. Loss of UBE3A has been linked to a number of diseases, including Angelman syndrome and Prader-Willi syndrome, both of which are characterised by cognitive deficits [220]. Further, UBE3A has been implicated in progression of Huntington's disease in mouse models [220]. Most relevant, previous studies in mouse models of AD have also shown that UBE3A deficiency showed both accelerated cognitive and motor decline, but also a decrease in amyloid plaque formation in the brain [220, 221]. In one of these studies, using a mouse model that over-expresses amyloid-β with the Swedish mutation, found that loss of the UBE3A ortholog preceded dendritic pruning and that the loss of this protein was mediated by a loss in its solubility [221]. This effect was reversed upon rescue, suggesting that UBE3A is a potential druggable target.

Our own study of Y92H12A.2 is consistent with the results from the mouse model. We show enhanced motility decline in Y92H12A.2-knockdown CL2355 worms compared to untreated controls (Fig. 5.9). Further, no significant, sustained decline can be seen in knockdowns of N2 worms. The motility decline in CL2355 worms is apparent on days 4 and 6 of adulthood, but is abated by day 8. This result may suggest that Y92H12A.2 is most active earlier in the life of the worm, although further study is needed to confirm this suspicion.

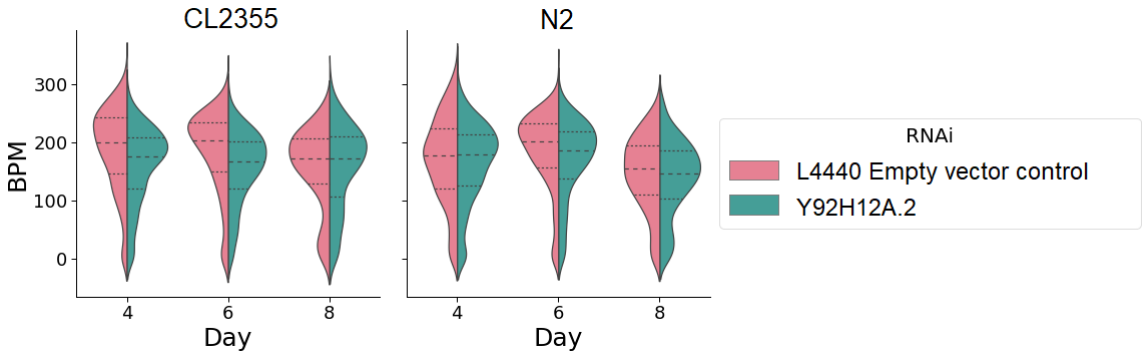

Fig. 5.9 **Results of thrashing motility assay upon *Y92H12A.2* knockdown.** Results of thrashing motility assay on *Y92H12A.2* knockdowns and controls using the WF-NTP. An enhancement of motility decline can be seen in the knockdown worms compared to controls.

Mirroring the findings in mouse models [220], we find that Y92H12A.2 knockdowns are associated with a steep decline in amyloid plaque formation. Interestingly, the authors of the study in mouse models propose increased activity of γ-secretase and ADAM10 that shifts proteolysis of APP toward the non-amyloidogenic pathway as the mechanism for the lack of amyloid plaque formation. Our model, however, expresses no APP (only Aβ1-42), suggesting that the link between Y92H12A.2 loss and plaque formation may be mediated through interaction with Aβ itself. The decline in motility could, as stated previously, be related to the failure to sequester Aβ oligomers in plaques.

5.3 Limitations

As previously discussed, inconsistency in the phenotype of CL2355 worms makes the results of this study difficult to interpret. Although the expression of amyloid-β in this strain has been verified by Western blot (Fig. 5.1A), this tells us very little about the variance of amyloid-β expression within the population. If we take fluorescence intensity of the intestinal transgene marker to be a reasonable facsimile of amyloid-β expression, it is evident that there is high variation in transgene expression in the CL2355 strain (Fig 5.10).

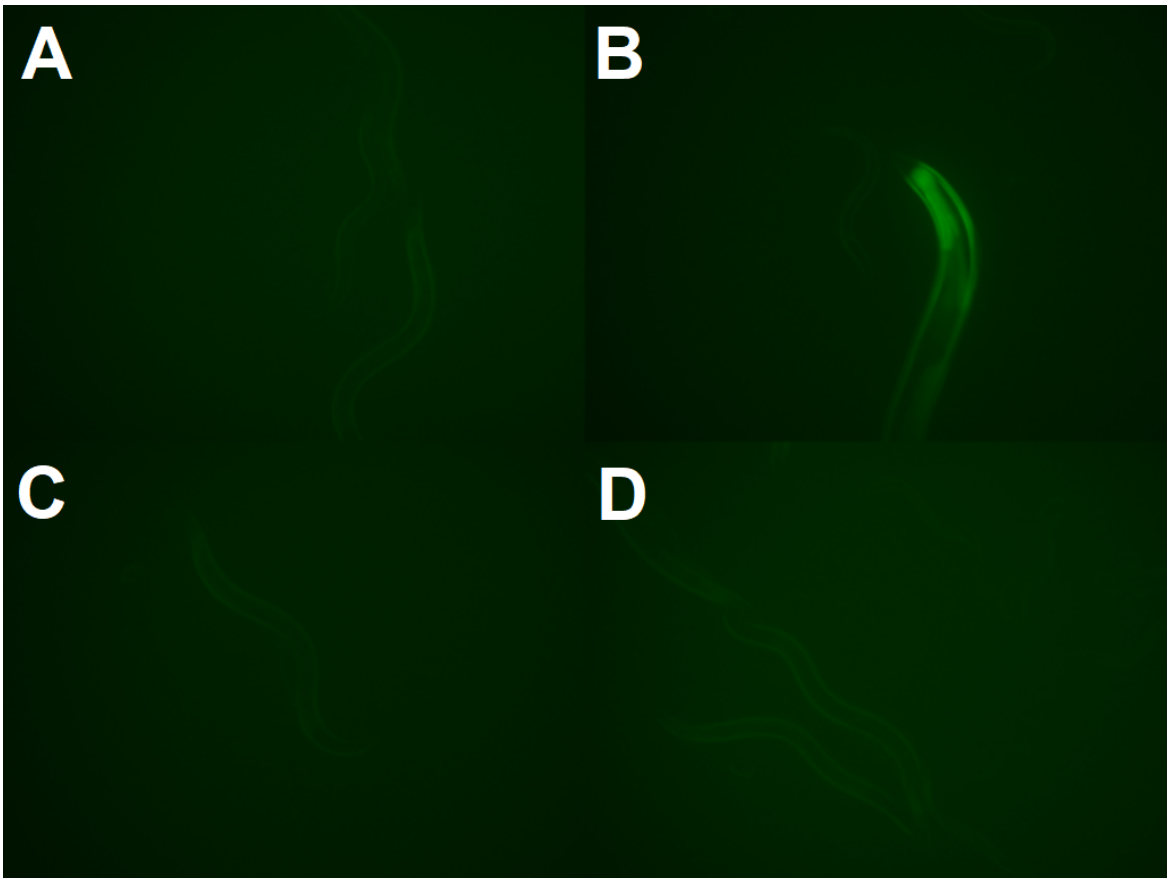

Fig. 5.10 **CL2355 worms show high variation in expression of the GFP intestinal marker.** CL2355 worms show a great deal of variation in expression of the GFP intestinal marker. The adult in the Panel B shows clear GFP fluorescence in the gut, whereas adults in the other three panels show limited gut fluorescence. All images were taken at the same light settings, adjusted to the minimum needed to visualise GFP fluorescence. Images were not brightened due to interference from intestinal autofluorescence.

Unfortunately, this inconsistency affects both of the read-outs in this study: motility screening and quantification of amyloid plaques. The effects on motility screening are quite evident. The effect size of RNAi treatment as measured by the thrashing assay strongly varies across worms raised from different bleaches, making it extremely difficult to reproduce motility results (Fig 5.11). In this case, we can clearly see that there is significant difference in motility between biological replicates of CL2355 worms. Not only is there a great degree of variation between replicates of CL2355 worms without knockdown (L4440 empty vector control), but also in the effect of the knockdown. For example, knockdown of K03A1.4 and skr-21 shows a results in a reduction of motility in Replicate 2, while the same knockdowns do not

result in substantial changes in the phenotype of worms from Replicate 1. Previous studies using the WF-NTP have demonstrated that the thrashing motility assay gives consistent, reproducible results in a number of strains, including GMC101 and N2 [188]. Results such as these could be due to differences in the penetrance of RNAi from replicate to replicate or from differences in expression of the transgene. It is highly likely that both contribute to problems with reproducibility. It is also possible that these issues may be overcome by vastly increasing the population sizes, as was done by Perni and colleagues [188]. However, this may have negative impacts on throughput.

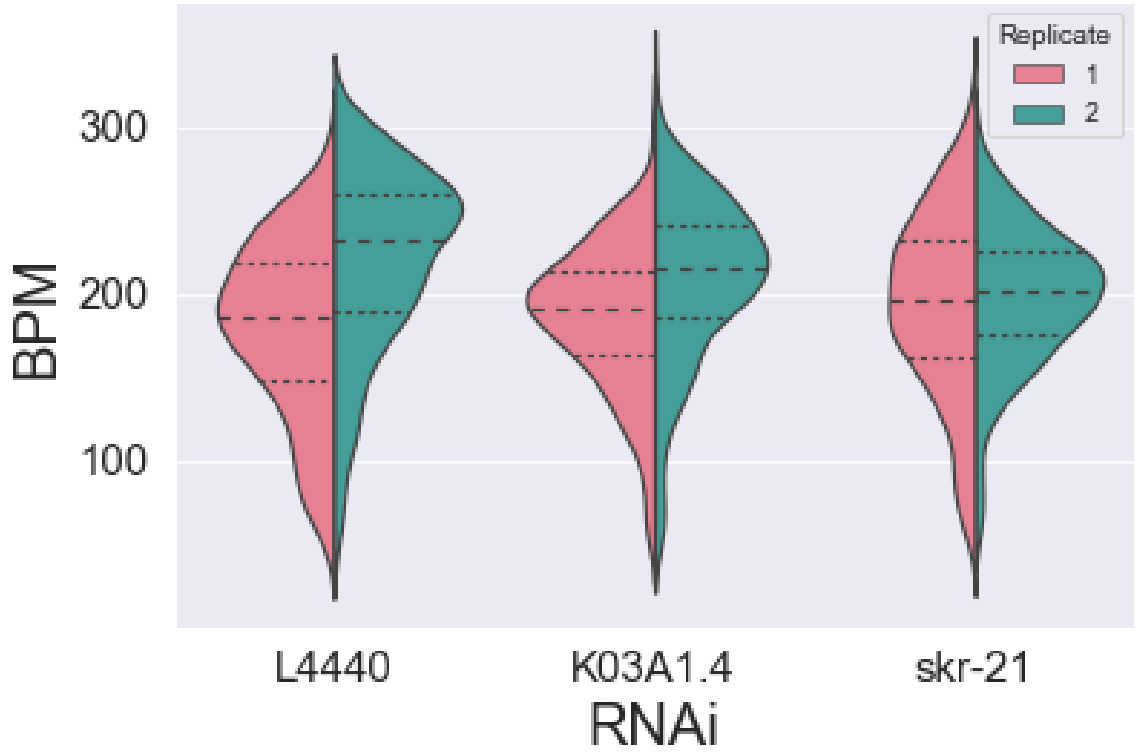

Fig. 5.11 **Comparison of thrashing motility assay results biological replicates of CL2355 worms** CL2355 worms show large variation across biological replicates in BPM calculated from the WF-NTP thrashing motility assay. Replicates compared here are all taken from day 4 of adulthood, and each biological replicate is itself data pooled from two technical replicates.

The same problems of reproducibility also affect plaque quantification, with plaques being visible in untreated CL2355 controls in only a fraction of biological replicates. Complicating matters, the nature of the imaging experiments required a relatively low number of worms (n=20-30). Live worms mounted on slides only

remain paralysed for a short period of time, and their movement can create a blurry image. And excessive crowding of worms on the slide results in overlaps, particularly once the agarose pad begins to dry and the worms are pulled closer together. Worms overlapping in an image cannot be considered for quantification, as it is impossible to determine which worm a plaque is in. As a result, even in the weeks where untreated controls have plaques that can be imaged, the reduction in plaque formation we see in some RNAi conditions could simply be due to sampling error.

If only one of these measures were potentially compromised, we could attempt to correlate them as an external check. However, the nature of the problem calls both BPM calculation and plaque quantification into question. Even still, we attempted to correlate dBPM Score with the Normalised %Area of the plaques (Fig 5.12). The dBPM Score was defined as the mean of the absolute value of the difference in the mean dBPM at each time point. The absolute value was used because the magnitude of the effect is more meaningful than its direction, particularly when considering aggregation-induced chorea. Because we could only successfully stain worms in 5 knockdown conditions, the data is extremely limited. While a vague trend can be seen, there is not a sufficiently clear relationship between the dBPM Score and plaque deposition to draw the conclusion that they correlate well, particularly given the small sample size. A summary of the data in Fig 5.12 can be found in Table 5.4.

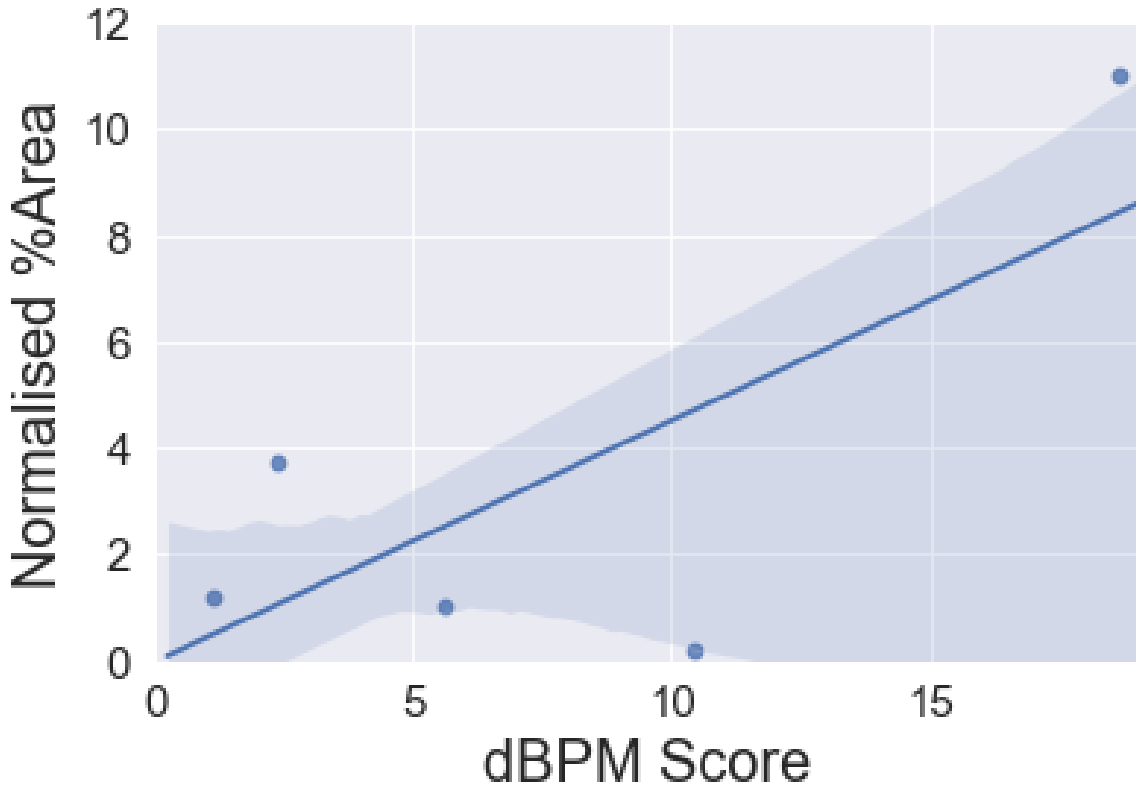

Fig. 5.12 **Correlation of dBPM Score and Normalised %Area of amyloid plaques.** There is no clear correlation between dBPM Score and the and total area of plaques in the heads of CL2355 worms. This may be reflective in the limitations of both measures stemming from variable phenotype in the CL2355 strain.

Gene name	dBPM score	Normalised %Area
Y92H12A.2	1.113	1.2
ckr-2	2.348	3.73
R03D7.5	5.614	1.01
skr-21	10.405	4.18
K03A1.4	18.631	11

Table 5.4 Table 5.4 dBPM Score and Normalised %Area of amyloid aggregates.

5.4 Conclusions

The three experimentally-validated hits from our study are members of two KEGG pathways: ubiqutin-mediated proteolysis (*skr-21* and *Y92H12A.2*) and neuroactive ligand-receptor interaction (*ckr-2*). Because we were only able to test a subset of our 23 hits, this does not suggest that these are the only pathways that interact with amyloid-β in our model. However, there may be useful information that can be extracted from these results. First, the fact some *skr* genes and not others appear to be hits despite the gene family's high sequence homology suggests that the differences in their sequences may reveal new information about the substrate specificity of SKP1. Upon further interrogation of the subset of *skr* genes that appear in our 23 hits (in addition to *skr-21*, *skr-16* and *skr-5* also remain to be evaluated), we will be able to see what sets apart the sequences of those *skr* family genes that are modulators of amyloid-β aggregation from those that are not. Furthermore, the finding that *Y92H12A.2* has an effect on amyloid-β aggregation in our model seems to confirm our methods, as this agrees with studies done on higher-order organisms.

Lastly, our finding that the CCK receptor ortholog *ckr-2* acts as a modulator of amyloid-β aggregation in our model means that *C. elegans* may be a suitable system in which to study the mechanism by which to study the involvement of CCK in AD. Although both older evidence from post-mortem brains [213] and newer studies [206] suggest that CCK is a biomarker for the disease, the mechanism remains unknown. Leveraging the ease of use of the *C. elegans* system and more advanced assay methods, we may be able to fully articulate this connection through further study.

The severe limitation imposed on this screen by the inconsistent phenotype of the CL2355 worm suggests that we must be cautious in our interpretation of these findings. What may appear to be an effect could simply be down to statistical noise. And those knockdowns that appeared to have no effect may have been masked by the poor phenotype. It is essential that this study be repeated in a more robust *C.*

elegans model. Thankfully, more pan-neuronal amyloid-β strains—such as GRU102—have been generated in recent years, and one of these strains may serve as a better model for a similar study.

5.5 Materials and Methods

5.5.1 Worm strains and maintenance

All *C. elegans* strains were grown at 20 °C unless otherwise specified. For the experiments carried out in this chapter, the CL2355 pan-neuronal Aβ (dvIs50 [pCL45 (snb-1::Abeta 1-42::3′ UTR(long) + mtl-2::GFP] I) and N2 Bristol wild-type strains were used. The CL2355 strain was maintained at 16°C to reduce selection against the transgene. Both strains were obtained from the Caenorhabditis Genetic Center at the University of Minnesota.

For RNAi experiments, worms were first raised on NGM plates seeded with OP50 E. coli and transferred to RNAi plates, a variant of NGM containing FUdR (12.5 mg/mL), ampicillin (50 µg/mL) and IPTG (15 µg/mL), seeded with dsRNA-expressing E. coli.

5.5.2 E. coli strains and culture

OP50 E. coli were cultured in LB medium overnight in 1 L flasks, spun down, and concentrate to a 10x solution before plating. RNAi-expressing bacteria (HT115(DE3)) were cultured overnight in LB medium plus 50 µg/mL ampicillin, spun down, and resuspended in water and 15 µg/mL IPTG before plating. OP50 bacteria were originally obtained from the Caenorhabditis Genetics Center, and RNAi-expressing bacteria from the Ahringer RNAi Library were kindly provided by the group of Ellen Nollen at the European Research Institute for the Biology of Ageing.

5.5.3 Worm thrashing assay

All worm populations were cultured at 20 °C and age-synchronized from a 4-hour egg lay and allowed to proceed through larval stages on OP50 E. coli. At 64 to 72 hours after egg lay (day 1 of adulthood), worms were shifted to NGM plates with HT115(DE3) E. coli[1]——an RNase III-deficient strain with IPTG-inducible T7

[1]The transfer from one strain of bacteria to another is intentional. In our experience, knockdowns before the L4 larval stage can cause larval arrest. And maintaining all strains on L4440 empty vector

polymerase activity——expressing dsRNAs from the Ahringer RNAi Library. To record videos for the assay, worms were washed from their original plates with 2 mL M9 buffer and transferred to tracking plates containing 4 mL M9 buffer each. Worms were then spread evenly across the tracking plate and 60-second videos were recorded at 20 fps on a homemade microscope setup at 0.75x magnification. Videos were recorded using the FlyCap2 video capture software. Experiments were conducted in duplicate, and each replicate contained 200-400 worms, with much of the variance arising from washing efficiency. Statistical analysis was carried out using the Python statistical packages SciPy and Sci-Kit Learn. A complete protocol follows with comments where relevant. Unless otherwise specified, all experimental conditions represent 1 biological replicate consisting of 2 technical replicates.

Protocol:

1. Transfer the required number of tracking plates from the cold room to the laboratory bench and allow them to warm to room temperature. Unstacking the plates greatly decreases the time taken for this step.

2. While the tracking plates warm, darken the room and remove RNAi plates from the incubator. Randomize the order of the knockdowns being assayed but keep the L4440 empty vector condition in the middle of the assay order. The randomization prevents any systematic bias arising from the order in which the plates are assayed. Assaying the controls in the middle of the assay order minimizes the time between any given knockdown condition and the control. While keeping the plates in order, wrap them in aluminium foil to prevent any effect created by leaving the worms in the light for varying amounts of time. At this point, lights may be turned back on in the room.

3. Line up tracking plates agar-side down on the bench and fill each with 4 mL M9 buffer. The 4 mL volume is recommended as it leaves a sufficient amount of liquid in the tracking plate for the worms not to immediately settle to the bottom while also not filling the plate so much as to make handling cumbersome.

4. Remove the appropriate number of RNAi plates from the stack, making sure to leave the rest of the plates under the foil. Gently wash worms from RNAi

bacteria prior to transfer to RNAi conditions compromises the assay due to novelty effects. Worms are known to avoid novel food sources and preserving food novelty for all conditions prevents confounds due to differences in the amount of bacteria consumed.

plates with 2 mL M9 buffer transferred using a P1000 micropipette. Take care not to wash too much bacteria from the plate, as cloudy buffer can occlude the tracking plate and make tracking impossible. When washing, hold the plate at a 45°-angle, and transfer M9 onto the top edge of the plate where no bacteria has grown. Then return the plate to a level surface and tilt the plate to allow the M9 to cover the entire surface of the plate. Finally, return the plate to a 45°-angle and allow the worms to fall to the bottom (this should only take a few seconds) and pipette up the remaining liquid. Approximately 1 mL of M9 will be absorbed by the plate during this process. If worms appear stuck in the bacteria, simply leave the plate level on the bench for 15-30 seconds after allowing the M9 to cover the surface; many of the worms will move from the bacterial lawn to the liquid during this time without excessively disrupting the bacteria.[2]

5. Transfer the worms to a tracking plate and spread the worms evenly across the surface. The most efficient way to do this is to hold the plate on a level surface and move it back-and-forth and side-to-side 2-3 times. Worm collisions reduce the reliability of tracking data and these motions have been found to be the quickest way to separate the majority of worms.

6. Place the tracking plate on the platform above the camera, making sure to centre it in the field-of-view. Zoom in using FlyCap2——not with the camera itself——to make sure the worms are in focus and adjust the focus as necessary. Never adjust the magnification on the camera during the assay. Pouring tracking plates at a consistent depth will prevent the number of times one must make focus adjustments.

7. Record the video. While the video records, proceed to the next set of RNAi plates and return to Step 4.

8. When the video has finished recording, you may discard the tracking plate or otherwise remove it from the immediate area.[3]

[2]Although the level of detail in this step may seem excessive, it is extremely important to get consistent results and videos that can be easily tracked. While one can always change parameters on the WF-NTP software to optimize worm tracking, an occluded video will never produce reliable tracking results.

[3]Because tracking plates are by their nature unlabeled, it is not recommended to keep more than one set of tracking plates with worms in them on the bench at a time. This reduces human error.

5.5.4 NIAD-4 staining

Unless otherwise specified, all steps after using NIAD-4 (Sigma) were performed in the dark to maintain the integrity of the stain. Worms were maintained as above, washed from RNAi plates as described in Step 4 of the thrashing assay, and transferred to 15 mL Falcon tubes using glass Pasteur pipettes. Worms were then allowed to sediment by gravity. After sedimentation, the worms were washed with M9 and allowed to sediment again. The worm pellet was then taken up and transferred to protein low-bind plastic test tubes. 1 mL of 10 µM NIAD-4 in 1% DMSO was then transferred to each tube. Worms were allowed to incubate in this solution for 4-6 hours with shaking. At the end of the incubation, worms were sedimented on the bench a final time. Pellets were then collected and transferred to tracking plates to de-stain overnight in a 24°C incubator.

For imaging, worms were washed from tracking plates and transferred to protein low-bind plastic test tubes. After sedimentation, 50 µL of the worm pellet was taken up and transferred to a 0.8mm agarose pad and anesthetized by the addition of a 5 µL drop of 50 µM sodium azide (Sigma). A glass cover slip was then placed over the pad and the slides were imaged immediately on an EVOS5000 light microscope with a Cy5 filter. A more detailed protocol follows.

Protocol:

1. Using approximately 2 mL of M9 buffer, wash worms off RNAi plates with a glass Pasteur pipette. Glass is less likely to retain worms and exact volumes are less important for this experiment. Transfer worms to a 15 mL Falcon tube.

2. Fill the Falcon tube to 10 mL with a serological pipette and leave it upright in a rack on the bench for 10-15 minutes. Allow worms to settle by gravity. This reduces the amount of bacteria that comes with the worms and improves the quality of the stain.

3. Remove supernatant with a serological pipette, being careful not to disturb the worm pellet. The worm pellet is extremely delicate and can be easily disrupted.

4. Refill the Falcon tube with M9 to 10 mL and allow the worms to settle again.

5. Transfer the pellet to a protein low-bind plastic test tube using a glass Pasteur pipette. In our experience, protein low-bind tubes are less likely to retain worms and do not allow worms to stick to the sides of the container during shaking. Label the test tube.

6. Turn off the lights and prepare 10 µM NIAD-4 staining solution in 1% DMSO. Add 1 mL of the staining solution to the test tube.

7. Place test tubes in a container and shield the tubes from light using aluminium foil. Place the container on an orbital shaker at room temperature for 4-6 hours. Longer incubation does not necessarily improve staining efficiency and requires longer de-staining times.

8. Retrieve the container from the shaker, turn off the lights, and allow worms to sediment on the bench for 10-15 minutes.

9. Using a P200 micropipette, transfer 20-50 µL of the worm pellet to a tracking plate. A P200 micropipette is the smallest one should use for the transfer of worms, as anything smaller has too narrow a mouth to prevent a great deal of sample loss.

10. Incubate tracking plates overnight at 24°C. This hastens aggregation slightly and allows for imageable amyloids.

11. Using approximately 1 mL M9, wash worms from the tracking plate into protein low-bind tubes using a glass Pasteur pipette. Allow worms to sediment. Gravity sedimentation at this step reduces the amount of NIAD-4 precipitate compared to sedimentation by centrifugation.

12. Transfer 40-50 µL of the worm pellet to a 0.8mm 5% agarose pad on a glass slide. Agarose pads should be prepared fresh to prevent excessive drying. A good tutorial on the preparation of agarose pads can be found on WormBook. The 0.8mm thickness was chosen over the more common 0.4mm as it gives more time to conduct imaging before sample desiccation.

13. Add 5 µL of 50 µM sodium azide to the drop on the agarose pad to anesthetize the worms. Place a glass cover slip onto the pad by dropping the slip onto the pad at a slight angle. This reduces the amount of air bubbles trapped under the slide.

14. Image the sample using a Cy5 or other appropriate filter.

5.5.5 Image analysis

Image analysis was conducted using ImageJ. Fluorescent images were first pre-processed using Phansalkar local thresholding with a radius of 20 pixels followed

by standard despeckling. Using the transilluminated image as a guide, head regions were defined for each worm in the image. The head region was defined as the area from the mouth to an area just caudal to the pharynx at the approximate location of the pharyngeal-intestinal valve. Particle analysis was carried out for each of these regions, and the %Area metric was extracted. Finally, %Area was normalised against untreated controls as baseline.

5.5.6 Statistical methods

Statistics in Phase I of the screen were conducted by dBPM calculation (the difference between each condition and untreated controls). These dBPMs were then plotted on a histogram, where three clusters of genes fairly obviously appeared. These clusters were then separated using k-means++ for 3 means.

In Phase II, statistics were conducted by first separating outlying data through deconvolution on the assumption that the data represented a mixture of Gaussian distributions. The deconvolution was done using the Sci-kit Learn package in Python. A distribution of dBPM within each strain was calculated using **Eqs. 1** and **2**. These dBPMs were then compared using a two-tailed Student's t-test with $\alpha = 0.05$ as the cut-off for significance.

For the image analysis, significance of %Area was established using a two-tailed Student's t-test with $\alpha = 0.05$ as the cut-off.

5.5.7 The adaptation of low-throughput methods for high-throughput experiments

The main set of experiments presented in this chapter, the thrashing motility assay, was conducted using the WF-NTP. Although the resolution of the data produced by the WF-NTP is far higher than motility data collected by traditional methods, the system was not designed with the throughput of a large screen in mind. Prior to its adaptation for this RNAi screen, the WF-NTP has chiefly been used for drug screening, only testing a few concentrations of a drug at a time: a far cry from the 142 genes screened in this study. Considering the optimization steps required for any such screen, as well as the usual challenges of laboratory work (contaminations, poor yields from bleaches, etc.), the only sure-fire way to screen all candidate genes in a reasonable timescale was to screen between 10 and 20 genes per week. As a result, our efforts for method development focused chiefly on performing the thrashing assay consistently and reliably at this volume of experiments. I present

in this section the various adaptations of the screening protocol that we attempted, including several experimental set-ups that were eventually abandoned and the rationale behind both the attempt and the eventual rejection of these methods. I also describe the solutions to these problems that we eventually reached. The aim of this section is two-fold: that others may benefit from the knowledge that these set-ups are not viable—and therefore they and similar set-ups should only be employed with the utmost caution—and that useful, generalisable principles regarding the adaptation of low-throughput methods for high-throughput experiments may be extracted from our setbacks and successes.

The volume of RNAi plates required poses an issue for reproducibility

Among the first issues we encountered was that variation across different batches of RNAi plates appeared to result in a variation of knockdown efficiency. We initially discovered this issue when a series of knockdowns induced a motility phenotype in one set of experiments and not in others. Although we were unsure of the precise source of this variation, we identified a reduction in the number of batches of plates produced as the obvious solution. In order to screen 20 genes at 4 time-points in 2 worm strains with 2 technical replicates for each day, 320 RNAi plates must be produced. We prepare media in 1 L Duran bottles, each producing approximately 45 RNAi plates. That means that 8 L—and therefore 8 batches—of RNAi medium had to be prepared for each week's experiments. Sufficient variation across these 8 batches would jeopardize the validity of our experiments.

To resolve this issue, we pursued the development of a liquid culture protocol, wherein worms would be raised in liquid medium on tissue culture plates. There were many potential benefits to this solution. First, the proposed culturing medium, S-complete, could be prepared in a single large batch and distributed over many culturing plates, eliminating issues associated with variation across batches. Second, since the thrashing assay could be conducted in the culturing plate itself, there was no need to transfer worms out of the plate at any point. As a result, the same plates of worms could be assayed for each screening day. This was particularly appealing because it would provide data on the rate of worm death in each condition. Finally, the reduction in the number of plates necessary to screen a given number of genes meant that the replicate count could be increased.

In practice, nearly all of what we believed about the liquid culture protocol was true, save for one complication. After several days in liquid culture, the worms began to stick together at the head or tail (Fig 5.13). At first, only one or two worms would

stick together, which did not seem to pose a serious threat to the experiment. But, with time, an increasing number of worms would join these aggregates. Eventually, nearly every worm on the plate would form a part of this ball. Not only was this an issue due to changes in motility behaviour, but the worms no longer occupied a single focal plane, making imaging impossible. Physically shaking the plates did little to disrupt these aggregates. Our initial assumption was that worms were coalescing around salts precipitating from solution, since we had observed solids gradually falling out of the S-complete buffer. However, tests we conducted using a wide variety of buffers demonstrated that the phenomenon occurred regardless of the buffer tested, although the rate of formation of the initial aggregate did seem to vary. It was only after correspondence with other experimentalists that we realised that the worms moulted inefficiently in liquid culture. The previous moults of the worms, still hanging from their bodies, formed sticky surfaces to which other worms would get stuck. A positive feedback loop then accelerated the process. Our conjecture is that this does not happen on solid media because the friction between the worm and the agar allows for the moult to slip away. Unfortunately, we were unable to solve this problem in a timely fashion and were forced to abandon optimization of the liquid culture protocol. If this problem can be solved, liquid culture may yet prove to be a powerful tool for the WF-NTP.

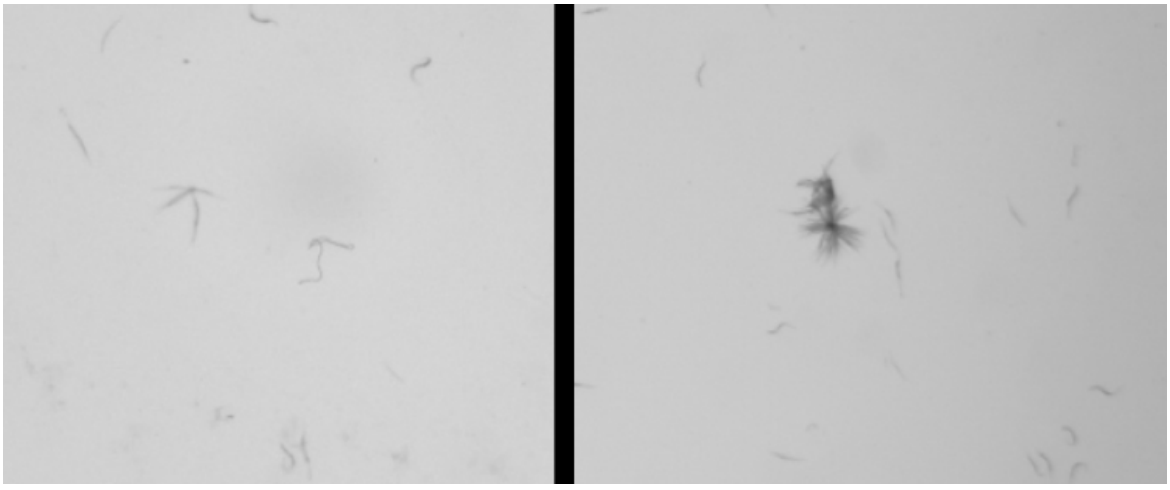

Fig. 5.13 **Agglomerations of worms.** Due to incomplete moulting, worms may stick together when raised in liquid culture. The left panel shows an agglomeration after only one day in liquid culture. The right panel shows a larger agglomeration after three days in liquid culture.

Ultimately, we found that the variance in the preparation of RNAi medium was due to variance in available IPTG. We had added IPTG to the RNAi medium while it

was still too hot, well above 65 °C. We tried to get around this by allowing the RNAi medium to cool sufficiently before the addition of IPTG, but cooling of the medium in local areas meant that some of the agar often set before the medium reached an average temperature of 65°C. Not only did this create waste, but it also meant that the IPTG concentration still varied across batches. Finally, we decided to resuspend the RNAi-expressing bacteria in a solution of water and IPTG prior to seeding and spread this solution across the plates. This ensured that the concentration of IPTG was consistent on every plate, regardless of the batch from which the plate was produced. Although we never conclusively proved that the issue was IPTG, our experiments were far more reproducible after this change in plate preparation protocol.

The use of FUdR for age-synchronisation may confound the Aβ-specificity of knockdown-induced phenotypes

It is well documented that FUdR exposure initiates a variety of transcriptional changes in both wild-type and mutant *C. elegans* strains. In our hands, knockdowns of certain genes (such as the E3 ubiquitin ligase uba-1) resulted in an increase in mortality in GMC101 worms raised on FUdR compared to those that were not. Although we made no note of such issues when doing knockdowns in CL2355 worms, our primary concern was the possibility that knockdown-induced phenotypes may be dependent on the Aβ-FUdR-RNAi interaction, rather than just the Aβ-RNAi interaction.

The most common alternative to chemical sterilization of worms for age-synchronization is age- synchronization by manual picking. Given the large number of worms per experiment—usually between 80-100,000—this was not a viable option. Instead, we collaborated with the group of Andrew de Mello at ETH Zürich to develop an improved version of their microfluidic worm sorter, which was designed to separate adult worms from larvae at all developmental stages (Fig 5.14). We hoped that we could adapt their device for high-throughput experiments, and that we could simply sort the worms each screening day prior to the motility assay.

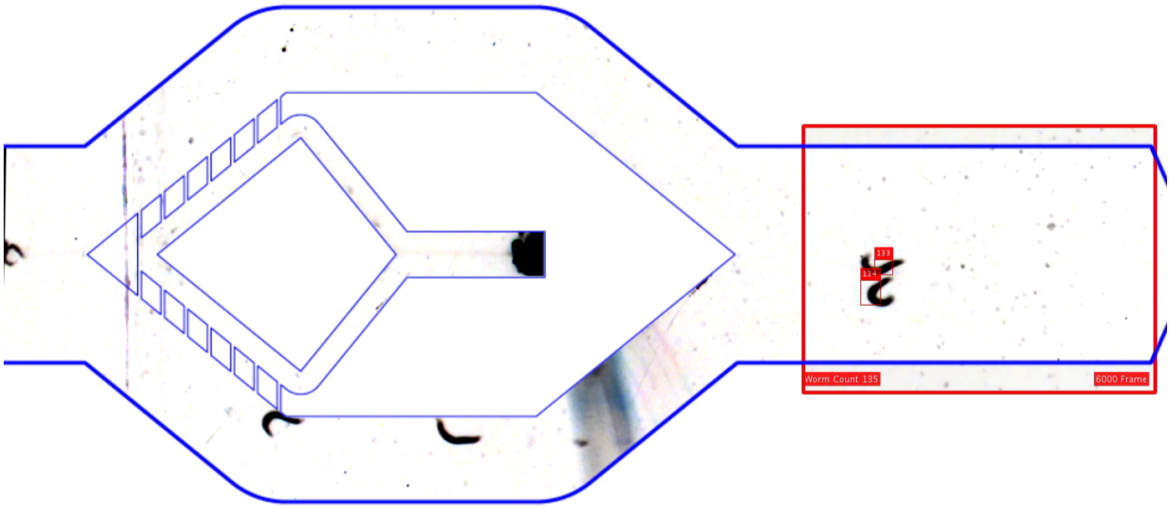

Fig. 5.14 **Microfluidic worm sorter.** The worm sorter developed in collaboration with the de Mello Group at ETH Zürich. A mixed population of worms enters the chamber on the left side of the chip. Larvae are pulled into the central chamber by fast currents through the smaller channels into a waste container. Adult worms (red box) are carried out to another container.

Even after correcting for potential operator error and many iterations on the design of the sorting chip, it still took approximately 3 hours to sort 300 worms: the equivalent of a single plate. In the end, the microfluidic worm sorter had to be abandoned as a mode of age-synchronization, and we returned to our use of FUdR, accepting the potential pitfalls that accompany it.

The length of screening time may make it difficult to compare measurements ostensibly taken at the same time point

We made several changes to adapt the protocol, primarily inspired by the assembly line. When a single person must perform every step of a protocol for each condition being assayed before moving to the next, completing a series of assays can be quite slow. However, when the same protocol is divided into discrete tasks that can be done all at once (i.e., do Step 1 50 times, proceed to Step 2)——essentially forming a one-person assembly line——a large amount of time can be saved. I attribute this increase in speed to "hitting a rhythm," wherein time taken for a given task is greatly reduced just because one does not have to switch between different tasks. This allows for an automation of movement that not only speeds up the work, but also provides more consistent results that are less prone to error or confusion due to

fatigue. For the same reasons, each task should be simplified to the greatest extent possible.

In concrete terms, we amended the WF-NTP protocol in the following ways: (1) Rather than filling each tracking plate with M9 buffer just prior to assaying the plate, we filled many tracking plates and lined them up on the bench. This way, when washing worms off the plate for the assay, one can simply pick up a pre-filled tracking plate, set up the assay, and move on to the next wash with no time in between. (2) Video file naming conventions had only two fields that needed to be changed between each assay: the gene name and the worm strain. The gene name was written as one would expect, and the strains were represented by a single letter ('A' for CL2355 and 'C' for N2, indicating 'Aβ' and 'control' respectively). When performing the assay, plates were ordered such that only one field had to be changed when switching between conditions. For example, if one were assaying GeneX and GeneY, one would assay GeneX_A, GeneX_C, GeneY_C, and GeneY_A in that order. Although this only saves a few seconds per plate, those seconds do add up. And only having to change one field reduced error when entering the file names into FlyCap. (3) Simple physical actions with reproducible results were found for the portions of the assay that were conditional upon the state of the plate. Namely, such actions were found for the worm washing and spreading steps of the assay, detailed at length in the protocols above. (4) The control group was always placed in the middle of the order of the assay, ensuring that the maximum difference in the time-point taken is half the length of the total screening time.

With all these changes, the screening time for each plate was reduced to 90 seconds, bringing the total time for screening 20 genes down to 2 hours—a 50% reduction. Human error during screening has also been abated. The rigidity of the organisation of the assay means that what few errors do occur can be corrected almost immediately and with little effort.

Considerations on the use of high-throughput and low-throughput methods

The core difference between low-throughput and high-throughput methods in a research setting is in the philosophy behind their design. While low-throughput methods can and should be optimized around ideal data collection for each sample, the pursuit of this kind of optimization for high-throughput methods ultimately compromises the integrity of every measurement taken. High-throughput methods should be designed with speed and simplicity in mind. Any method that requires heavy monitoring or intervention by the practitioner should be approached with

caution, and any adaptations that can be made to reduce such steps while preserving consistency and reliability in data collection should be employed.

Lastly, the importance of iterative development cannot be overstated. Although a common impulse is to try to account for all possible pitfalls before undertaking an experiment, I have learned that this is a strategic error. Experiments should be attempted and post-evaluated as many times as necessary to both build physical skill in performing the assay and determine what procedures succeed or fail in practice. In the words of boxing heavyweight Mike Tyson, "Everyone has a plan until they get punched in the mouth."

All that begins also ends.

Seneca, *Of Consolation, To Polybius* (43 AD)

This is my conclusion for now.

The Cranberries, *Illusion* (2019)

6

Conclusions and Future Directions

The aim of the studies presented in this work has been to improve animal models of sAD. Our initial attempt to develop an sAD model in *C. elegans*, the BAG-Aβ worm, was successful in that it demonstrated a subtle, but measurable phenotype. But it fell short of our goal, in that the methods needed to quantify these effects were, unfortunately, difficult to assay at high-throughput. As a result, this early model was unsuitable for screening the nTWAS-generated AD Gene List down the line.

Our next attempt, using an existing *C. elegans* amyloid-β pan-neuronal model (CL2355), appeared more fruitful albeit with significant limitations. From a list of 142 potential modulators of amyloid-β aggregation, we were able to extract a core list of 23 hits. These genes represent members of several biochemical pathways that are related to AD, and the validation of three of these hits—namely, *ckr-2*, *skr-21*, and *Y92H12A.2*—both through our motility assay and by staining and imaging. The variability in the phenotype of the CL2355 worm strain, however, poses significant challenges for interpretation of these results. There is some irony that a study intended to improve animal models of sAD was itself hampered by an imperfect model. I am hopeful that this project will yet yield useful information about the underlying causes of AD upon the full validation of our hits in another *C. elegans* model system. The fact that our early results are well-evidenced by both historical

and contemporary literature indicates that our findings may still be valid. In time, the culmination of this work will be to use our final results to inform further research in other models, including induced pluripotent stem cells. I can only imagine what insights these future studies may bring.

Even so, there remains work to be done even in the model system presented here. These experiments must be repeated in a more robust pan-neuronal amyloid-β worm strain. Ideally, this strain should be crossed into an RNAi-sensitive strain, particularly one with additional RNAi-sensitivity in neurons. Upon completion of that screen, the hits must be experimentally validated by imaging, and the knockdowns we perform must be verified by qRT-PCR. Time should be taken to design primers that do not give false negatives by amplifying the wrong sequence and to optimise other elements of the experiment. However, the induction of a phenotype is typically a good indication that the knockdown has been successful, as the false positive rate is less than 1%, albeit this figure was judged by traditional assay methods [198].

Second, the statistical methods presented here bear revisiting. Although the dBPM calculation and comparison may be mathematically and statistically sound, it does not always yield biologically relevant results. Two dBPM distributions having statistically significant differences says little about the magnitude of that effect. To quote Rosnow and Rosenthal, "Surely, God loves the 0.06 nearly as much as the 0.05" [222]. The most common methods for analysing RNAi and drug treatment data—namely, the calculation of interaction terms and their p-values from linear regressions—also do not address this problem. There are standardised measures of effect size calculated from differences in means, such as Cohen's d, but these are not directly comparable to one another. That is to say, there is not an obvious way to compare size of the effect of RNAi treatment within the amyloid-β strain to the effect size of the same in the control strain. Ultimately, some combination of these statistical methods should be employed for ideal hit selection.

Third, we must consider the use of complementary assays of worm motility and health. Although the WF-NTP is an extremely powerful screening platform, our results suggest some ambiguity in the interpretation of the results of a thrashing assay in a neurodegenerative model. Although there is a phenotype, determining what kinds of dysfunction are occurring may only be possible with further investigation. Consequently, assays analysing movement on solid media—as well as lifespan assays, calcium imaging, electrophysiology, and other neurophysiological assays—should be employed to determine the precise nature of the molecular mechanisms underlying the phenotypes we have induced by knockdown. Because

these methods are time-consuming and unsuitable for high-throughput screens, we would not be able to undertake experiments of this kind without the combination of high-resolution and high-throughput that the WF-NTP affords.

Fourth, when the hits have been fully-validated, we must begin the work of confirming that it is these genes in particular that are responsible for the phenotype produced. This means performing knockdowns of closely-related genes, as well as corroborating these results by means of rescues.

Even when these tasks have been accomplished, there is yet more promising research to be done. Once we have a confirmed AD Gene List in *C. elegans*, will perturbations in these genes produce noticeable phenotype and aggregation in yet-more subtle models such as the BAG-Aβ worm? If so, can we use them to build better models? Engineering worms with lowered or abolished expression of the genes on our list, as well as worms with partially-defective versions of these genes, seems to me to be the most straightforward way of recapitulating sAD in *C. elegans*. Once we have developed and characterised new and more effective models of sAD, we can use them to test panels of pharmacological interventions. In this way, our *C. elegans* models may act as an effective filter for drugs that may have an effect in higher-order models of AD and the patients for whom all this work is ultimately conducted.

References

[1] Elizabeth Joe and John M. Ringman. Cognitive symptoms of Alzheimer's disease: Clinical management and prevention, dec 2019.

[2] Jens Pahnke, Lary C Walker, Katja Scheffler, and Markus Krohn. Alzheimer's disease and blood–brain barrier function—why have anti-β-amyloid therapies failed to prevent dementia progression? *Neuroscience & Biobehavioral Reviews*, 33(7):1099–1108, 2009.

[3] George G. Glenner and Caine W. Wong. Alzheimer's disease and Down's syndrome: Sharing of a unique cerebrovascular amyloid fibril protein. *Biochemical and Biophysical Research Communications*, 122(3):1131–1135, aug 1984.

[4] Siqiang Ren, Lionel Breuillaud, Wen Yao, Tao Yin, Kelly A Norris, Simone P Zehntner, and & Luciano D'adamio. Trem2 mutation, TNF-a and inhibitory transmission TNF-α-mediated reduction in inhibitory neurotransmission precedes sporadic Alzheimer's disease pathology in young Trem2 R47H rats.

[5] Fabrizio Chiti and Christopher M. Dobson. Protein Misfolding, Amyloid Formation, and Human Disease: A Summary of Progress Over the Last Decade. *Annual Review of Biochemistry*, 86(1):27–68, jun 2017.

[6] Tuomas PJ Knowles, Michele Vendruscolo, and Christopher M Dobson. The amyloid state and its association with protein misfolding diseases. *Nature reviews. Molecular cell biology*, 15(6):384, 2014.

[7] Mark S. Hipp, Prasad Kasturi, and F. Ulrich Hartl. The proteostasis network and its decline in ageing, 2019.

[8] Johnathan Labbadia and Richard I. Morimoto. The biology of proteostasis in aging and disease, 2015.

[9] Christian B Anfinsen. Studies on the principles that govern the folding of protein chains. 1972.

[10] Christopher M Dobson, Andrej Šali, and Martin Karplus. Protein folding: a perspective from theory and experiment. *Angewandte Chemie International Edition*, 37(7):868–893, 1998.

[11] Sheena E Radford and Christopher M Dobson. From computer simulations to human disease. *Cell*, 97(3):291–298, 1999.

[12] Michele Vendruscolo, Jesús Zurdo, Cait E MacPhee, and Christopher M Dobson. Protein folding and misfolding: a paradigm of self–assembly and regulation in complex biological systems. *Philosophical Transactions of the Royal Society of London A: Mathematical, Physical and Engineering Sciences*, 361(1807):1205–1222, 2003.

[13] Alan R Fersht. Transition-state structure as a unifying basis in protein-folding mechanisms: contact order, chain topology, stability, and the extended nucleus mechanism. *Proceedings of the National Academy of Sciences*, 97(4):1525–1529, 2000.

[14] Stefan Walter and Johannes Buchner. Molecular chaperones - Cellular machines for protein folding, apr 2002.

[15] Boyd Hardesty and Gisela Kramer. Folding of a nascent peptide on the ribosome. *Progress in nucleic acid research and molecular biology*, 66:41–66, 2000.

[16] Bernd Bukau and Arthur L Horwich. The hsp70 and hsp60 chaperone machines. *Cell*, 92(3):351–366, 1998.

[17] F Ulrich Hartl and Manajit Hayer-Hartl. Molecular chaperones in the cytosol: from nascent chain to folded protein. *Science*, 295(5561):1852–1858, 2002.

[18] Christopher M Dobson. Protein folding and misfolding. *Nature*, 426(6968):884–890, 2003.

[19] R John Ellis. Macromolecular crowding: an important but neglected aspect of the intracellular environment. *Current opinion in structural biology*, 11(1):114–119, 2001.

[20] Margaret Sunde and Colin Blake. The structure of amyloid fibrils by electron microscopy and x-ray diffraction. *Advances in protein chemistry*, 50:123–159, 1997.

[21] Jean D. Sipe and Alan S. Cohen. Review: History of the amyloid fibril, jun 2000.

[22] Bede M Broome and Michael H Hecht. Nature disfavors sequences of alternating polar and non-polar amino acids: implications for amyloidogenesis. *Journal of molecular biology*, 296(4):961–968, 2000.

[23] Alex Santoso, Peter Chien, Lev Z Osherovich, and Jonathan S Weissman. Molecular basis of a yeast prion species barrier. *Cell*, 100(2):277–288, 2000.

[24] Peter Chien and Jonathan S Weissman. Conformational diversity in a yeast prion dictates its seeding specificity. *Nature*, 410(6825):223–227, 2001.

[25] Yoshiko Miura, Kikuko Yasuda, Kiyofumi Yamamoto, Mihoko Koike, Yoshihiro Nishida, and Kazukiyo Kobayashi. Inhibition of Alzheimer amyloid aggregation with sulfated gycopolymers. *Biomacromolecules*, 8(7):2129–2134, jul 2007.

[26] JJM Hoozemans, R Veerhuis, ES Van Haastert, JM Rozemuller, F Baas, P Eikelenboom, and W Scheper. The unfolded protein response is activated in alzheimer's disease. *Acta neuropathologica*, 110(2):165–172, 2005.

[27] Maya A Hanspal, Christopher M Dobson, Justin J Yerbury, and Janet R Kumita. The relevance of contact-independent cell-to-cell transfer of tdp-43 and sod1 in amyotrophic lateral sclerosis. *Biochimica et Biophysica Acta (BBA)-Molecular Basis of Disease*, 2017.

[28] Neil F Bence, Roopal M Sampat, and Ron R Kopito. Impairment of the ubiquitin-proteasome system by protein aggregation. *Science*, 292(5521):1552–1555, 2001.

[29] Christopher A Ross and Michelle A Poirier. Protein aggregation and neurodegenerative disease. 2004.

[30] Michael H Glickman and Aaron Ciechanover. The ubiquitin-proteasome proteolytic pathway: destruction for the sake of construction. *Physiological reviews*, 82(2):373–428, 2002.

[31] Amol P Pawar, Kateri F DuBay, Jesus Zurdo, Fabrizio Chiti, Michele Vendruscolo, and Christopher M Dobson. Prediction of "aggregation-prone" and "aggregation-susceptible" regions in proteins associated with neurodegenerative diseases. *Journal of molecular biology*, 350(2):379–392, 2005.

[32] Jane S Richardson and David C Richardson. Natural β-sheet proteins use negative design to avoid edge-to-edge aggregation. *Proceedings of the National Academy of Sciences*, 99(5):2754–2759, 2002.

[33] Peter M. Douglas and Andrew Dillin. Protein homeostasis and aging in neurodegeneration, sep 2010.

[34] William E Balch, Richard I Morimoto, Andrew Dillin, and Jeffery W Kelly. Adapting proteostasis for disease intervention. *science*, 319(5865):916–919, 2008.

[35] Richard I Morimoto. Proteotoxic stress and inducible chaperone networks in neurodegenerative disease and aging. *Genes & development*, 22(11):1427–1438, 2008.

[36] Ehud Cohen and Andrew Dillin. The insulin paradox: aging, proteotoxicity and neurodegeneration. *Nature Reviews Neuroscience*, 9(10):759–767, 2008.

[37] Noboru Mizushima, Beth Levine, Ana Maria Cuervo, and Daniel J Klionsky. Autophagy fights disease through cellular self-digestion. *Nature*, 451(7182):1069–1075, 2008.

[38] Richard I Morimoto and Ana M Cuervo. Protein homeostasis and aging: taking care of proteins from the cradle to the grave. *The Journals of Gerontology Series A: Biological Sciences and Medical Sciences*, page gln071, 2009.

[39] Alexander Buchberger, Bernd Bukau, and Thomas Sommer. Protein quality control in the cytosol and the endoplasmic reticulum: brothers in arms. *Molecular cell*, 40(2):238–252, 2010.

[40] Sara M Butterfield and Hilal A Lashuel. Amyloidogenic protein–membrane interactions: mechanistic insight from model systems. *Angewandte Chemie International Edition*, 49(33):5628–5654, 2010.

[41] Thomas Wisniewski and Blas Frangione. Apolipoprotein e: a pathological chaperone protein in patients with cerebral and systemic amyloid. *Neuroscience letters*, 135(2):235–238, 1992.

[42] Holly Oakley, Sarah L Cole, Sreemathi Logan, Erika Maus, Pei Shao, Jeffery Craft, Angela Guillozet-Bongaarts, Masuo Ohno, John Disterhoft, Linda Van Eldik, et al. Intraneuronal β-amyloid aggregates, neurodegeneration, and neuron loss in transgenic mice with five familial alzheimer's disease mutations: potential factors in amyloid plaque formation. *Journal of Neuroscience*, 26(40):10129–10140, 2006.

[43] Silvia Campioni, Benedetta Mannini, Mariagioia Zampagni, Anna Pensalfini, Claudia Parrini, Elisa Evangelisti, Annalisa Relini, Massimo Stefani, Christopher M Dobson, Cristina Cecchi, et al. A causative link between the structure of aberrant protein oligomers and their toxicity. *Nature chemical biology*, 6(2):140, 2010.

[44] Paolo Arosio, Risto Cukalevski, Birgitta Frohm, Tuomas PJ Knowles, and Sara Linse. Quantification of the concentration of aβ42 propagons during the lag phase by an amyloid chain reaction assay. *Journal of the American Chemical Society*, 136(1):219–225, 2013.

[45] Ganesh M Shankar, Shaomin Li, Tapan H Mehta, Amaya Garcia-Munoz, Nina E Shepardson, Imelda Smith, Francesca M Brett, Michael A Farrell, Michael J Rowan, Cynthia A Lemere, et al. Amyloid-β protein dimers isolated directly from alzheimer's brains impair synaptic plasticity and memory. *Nature medicine*, 14(8):837–842, 2008.

[46] Benedetta Mannini, Estefania Mulvihill, Caterina Sgromo, Roberta Cascella, Reza Khodarahmi, Matteo Ramazzotti, Christopher M Dobson, Cristina Cecchi, and Fabrizio Chiti. Toxicity of protein oligomers is rationalized by a function combining size and surface hydrophobicity. *ACS chemical biology*, 9(10):2309–2317, 2014.

[47] Dominic M Walsh and Dennis J Selkoe. Aβ oligomers–a decade of discovery. *Journal of neurochemistry*, 101(5):1172–1184, 2007.

[48] Johnny Habchi, Paolo Arosio, Michele Perni, Ana Rita Costa, Maho Yagi-Utsumi, Priyanka Joshi, Sean Chia, Samuel IA Cohen, Martin BD Müller, Sara Linse, et al. An anticancer drug suppresses the primary nucleation reaction that initiates the production of the toxic aβ42 aggregates linked with alzheimer's disease. *Science advances*, 2(2):e1501244, 2016.

[49] Konstanze F Winklhofer, Jörg Tatzelt, and Christian Haass. The two faces of protein misfolding: gain-and loss-of-function in neurodegenerative diseases. *The EMBO journal*, 27(2):336–349, 2008.

[50] J Paul Taylor, John Hardy, and Kenneth H Fischbeck. Toxic proteins in neurodegenerative disease. *Science*, 296(5575):1991–1995, 2002.

[51] Helena Decker, Karen Y Lo, Sandra M Unger, Sergio T Ferreira, and Michael A Silverman. Amyloid-β peptide oligomers disrupt axonal transport through an nmda receptor-dependent mechanism that is mediated by glycogen synthase kinase 3β in primary cultured hippocampal neurons. *Journal of Neuroscience*, 30(27):9166–9171, 2010.

[52] Charles G Glabe. Common mechanisms of amyloid oligomer pathogenesis in degenerative disease. *Neurobiology of aging*, 27(4):570–575, 2006.

[53] Nelson Arispe, Harvey B Pollard, and Eduardo Rojas. Zn2+ interaction with alzheimer amyloid beta protein calcium channels. *Proceedings of the National Academy of Sciences*, 93(4):1710–1715, 1996.

[54] Nelson Arispe, Eduardo Rojas, and Harvey B Pollard. Alzheimer disease amyloid beta protein forms calcium channels in bilayer membranes: blockade by tromethamine and aluminum. *Proceedings of the National Academy of Sciences*, 90(2):567–571, 1993.

[55] Dominic M Walsh, Igor Klyubin, Julia V Fadeeva, William K Cullen, Roger Anwyl, Michael S Wolfe, Michael J Rowan, and Dennis J Selkoe. Naturally secreted oligomers of amyloid β protein potently inhibit hippocampal long-term potentiation in vivo. *Nature*, 416(6880):535–539, 2002.

[56] Byron Caughey and Peter T Lansbury Jr. Protofibrils, pores, fibrils, and neurodegeneration: separating the responsible protein aggregates from the innocent bystanders. *Annual review of neuroscience*, 26(1):267–298, 2003.

[57] Irene H Cheng, Kimberly Scearce-Levie, Justin Legleiter, Jorge J Palop, Hilary Gerstein, Nga Bien-Ly, Jukka Puoliväli, Sylvain Lesné, Karen H Ashe, Paul J Muchowski, et al. Accelerating amyloid-β fibrillization reduces oligomer levels and functional deficits in alzheimer disease mouse models. *Journal of Biological Chemistry*, 282(33):23818–23828, 2007.

[58] Meenakshi Verma, Abhishek Vats, and Vibha Taneja. Toxic species in amyloid disorders: Oligomers or mature fibrils. *Annals of Indian Academy of Neurology*, 18(2):138, 2015.

[59] Renee C. Gaspar, Stephanie A. Villarreal, Nicole Bowles, Robert W. Hepler, Joseph G. Joyce, and Paul J. Shughrue. Oligomers of β-amyloid are sequestered into and seed new plaques in the brains of an AD mouse model. *Experimental Neurology*, 223(2):394–400, jun 2010.

[60] Mohammad Javad Hajipour, Hossein Mohammad-Beigi, Iraj Nabipour, Negar Mahmoudi, Morteza Azhdarzadeh, Hossein Derakhshankhah, Dina El Dawud, Reza Mohammadinejad, and Daniel E. Otzen. Amyloid fibril inhibition, acceleration, or fragmentation; Are nano-based approaches advance in the right direction? *Nano Today*, 35:100983, dec 2020.

[61] Fabrizio Chiti and Christopher M. Dobson. Protein Misfolding, Functional Amyloid, and Human Disease. *Annual Review of Biochemistry*, 75(1):333–366, jun 2006.

[62] Henriette van Praag. Lifestyle Factors and Alzheimer's Disease. *Brain Plasticity*, 4(1):1–2, dec 2018.

[63] Bruno Dubois, Harald Hampel, Howard H. Feldman, Philip Scheltens, Paul Aisen, Sandrine Andrieu, Hovagim Bakardjian, Habib Benali, Lars Bertram, Kaj Blennow, Karl Broich, Enrica Cavedo, Sebastian Crutch, Jean-François Dartigues, Charles Duyckaerts, Stéphane Epelbaum, Giovanni B. Frisoni, Serge Gauthier, Remy Genthon, Alida A. Gouw, Marie-Odile Habert, David M. Holtzman, Miia Kivipelto, Simone Lista, José-Luis Molinuevo, Sid E. O'Bryant, Gil D. Rabinovici, Christopher Rowe, Stephen Salloway, Lon S. Schneider, Reisa Sperling, Marc Teichmann, Maria C. Carrillo, Jeffrey Cummings, and Cliff R. Jack. Preclinical Alzheimer's disease: Definition, natural history, and diagnostic criteria. *Alzheimer's & Dementia*, 12(3):292–323, mar 2016.

[64] Debra A. Fleischman and John Gabrieli. Long-term memory in Alzheimer's disease. *Current Opinion in Neurobiology*, 9(2):240–244, apr 1999.

[65] Myron F. Weiner, Katherine E. Neubecker, Mary E. Bret, and Linda S. Hynan. Language in Alzheimer's disease. *Journal of Clinical Psychiatry*, 69(8):1223–1227, 2008.

[66] Mathieu Lesourd, Didier Le Gall, Josselin Baumard, Bernard Croisile, Christophe Jarry, and François Osiurak. Apraxia and alzheimer's disease: Review and perspectives. *Neuropsychology Review*, 23(3):234–256, 2013.

[67] P. Giannakopoulos, G. Gold, M. Duc, J. P. Michel, P. R. Hof, and C. Bouras. Neuroanatomic correlates of visual agnosia in Alzheimer's disease: A clinicopathologic study. *Neurology*, 52(1):71–77, jan 1999.

[68] Ayako Edahiro, Hirohiko Hirano, Ritsuko Yamada, Yumi Chiba, Yutaka Watanabe, Morio Tonogi, and Gen-yuki Yamane. Factors affecting independence in eating among elderly with Alzheimer's disease. *Geriatrics & Gerontology International*, 12(3):481–490, jul 2012.

[69] Clement T. Loy, Peter R. Schofield, Anne M. Turner, and John B.J. Kwok. Genetics of dementia. *The Lancet*, 383(9919):828–840, 2014.

[70] Heiko Braak, Dietmar R. Thal, Estifanos Ghebremedhin, and Kelly Del Tredici. Stages of the Pathologic Process in Alzheimer Disease: Age Categories From 1 to 100 Years. *Journal of Neuropathology & Experimental Neurology*, 70(11):960–969, nov 2011.

[71] A. Alzheimer, Hans Förstl, and Raymond Levy. On certain peculiar diseases of old age. *History of Psychiatry*, 2(5):71–73, mar 1991.

[72] Dolores Del Prete, Frédéric Checler, and Mounia Chami. Ryanodine receptors: Physiological function and deregulation in Alzheimer disease, jun 2014.

[73] Gary P. Morris, Ian A. Clark, and Bryce Vissel. Inconsistencies and Controversies Surrounding the Amyloid Hypothesis of Alzheimer's Disease, jan 2014.

[74] Nikolai D Belyaev, Natalia N Nalivaeva, Natalia Z Makova, and Anthony J Turner. Neprilysin gene expression requires binding of the amyloid precursor protein intracellular domain to its promoter: implications for Alzheimer disease. *EMBO reports*, 10(1):94–100, jan 2009.

[75] Lina Adwan and Nasser H. Zawia. Epigenetics: A novel therapeutic approach for the treatment of Alzheimer's disease. *Pharmacology and Therapeutics*, 139(1):41–50, 2013.

[76] Robert J. Andrew, Katherine A.B. Kellett, Gopal Thinakaran, and Nigel M. Hooper. A Greek tragedy: The growing complexity of Alzheimer amyloid precursor protein proteolysis, 2016.

[77] Daniela Kaden, Anja Harmeier, Christoph Weise, Lisa M. Munter, Veit Althoff, Benjamin R. Rost, Peter W. Hildebrand, Dietmar Schmitz, Michael Schaefer, Rudi Lurz, Sabine Skodda, Raina Yamamoto, Sönke Arlt, Ulrich Finckh, and Gerd Multhaup. Novel APP/Aβ mutation K16N produces highly toxic heteromeric Aβ oligomers. *EMBO Molecular Medicine*, 2012.

[78] Anna Ochalek, Balázs Mihalik, Hasan X. Avci, Abinaya Chandrasekaran, Annamária Téglási, István Bock, Maria Lo Giudice, Zsuzsanna Táncos, Kinga Molnár, Lajos László, Jørgen E. Nielsen, Bjørn Holst, Kristine Freude, Poul Hyttel, Julianna Kobolák, and András Dinnyés. Neurons derived from sporadic Alzheimer's disease iPSCs reveal elevated TAU hyperphosphorylation, increased amyloid levels, and GSK3B activation. *Alzheimer's Research and Therapy*, 9(1):90, dec 2017.

[79] Tiantian Guo, Denghong Zhang, Yuzhe Zeng, Timothy Y. Huang, Huaxi Xu, and Yingjun Zhao. Molecular and cellular mechanisms underlying the pathogenesis of Alzheimer's disease, jul 2020.

[80] Heiko Braak and Eva Braak. Neuropathological stageing of alzheimer-related changes. *Acta neuropathologica*, 82(4):239–259, 1991.

[81] S. Swarbrick, N. Wragg, S. Ghosh, and Alexandra Stolzing. Systematic Review of miRNA as Biomarkers in Alzheimer's Disease, sep 2019.

[82] John Hardy and David Allsop. Amyloid deposition as the central event in the aetiology of Alzheimer's disease, 1991.

[83] John A. Hardy and Gerald A. Higgins. Alzheimer's disease: The amyloid cascade hypothesis, apr 1992.

[84] Bart De Strooper and Eric Karran. The Cellular Phase of Alzheimer's Disease, feb 2016.

[85] Dennis J Selkoe and John Hardy. The amyloid hypothesis of alzheimer9s disease at 25 years. *EMBO molecular medicine*, 8(6):595–608, 2016.

[86] Maria Bjerke, Erik Portelius, Lennart Minthon, Anders Wallin, Henrik Anckarster, Rolf Anckarster, Niels Andreasen, Henrik Zetterberg, Ulf Andreasson, and Kaj Blennow. Confounding factors influencing amyloid beta concentration in cerebrospinal fluid. *International Journal of Alzheimer's Disease*, 2010.

[87] Philip Scheltens, Kaj Blennow, Monique M.B. Breteler, Bart de Strooper, Giovanni B. Frisoni, Stephen Salloway, and Wiesje Maria Van der Flier. Alzheimer's disease. *The Lancet*, 388(10043):505–517, 2016.

[88] Jie Shen and Raymond J Kelleher III. The presenilin hypothesis of Alzheimer's disease: Evidence for a loss-of-function pathogenic mechanism. Technical report, 2006.

[89] Inelia Morales, Leonardo GuzmÃ¡n-MartÃnez, CristÃ³bal Cerda-Troncoso, Gonzalo A. FarÃas, and Ricardo B. Maccioni. Neuroinflammation in the pathogenesis of Alzheimerâ€™s disease. A rational framework for the search of novel therapeutic approaches. *Frontiers in Cellular Neuroscience*, 8(1 APR):112, apr 2014.

[90] Michael R. Hoane, Nicholas Kaufman, Michael P. Vitek, and Suzanne E. McKenna. COG1410 improves cognitive performance and reduces cortical neuronal loss in the traumatically injured brain. *Journal of Neurotrauma*, 2009.

[91] Elena A. Tukhovskaya, Alexey Yu Yukin, Oksana N. Khokhlova, Arkady N. Murashev, and Michael P. Vitek. COG1410, a novel apolipoprotein-E mimetic, improves functional and morphological recovery in a rat model of focal brain ischemia. *Journal of Neuroscience Research*, 2009.

[92] M. P. Vitek, D. J. Christensen, D. Wilcock, J. Davis, W. E. Van Nostrand, F. Q. Li, and C. A. Colton. APOE-mimetic peptides reduce behavioral deficits, plaques and tangles in Alzheimer's disease transgenics. *Neurodegenerative Diseases*, 2012.

[93] Michael J. Berridge. Calcium hypothesis of Alzheimer's disease, feb 2010.

[94] Elena Popugaeva, Ekaterina Pchitskaya, and Ilya Bezprozvanny. Dysregulation of Intracellular Calcium Signaling in Alzheimer's Disease, oct 2018.

[95] Calcium Hypothesis of Alzheimer's disease and brain aging: A framework for integrating new evidence into a comprehensive theory of pathogenesis. *Alzheimer's and Dementia*, 2017.

[96] Vathany Kulasingam and Eleftherios P. Diamandis. Strategies for discovering novel cancer biomarkers through utilization of emerging technologies, aug 2008.

[97] M Pek, Smjm Yatim, Y Chen, J Li, M Gong, X Jiang, F Zhang, J Zheng, X Wu, and Q Yu. Oncogenic KRAS-associated gene signature defines co-targeting of CDK4/6 and MEK as a viable therapeutic strategy in colorectal cancer. 2017.

[98] Christos Sotiriou and Lajos Pusztai. Gene-Expression Signatures in Breast Cancer. *New England Journal of Medicine*, 360(8):790–800, feb 2009.

[99] Catherine Dulac. Brain function and chromatin plasticity, 2010.

[100] Kouichi Ozaki, Yozo Ohnishi, Aritoshi Iida, Akihiko Sekine, Ryo Yamada, Tatsuhiko Tsunoda, Hiroshi Sato, Hideyuki Sato, Masatsugu Hori, Yusuke Nakamura, and Toshihiro Tanaka. Functional SNPs in the lymphotoxin-α gene that are associated with susceptibility to myocardial infarction. 2002.

[101] David M. Howard, Mark J. Adams, Toni Kim Clarke, Jonathan D. Hafferty, Jude Gibson, Masoud Shirali, Jonathan R.I. Coleman, Saskia P. Hagenaars, Joey Ward, Eleanor M. Wigmore, Clara Alloza, Xueyi Shen, Miruna C. Barbu, Eileen Y. Xu, Heather C. Whalley, Riccardo E. Marioni, David J. Porteous, Gail Davies, Ian J. Deary, Gibran Hemani, Klaus Berger, Henning Teismann, Rajesh Rawal, Volker Arolt, Bernhard T. Baune, Udo Dannlowski, Katharina Domschke, Chao Tian, David A. Hinds, Maciej Trzaskowski, Enda M. Byrne, Stephan Ripke, Daniel J. Smith, Patrick F. Sullivan, Naomi R. Wray, Gerome Breen, Cathryn M. Lewis, and Andrew M. McIntosh. Genome-wide meta-analysis of depression identifies 102 independent variants and highlights the importance of the prefrontal brain regions. *Nature Neuroscience*, 22(3):343–352, mar 2019.

[102] Schizophrenia Working Group of the Psychiatric Genomics Consortium. Biological insights from 108 schizophrenia-associated genetic loci. 2014.

[103] Hunna J. Watson, Zeynep Yilmaz, Laura M. Thornton, Christopher Hübel, Jonathan R.I. Coleman, Héléna A. Gaspar, Julien Bryois, Anke Hinney, Virpi M. Leppä, Manuel Mattheisen, Sarah E. Medland, Stephan Ripke, Shuyang Yao, Paola Giusti-Rodríguez, Ken B. Hanscombe, Kirstin L. Purves, Roger A.H. Adan, Lars Alfredsson, Tetsuya Ando, Ole A. Andreassen, Jessica H. Baker, Wade H. Berrettini, Ilka Boehm, Claudette Boni, Vesna Boraska Perica, Katharina Buehren, Roland Burghardt, Matteo Cassina, Sven Cichon, Maurizio Clementi, Roger D. Cone, Philippe Courtet, Scott Crow, James J. Crowley, Unna N. Danner, Oliver S.P. Davis, Martina de Zwaan, George Dedoussis, Daniela Degortes, Janiece E. DeSocio, Danielle M. Dick, Dimitris Dikeos, Christian Dina, Monika Dmitrzak-Weglarz, Elisa Docampo, Laramie E. Duncan, Karin Egberts, Stefan Ehrlich, Geòrgia Escaramís, Tõnu Esko, Xavier Estivill, Anne Farmer, Angela Favaro, Fernando Fernández-Aranda, Manfred M. Fichter, Krista Fischer, Manuel Föcker, Lenka Foretova, Andreas J. Forstner, Monica Forzan, Christopher S. Franklin, Steven Gallinger, Ina Giegling, Johanna Giuranna, Fragiskos Gonidakis, Philip Gorwood, Monica Gratacos Mayora, Sébastien Guillaume, Yiran Guo, Hakon Hakonarson, Konstantinos Hatzikotoulas, Joanna Hauser, Johannes Hebebrand, Sietske G. Helder, Stefan Herms, Beate Herpertz-Dahlmann, Wolfgang Herzog, Laura M. Huckins, James I. Hudson, Hartmut Imgart, Hidetoshi Inoko, Vladimir Janout,

Susana Jiménez-Murcia, Antonio Julià, Gursharan Kalsi, Deborah Kaminská, Jaakko Kaprio, Leila Karhunen, Andreas Karwautz, Martien J.H. Kas, James L. Kennedy, Anna Keski-Rahkonen, Kirsty Kiezebrink, Youl Ri Kim, Lars Klareskog, Kelly L. Klump, Gun Peggy S. Knudsen, Maria C. La Via, Stephanie Le Hellard, Robert D. Levitan, Dong Li, Lisa Lilenfeld, Bochao Danae Lin, Jolanta Lissowska, Jurjen Luykx, Pierre J. Magistretti, Mario Maj, Katrin Mannik, Sara Marsal, Christian R. Marshall, Morten Mattingsdal, Sara McDevitt, Peter McGuffin, Andres Metspalu, Ingrid Meulenbelt, Nadia Micali, Karen Mitchell, Alessio Maria Monteleone, Palmiero Monteleone, Melissa A. Munn-Chernoff, Benedetta Nacmias, Marie Navratilova, Ioanna Ntalla, Julie K. O'Toole, Roel A. Ophoff, Leonid Padyukov, Aarno Palotie, Jacques Pantel, Hana Papezova, Dalila Pinto, Raquel Rabionet, Anu Raevuori, Nicolas Ramoz, Ted Reichborn-Kjennerud, Valdo Ricca, Samuli Ripatti, Franziska Ritschel, Marion Roberts, Alessandro Rotondo, Dan Rujescu, Filip Rybakowski, Paolo Santonastaso, André Scherag, Stephen W. Scherer, Ulrike Schmidt, Nicholas J. Schork, Alexandra Schosser, Jochen Seitz, Lenka Slachtova, P. Eline Slagboom, Margarita C.T. Slof-Op 't Landt, Agnieszka Slopien, Sandro Sorbi, Beata Świątkowska, Jin P. Szatkiewicz, Ioanna Tachmazidou, Elena Tenconi, Alfonso Tortorella, Federica Tozzi, Janet Treasure, Artemis Tsitsika, Marta Tyszkiewicz-Nwafor, Konstantinos Tziouvas, Annemarie A. van Elburg, Eric F. van Furth, Gudrun Wagner, Esther Walton, Elisabeth Widen, Eleftheria Zeggini, Stephanie Zerwas, Stephan Zipfel, Andrew W. Bergen, Joseph M. Boden, Harry Brandt, Steven Crawford, Katherine A. Halmi, L. John Horwood, Craig Johnson, Allan S. Kaplan, Walter H. Kaye, James E. Mitchell, Catherine M. Olsen, John F. Pearson, Nancy L. Pedersen, Michael Strober, Thomas Werge, David C. Whiteman, D. Blake Woodside, Garret D. Stuber, Scott Gordon, Jakob Grove, Anjali K. Henders, Anders Juréus, Katherine M. Kirk, Janne T. Larsen, Richard Parker, Liselotte Petersen, Jennifer Jordan, Martin Kennedy, Grant W. Montgomery, Tracey D. Wade, Andreas Birgegård, Paul Lichtenstein, Claes Norring, Mikael Landén, Nicholas G. Martin, Preben Bo Mortensen, Patrick F. Sullivan, Gerome Breen, and Cynthia M. Bulik. Genome-wide association study identifies eight risk loci and implicates metabo-psychiatric origins for anorexia nervosa. *Nature Genetics*, 51(8):1207–1214, aug 2019.

[104] Vijay K Ramanan and Andrew J Saykin. (No Title). Technical Report 3, 2013.

[105] Vivian Tam, Nikunj Patel, Michelle Turcotte, Yohan Bossé, Guillaume Paré, and David Meyre. Benefits and limitations of genome-wide association studies. *Nature Reviews Genetics*, 20(8):467–484, 2019.

[106] Lucia A Hindorff, Praveen Sethupathy, Heather A Junkins, Erin M Ramos, Jayashri P Mehta, Francis S Collins, and Teri A Manolio. Potential etiologic and functional implications of genome-wide association loci for human diseases and traits. Technical report.

[107] Wen Hua Wei, Gibran Hemani, and Chris S. Haley. Detecting epistasis in human complex traits. *Nature Reviews Genetics*, 15(11):722–733, 2014.

[108] Minoru Kanehisa and Susumu Goto. KEGG: Kyoto Encyclopedia of Genes and Genomes, 2000.

[109] Brad T. Sherman, Da Wei Huang, Qina Tan, Yongjian Guo, Stephan Bour, David Liu, Robert Stephens, Michael W. Baseler, Clifford H. Lane, and Richard A. Lempicki. DAVID Knowledgebase: A gene-centered database integrating heterogeneous gene annotation resources to facilitate high-throughput gene functional analysis. *BMC Bioinformatics*, 2007.

[110] Qunxing Ding, William R. Markesbery, Qinghua Chen, Feng Li, and Jeffrey N. Keller. Ribosome dysfunction is an early event in Alzheimer's disease. *Journal of Neuroscience*, 2005.

[111] Michael T. Lin and M. Flint Beal. Mitochondrial dysfunction and oxidative stress in neurodegenerative diseases, 2006.

[112] R. Milo, S. Shen-Orr, S. Itzkovitz, N. Kashtan, D. Chklovskii, and U. Alon. Network motifs: Simple building blocks of complex networks. *Science*, 2002.

[113] Lewi Stone, Daniel Simberloff, and Yael Artzy-Randrup. Network motifs and their origins. *PLoS Computational Biology*, 2019.

[114] Anna C.F. Lewis, Nick S. Jones, Mason A. Porter, and Deane M. Charlotte. The function of communities in protein interaction networks at multiple scales. *BMC Systems Biology*, 2010.

[115] Elisabeth Wong, Brittany Baur, Saad Quader, and Chun Hsi Huang. Biological network motif detection: Principles and practice. *Briefings in Bioinformatics*, 2012.

[116] Rohit Gupta, S. M. Fayaz, and Sanjay Singh. Identification of gene network motifs for cancer disease diagnosis. In *2016 IEEE International Conference on Distributed Computing, VLSI, Electrical Circuits and Robotics, DISCOVER 2016 - Proceedings*, 2016.

[117] Bo Wang, Armin Pourshafeie, Marinka Zitnik, Junjie Zhu, Carlos D. Bustamante, Serafim Batzoglou, and Jure Leskovec. Network enhancement as a general method to denoise weighted biological networks. *Nature Communications*, 2018.

[118] William Dauer and Serge Przedborski. Parkinson's disease: Mechanisms and models, 2003.

[119] Alain Dagher and Trevor W. Robbins. Personality, Addiction, Dopamine: Insights from Parkinson's Disease, 2009.

[120] Sangjune Kim, Seung Hwan Kwon, Tae In Kam, Nikhil Panicker, Senthilkumar S. Karuppagounder, Saebom Lee, Jun Hee Lee, Wonjoong Richard Kim, Minjee Kook, Catherine A. Foss, Chentian Shen, H. Lee, Subhash Kulkarni, Pankaj J. Pasricha, Gabsang Lee, Martin G. Pomper, Valina L. Dawson, T. M. Dawson, and Han Seok Ko. Transneuronal Propagation of Pathologic α-Synuclein from the Gut to the Brain Models Parkinson's Disease. *Neuron*, 2019.

[121] Guglielmo Foffani and José A. Obeso. A Cortical Pathogenic Theory of Parkinson's Disease, 2018.

[122] Bin Zheng, Zhixiang Liao, Joseph J. Locascio, Kristen A. Lesniak, Sarah S. Roderick, Marla L. Watt, Aron C. Eklund, Yanli Zhang-James, Peter D. Kim, Michael A. Hauser, Edna Grünblatt, Linda B. Moran, Silvia A. Mandel, Peter Riederer, Renee M. Miller, Howard J. Federoff, Ullrich Wüllner, Spyridon Papapetropoulos, Moussa B. Youdim, Ippolita Cantuti-Castelvetri, Anne B. Young, Jeffery M. Vance, Richard L. Davis, John C. Hedreen, Charles H. Adler, Thomas G. Beach, Manuel B. Graeber, Frank A. Middleton, Jean Christophe Rochet, and Clemens R. Scherzer. PGC-1α, a potential therapeutic target for early intervention in Parkinson's disease. *Science Translational Medicine*, 2010.

[123] Nicolas X. Tritsch and Bernardo L. Sabatini. Dopaminergic Modulation of Synaptic Transmission in Cortex and Striatum, 2012.

[124] Lara Lourenço Venda, Stephanie J. Cragg, Vladimir L. Buchman, and Richard Wade-Martins. α-Synuclein and dopamine at the crossroads of Parkinson's disease, 2010.

[125] Eduardo E. Benarroch. Glutamatergic synaptic plasticity and dysfunction in Alzheimer disease: Emerging mechanisms. *Neurology*, 91(3):125–132, jul 2018.

[126] Barry J. Everitt and Trevor W. Robbins. Central cholinergic systems and cognition. *Annual Review of Psychology*, 1997.

[127] Balázs Hangya, Sachin P. Ranade, Maja Lorenc, and Adam Kepecs. Central Cholinergic Neurons Are Rapidly Recruited by Reinforcement Feedback. *Cell*, 2015.

[128] Antonio Contestabile. The history of the cholinergic hypothesis, 2011.

[129] Laura A. Craig, Nancy S. Hong, and Robert J. McDonald. Revisiting the cholinergic hypothesis in the development of Alzheimer's disease, 2011.

[130] Harald Hampel, M. Marsel Mesulam, A. Claudio Cuello, Martin R. Farlow, Ezio Giacobini, George T. Grossberg, Ara S. Khachaturian, Andrea Vergallo, Enrica Cavedo, Peter J. Snyder, and Zaven S. Khachaturian. The cholinergic system in the pathophysiology and treatment of Alzheimer's disease, 2018.

[131] Sagar H. Barage and Kailas D. Sonawane. Amyloid cascade hypothesis: Pathogenesis and therapeutic strategies in Alzheimer's disease, 2015.

[132] B. M. McGleenon, K. B. Dynan, and A. P. Passmore. Acetylcholinesterase inhibitors in Alzheimer's disease, 1999.

[133] Mona Mehta, Abdu Adem, and Marwan Sabbagh. New acetylcholinesterase inhibitors for alzheimer's disease. *International Journal of Alzheimer's Disease*, 2012.

[134] David S. Geldmacher. Acetylcholinesterase inhibitors for Alzheimer's disease, 2007.

[135] Mirjana B. Colovic, Danijela Z. Krstic, Tamara D. Lazarevic-Pasti, Aleksandra M. Bondzic, and Vesna M. Vasic. Acetylcholinesterase Inhibitors: Pharmacology and Toxicology. *Current Neuropharmacology*, 2013.

[136] Alessandro Martorana, Zaira Esposito, and Giacomo Koch. Beyond the Cholinergic Hypothesis: Do Current Drugs Work in Alzheimer's Disease? *CNS Neuroscience & Therapeutics*, 16(4):no–no, jun 2010.

[137] Suzanne M. De La Monte and Jack R. Wands. Alzheimer's disease is type 3 diabetes-evidence reviewed, 2008.

[138] Thomas Diehl, Roger Mullins, and Dimitrios Kapogiannis. Insulin resistance in Alzheimer's disease, 2017.

[139] Suzanne M. de la Monte. Insulin resistance and Alzheimer's disease, 2009.

[140] Kelly T. Dineley, Jordan B. Jahrling, and Larry Denner. Insulin resistance in Alzheimer's disease, 2014.

[141] Allen Thomson. XXII. The Reproduction o f the Ascaris mystax. B y H enry N elson, Communicated by. Technical report.

[142] Victor M (Université de Lyon) Nigon and Marie-Ann (Ecole Normale Supérieure) Félix. History of research on C. elegans and other free-living nematodes as model organisms. In *WormBook: The Online Review of C. Elegans Biology*, pages 1–22. 2013.

[143] Edouard van Beneden. *Recherches sur la maturation de l'oeuf, la fécondation, et la division ... - Édouard van Beneden - Google Books*. 1883.

[144] John H. Cross. *Enteric Nematodes of Humans*. University of Texas Medical Branch at Galveston, 1996.

[145] E Maupas. La mue et l'enkystement chez les nématodes. *Arch Zool exp gén,(3e. Série)*, 7:563–628, 1899.

[146] Maupas E (1900) Archives de Zoologie Experimentale et Generale "Modes et formes de reproduction des nematodes." (paper) - WormBase : Nematode Information Resource.

[147] Eva Kruger. Fortpflanzung und keimzellenbildung von rhabditis aberrans n. sp. *Z Wiss Zool*, 105:87–124, 1913.

[148] Paula Hertwig. Abweichende form der parthenogenese bei einer mutation von rhabditis pellio. *Archiv für mikroskopische Anatomie*, 94(1):303–337, 1920.

[149] Karl Belar. Über den chromosomenzyklus von parthenogenetischen erdnematoden. *Biol. Zbl.*, 43:513–518, 1923.

[150] Karl Bělař. Die cytologie der merospermie bei freilebenden rhabditis-arten. *Zeitschrift für Zellforschung und Mikroskopische Anatomie*, 1(1):1–21, 1924.

[151] Hikokuro Honda. Experimental and cytological studies on bisexual and hermaphrodite free-living nematodes, with special reference to problems of sex. *Journal of morphology*, 40(2):191–233, 1925.

[152] Haven Metcalf. Cultural studies of a nematode associated with plant decay. *Transactions of the American Microscopical Society*, 24:89–102, nov 1903.

[153] V Nigon. Le déterminisme du sexe chez un Nématode libre hermaphrodite, Rhabditis elegans Maupas. *Compt. Rendus. Soc. Biol*, 137:40–41, 1943.

[154] Victor Nigon. Les modalites de la reproduction et le determinisme due sexe chez quelques nematodes libres. *Ann. Sci. Nat.*, 11:1–132, 1949.

[155] EC Dougherty, Hermione G Calhoun, et al. Experiences in culturing rhabditis pellio (schneider, 1866) bütschli, 1873 (nematoda: Rhabditidae), and related soil nematodes. *Proceedings of the Helminthological Society of Washington*, 15(2):55–68, 1948.

[156] Ellsworth C Dougherty et al. Introduction to axenic culture of invertebrate metazoa: a goal. *Annals of the New York Academy of Sciences*, 77(2):27–54, 1959.

[157] Bob Goldstein. Sydney brenner on the genetics of caenorhabditis elegans, sep 2016.

[158] Brenner S Wood WB. The nematode caenorhabditis elegans. *Cold Spring Harbor Laboratory*, 1:988, 1988.

[159] Rachel A. Ankeny. The natural history of Caenorhabditis elegans. *Nature*, 2(22):474–479, 2001.

[160] JG White, E Southgate, JN Thompson, and S Brenner. The structure of the nervous system of the nematode c. elegans (aka" the mind of a worm"). *Phil Trans R Soc Lond*, 314:1–340, 1986.

[161] The C. elegans Sequencing Consortium*. Genome sequence of the nematode C. elegans: A platform for investigating biology, dec 1998.

[162] David M Eisenmann. WormBook. *WormBook : the online review of C. elegans biology*, 2005.

[163] Lisa R. Girard, Tristan J. Fiedler, Todd W. Harris, Felicia Carvalho, Igor Antoshechkin, Michael Han, Paul W. Sternberg, Lincoln D. Stein, and Martin Chalfie. WormBook: The online review of Caenorhabditis elegans biology, 2007.

[164] Zeynep F. Altun and David H. Hall. WormAtas Hermaphrodite Handbook - Introduction. *WormAtlas*, 2006.

[165] Thomas Evans. Transformation and microinjection, 2006.

[166] Michael R. Klass. Aging in the nematode Caenorhabditis elegans: Major biological and environmental factors influencing life span. *Mechanisms of Ageing and Development*, 1977.

[167] T A Forge and A E Macguidwin. Nematode autofluorescence and its use as an indicator of viability. *Journal of nematology*, 1989.

[168] Zachary Pincus, Travis C. Mazer, and Frank J. Slack. Autofluorescence as a measure of senescence in C. elegans: Look to red, not blue or green. *Aging*, 2016.

[169] A. Fire, S. Xu, M. K. Montgomery, S. A. Kostas, S. E. Driver, and C. C. Mello. Potent and specific genetic interference by double-stranded RNA in caenorhabditis elegans. *Nature*, 1998.

[170] Marcel Tijsterman and Ronald H.A. Plasterk. Dicers at RISC: The mechanism of RNAi, apr 2004.

[171] Kazuko Nishikura. A short primer on RNAi: RNA-directed RNA polymerase acts as a key catalyst, nov 2001.

[172] Erik M. Jorgensen and Susan E. Mango. The art and design of genetic screens: Caenorhabditis elegans, 2002.

[173] Tessa Sinnige, Prashanth Ciryam, Samuel Casford, Christopher M. Dobson, Mario De Bono, and Michele Vendruscolo. Expression of the amyloid-β peptide in a single pair of C. elegans sensory neurons modulates the associated behavioural response. *PLoS ONE*, 14(5), may 2019.

[174] Collin Y Ewald, Daniel A Raps, and Chris Li. Apl-1, the alzheimer's amyloid precursor protein in caenorhabditis elegans, modulates multiple metabolic pathways throughout development. *Genetics*, 191(2):493–507, 2012.

[175] Gawain Mccoll, Blaine R. Roberts, Tara L. Pukala, Vijaya B. Kenche, Christine M. Roberts, Christopher D. Link, Timothy M. Ryan, Colin L. Masters, Kevin J. Barnham, Ashley I. Bush, and Robert A. Cherny. Utility of an improved model of amyloid-beta (Aβ1-42) toxicity in Caenorhabditis elegans for drug screening for Alzheimer's disease. *Molecular Neurodegeneration*, 2012.

[176] Christopher D. Link. Expression of human β-amyloid peptide in transgenic Caenorhabditis elegans. *Proceedings of the National Academy of Sciences of the United States of America*, 1995.

[177] Christopher D Link. C. elegans models of age-associated neurodegenerative diseases: lessons from transgenic worm models of alzheimer's disease. *Experimental gerontology*, 41(10):1007–1013, 2006.

[178] Andrew Jonathan Bretscher, Eiji Kodama-Namba, Karl Emanuel Busch, Robin Joseph Murphy, Zoltan Soltesz, Patrick Laurent, and Mario de Bono. Temperature, oxygen, and salt-sensing neurons in C. elegans are carbon dioxide sensors that control avoidance behavior. *Neuron*, 2011.

[179] Francis PT. The interplay of neurotransmitters in Alzheimer's disease. LinkOut -more resources. *CNS Spectr*, 2005.

[180] Zaira Esposito, Lorena Belli, Sofia Toniolo, Giuseppe Sancesario, Claudio Bianconi, and Alessandro Martorana. Amyloid β, glutamate, excitotoxicity in alzheimer's disease: Are we on the right track?, 2013.

[181] Timothy J. Revett, Glen B. Baker, Jack Jhamandas, and Satyabrata Kar. Glutamate system, amyloid β peptides and tau protein: Functional interrelationships and relevance to Alzheimer disease pathology, 2013.

[182] Hongjun Fu, Andrea Possenti, Rosie Freer, Yoshikazu Nakano, Nancy C.Hernandez Villegas, Maoping Tang, Paula V.M. Cauhy, Benjamin A. Lassus, Shuo Chen, Stephanie L. Fowler, Helen Y. Figueroa, Edward D. Huey, Gail V.W. Johnson, Michele Vendruscolo, and Karen E. Duff. A tau homeostasis signature is linked with the cellular and regional vulnerability of excitatory neurons to tau pathology. *Nature Neuroscience*, 2019.

[183] Jesse M. Gray, David S. Karow, Hang Lu, Andy J. Chang, Jennifer S. Chang, Ronald E. Ellis, Michael A. Marietta, and Cornelia I. Bargmann. Oxygen sensation and social feeding mediated by a C. elegans guanylate cyclase homologue. *Nature*, 2004.

[184] Manuel Zimmer, Jesse M. Gray, Navin Pokala, Andy J. Chang, David S. Karow, Michael A. Marletta, Martin L. Hudson, David B. Morton, Nikos Chronis, and Cornelia I. Bargmann. Neurons Detect Increases and Decreases in Oxygen Levels Using Distinct Guanylate Cyclases. *Neuron*, 2009.

[185] Elissa A. Hallem and Paul W. Sternberg. Acute carbon dioxide avoidance in Caenorhabditis elegans. *Proceedings of the National Academy of Sciences of the United States of America*, 2008.

[186] Elissa A. Hallem, W. Clay Spencer, Rebecca D. McWhirter, Georg Zeller, Stefan R. Henz, Gunnar Rätsch, David M. Miller, H. Robert Horvitz, Paul W. Sternberg, and Niels Ringstad. Receptor-type guanylate cyclase is required for carbon dioxide sensation by Caenorhabditis elegans. *Proceedings of the National Academy of Sciences of the United States of America*, 2011.

[187] Christian Frøkjær-Jensen, M. Wayne Davis, Mihail Sarov, Jon Taylor, Stephane Flibotte, Matthew LaBella, Andrei Pozniakovsky, Donald G. Moerman, and Erik M. Jorgensen. Random and targeted transgene insertion in Caenorhabditis elegans using a modified Mos1 transposon. *Nature Methods*, 2014.

[188] Michele Perni, Pavan K. Challa, Julius B. Kirkegaard, Ryan Limbocker, Mandy Koopman, Maarten C. Hardenberg, Pietro Sormanni, Thomas Müller, Kadi L. Saar, Lianne W.Y. Roode, Johnny Habchi, Giulia Vecchi, Nilumi Fernando, Samuel Casford, Ellen A.A. Nollen, Michele Vendruscolo, Christopher M. Dobson, and Tuomas P.J. Knowles. Massively parallel C. elegans tracking provides multi-dimensional fingerprints for phenotypic discovery. *Journal of Neuroscience Methods*, 2018.

[189] Manon L. Guillermin, Mayra A. Carrillo, and Elissa A. Hallem. A Single Set of Interneurons Drives Opposite Behaviors in C. elegans. *Current Biology*, 2017.

[190] Takeharu Nagai, Shuichi Yamada, Takashi Tominaga, Michinori Ichikawa, and Atsushi Miyawaki. Expanded dynamic range of fluorescent indicators for Ca2+ by circularly permuted yellow fluorescent proteins. *Proceedings of the National Academy of Sciences of the United States of America*, 2004.

[191] Jorge J. Palop and Lennart Mucke. Network abnormalities and interneuron dysfunction in Alzheimer disease, 2016.

[192] Oliver Rackham and Chris M. Brown. Visualization of RNA-protein interactions in living cells: FMRP and IMP1 interact on mRNAs. *EMBO Journal*, 2004.

[193] Andreas Grote, Karsten Hiller, Maurice Scheer, Richard Münch, Bernd Nörtemann, Dietmar C. Hempel, and Dieter Jahn. JCat: A novel tool to adapt codon usage of a target gene to its potential expression host. *Nucleic Acids Research*, 2005.

[194] C. D. Link, M. A. Silverman, M. Breen, K. E. Watt, and S. A. Dames. Characterization of Caenorhabditis elegans lectin-binding mutants. *Genetics*, 1992.

[195] Steven L. McIntire, Gian Garriga, John White, Dean Jacobson, and H. Robert Horvitz. Genes necessary for directed axonal elongation or fasciculation in C. elegans. *Neuron*, 1992.

[196] George P. Rédei. BLASTP. In *Encyclopedia of Genetics, Genomics, Proteomics and Informatics*. 2008.

[197] Andrew G. Fraser, Ravi S. Kamath, Peder Zipperlen, Maruxa Martinez-Campos, Marc Sohrmann, and Julie Ahringer. Functional genomic analysis of C. elegans chromosome I by systematic RNA interference. *Nature*, 2000.

[198] Ravi S. Kamath and Julie Ahringer. Genome-wide RNAi screening in Caenorhabditis elegans. *Methods*, 2003.

[199] Edward T. Kipreos. Ubiquitin-mediated pathways in C. elegans., 2005.

[200] Avram Hershko. Roles of ubiquitin-mediated proteolysis in cell cycle control. *Current Opinion in Cell Biology*, 9(6):788–799, dec 1997.

[201] David Arthur and Sergei Vassilvitskii. K-means++: The advantages of careful seeding. In *Proceedings of the Annual ACM-SIAM Symposium on Discrete Algorithms*, 2007.

[202] Raymund A.C. Roos. Huntington's disease: A clinical review, 2010.

[203] Evgueni E. Nesterov, Jesse Skoch, Bradley T. Hyman, William E. Klunk, Brian J. Bacskai, and Timothy M. Swager. In vivo optical imaging of amyloid aggregates in brain: Design of fluorescent markers. *Angewandte Chemie - International Edition*, 2005.

[204] Neerad Phansalkar, Sumit More, Ashish Sabale, and Madhuri Joshi. Adaptive local thresholding for detection of nuclei in diversity stained cytology images. In *ICCSP 2011 - 2011 International Conference on Communications and Signal Processing*, pages 218–220, 2011.

[205] Maggie C. Lee, Susan S. Schiffman, and Theodore N. Pappas. Role of neuropeptides in the regulation of feeding behavior: A review of cholecystokinin, bombesin, neuropeptide Y, and galanin. *Neuroscience and Biobehavioral Reviews*, 18(3):313–323, sep 1994.

[206] Alexandra Plagman, Siobhan Hoscheidt, Kelsey E. McLimans, Brandon Klinedinst, Colleen Pappas, Vellareddy Anantharam, Anumantha Kanthasamy, and Auriel A. Willette. Cholecystokinin and Alzheimer's disease: a biomarker of metabolic function, neural integrity, and cognitive performance. *Neurobiology of Aging*, 76:201–207, apr 2019.

[207] Harold J.G.M. Van Megen, Herman G.M. Westenberg, Johan A. Den Boer, and René S. Kahn. Cholecystokinin in anxiety, nov 1996.

[208] M. Bourin, M. Malinge, E. Vasar, and J. Bradwejn. Two faces of cholecystokinin: anxiety and schizophrenia. *Fundamental & Clinical Pharmacology*, 10(2):116–126, mar 1996.

[209] Emma Roth, Simon Benoit, Baptiste Quentin, Brian Lam, Sarah Will, Marcella Ma, Nick Heeley, Tamana Darwish, Yashaswi Shrestha, Fiona Gribble, Frank Reimann, Irina Pshenichnaya, Giles Yeo, David J. Baker, James L. Trevaskis, and Clemence Blouet. Behavioural and neurochemical mechanisms underpinning the feeding-suppressive effect of GLP-1/CCK combinatorial therapy. *Molecular Metabolism*, page 101118, nov 2020.

[210] Mare Lõhmus, Peter A. Raven, L. Fredrik Sundström, and Robert H. Devlin. Disruption of seasonality in growth hormone-transgenic coho salmon (Oncorhynchus kisutch) and the role of cholecystokinin in seasonal feeding behavior. *Hormones and Behavior*, 54(4):506–513, sep 2008.

[211] Franco J. Vaccarino and Judy Rankin. Nucleus Accumbens Cholecystokinin (CCK) Can Either Attenuate or Potentiate Amphetamine-Induced Locomotor Activity: Evidence for Rostral-Caudal Differences in Accumbens CCK Function. *Behavioral Neuroscience*, 103(4):831–836, aug 1989.

[212] Alexandra Oranth, Christian Schultheis, Oleg Tolstenkov, Karen Erbguth, Jatin Nagpal, David Hain, Martin Brauner, Sebastian Wabnig, Wagner Steuer Costa, Rebecca D. McWhirter, Sven Zels, Sierra Palumbos, David M. Miller, Isabel Beets, and Alexander Gottschalk. Food Sensation Modulates Locomotion by Dopamine and Neuropeptide Signaling in a Distributed Neuronal Network. *Neuron*, 100(6):1414–1428.e10, dec 2018.

[213] Michael F. Mazurek and M. Flint Beal. Cholecystokinin and somatostatin in Alzheimer's disease postmortem cerebral cortex. *Neurology*, 41(5):716–719, may 1991.

[214] Raja Bhattacharya, Denis Touroutine, Belinda Barbagallo, Jason Climer, Christopher M. Lambert, Christopher M. Clark, Mark J. Alkema, and Michael M. Francis. A Conserved Dopamine-Cholecystokinin Signaling Pathway Shapes Context–Dependent Caenorhabditis elegans Behavior. *PLoS Genetics*, 10(8):e1004584, aug 2014.

[215] Tom Janssen, Ellen Meelkop, Marleen Lindemans, Karen Verstraelen, Steven J. Husson, Liesbet Temmerman, Ronald J. Nachman, and Liliane Schoofs. Discovery of a Cholecystokinin-Gastrin-Like Signaling System in Nematodes. *Endocrinology*, 149(6):2826–2839, jun 2008.

[216] Rasoul Godini, Roger Pocock, and Hossein Fallahi. Caenorhabditis elegans hub genes that respond to amyloid beta are homologs of genes involved in human Alzheimer's disease. *PLoS ONE*, 14(7), jul 2019.

[217] Sudhir Nayak, Fernando E. Santiago, Hui Jin, Debbie Lin, Tim Schedl, and Edward T. Kipreos. The Caenorhabditis elegans Skp1-related gene family: Diverse functions in cell proliferation, morphogenesis, and meiosis. *Current Biology*, 12(4):277–287, feb 2002.

[218] Atsushi Yamanaka, Masayoshi Yada, Hiroyuki Imaki, Makoto Koga, Yasumi Ohshima, and Kei Ichi Nakayama. Multiple Skp1-related proteins in Caenorhabditis elegans: Diverse patterns of interaction with Cullins and F-box proteins. *Current Biology*, 12(4):267–275, feb 2002.

[219] Kan He, Tao Zhou, Jiaofang Shao, Xiaoliang Ren, Zhongying Zhao, and Dahai Liu. Dynamic regulation of genetic pathways and targets during aging in Caenorhabditis elegans. *Aging*, 6(3):215–230, 2014.

[220] Brijesh Kumar Singh, Naman Vatsa, Vipendra Kumar, Shashi Shekhar, Ankit Sharma, and Nihar Ranjan Jana. Ube3a deficiency inhibits amyloid plaque formation in APPswe/PS1δE9 mouse model of Alzheimer's disease. *Human Molecular Genetics*, 26(20):4042–4054, oct 2017.

[221] Markel Olabarria, Silvia Pasini, Carlo Corona, Pablo Robador, Cheng Song, Hardik Patel, and Roger Lefort. Dysfunction of the ubiquitin ligase E3A Ube3A/E6-AP contributes to synaptic pathology in Alzheimer's disease. *Communications Biology*, 2(1):1–14, 2019.

[222] Ralph L Rosnow and Robert Rosenthal. Statistical procedures and the justification of knowledge in psychological science. 1992.